A Nonlinear Thermoviscoelastic Stress and Fracture Analysis Of An Adhesive Bond

Thesis by

Cong Duong

In Partial Fulfillment of the Requirements

for the Degree of

Doctor of Philosophy

California Institute of Technology

Pasadena, California

1994

(Submitted December 6, 1993)

Acknowledgements

It is difficult to summarize in a few lines the help and encouragement I have received while pursuing my doctoral degree. First of all, I would like to express my appreciation and thank Professor W. G. Knauss for his guidance during the course of this work. I also thank Professor J. Hall for his invaluable help on the computational aspects of this research. I am also grateful to Professors G. Ravichandran, A. Rosakis, and K. Bhattacharya for taking time to review this thesis. My thanks also go to all students of the Caltech Solid Mechanics group for their comments and suggestions throughout this research.

I would like to acknowledge the Office of Naval Research for the financial support under grant N00014-91-J-1427 and under the supervision of Dr. P. Schmidt. The computational part of the dissertation has been performed on the Cray-YMP of the San Diego Supercomputing center through a grant by the NSF to the GALCIT Solid Mechanics Group.

Above all, I would like to thank my parents for their love and support during my years at Caltech.

Abstract

The evolution of residual stresses resulting from cooling an adhesive bond configuration on its lateral surfaces at a constant rate through the glass transition of the polymer are considered. A nonlinear, viscoelastic (free-volume) model serves for the thermo-viscoelastic characterization of the polymer. The simultaneous solution to the heat diffusion and the transient thermoviscoelatic problems are addressed. Both an infinite (one-dimensional) and a finite (two-dimensional) domain are studied. A "critical" cooling time exists, in the present case on the order of a few seconds, which separates the control of the solidification process according to whether the relaxation or thermal diffusion time scale governs. The short time "quenching process," *i.e.*, when the time scale is governed by thermal diffusion, leads to essentially constant residual stresses. Slower cooling increasingly invokes the time and rate sensitive properties of the polymer and leads to monotically decreasing residual stresses with longer cooling times. To reduce residual stresses by a factor of two from their maximal values requires cooling times on the order of one or two days. These results are not drastically altered by changes in the thicknesses of the bond components. Apart from singular behavior of the stress components in the two-dimensionally finite domain "quenching" has the effect of producing significantly different stress distributions (including stress "spikes") than slow or thermoelastic analyses would suggest. This observation is attributed to the interaction of the bending response of the metal components early in the cooling history under the high thermal gradients, which deformations are then partially frozen in during the subsequent cooling of the polymer. Implications of these results for systems possessing geometric and material differences subjected to various thermal cooling ranges are also discussed. The results demonstrate the importance of knowing the bulk relaxation or creep spectrum for the polymer.

In the second part of the thesis the effect of the residual stresses on fracture behavior of an adhesive bond are addressed within the context of linear fracture mechanics for

dissimilar materials. The crack faces are found to be in contact at the fractured end during the (residually stress) unloading process. A significantly error results if this contact zone is not taken into account. The combined effect of the mechanical loads and the residual stresses on the energy release rate is also studied. The total energy release rate from the combined effect is not necessarily higher or equal to the sum of the individual contribution from external loads and from residual stresses separately.

Table of Contents

List of Figures

Introductory Remark

The purpose of this thesis is to advance our understanding of the failure of adhesive joints with special emphasis on the residual stresses which arise under thermal cool-down across the glass transition during bond formation. This document is organized in three chapters, each containing its own introduction and conclusions. In the first chapter, the constitutive model employed in the study for the adhesive polymer based on the free volume theory is reviewed. This material description incorporates a nonlinear stress effect in addition to the long recognized influence of temperature on the material properties and response of polymers. This development is followed by the thermoviscoelastic stress analysis of bonded joints in chapter 2. In this chapter the thermoviscoelastic boundary value problem is formulated and is solved within the context of the finite element method. The residual stresses for a wide range of processing conditions and for different viscoelastic polymer properties are examined. Finally the effect of residual stresses on fracture of the adhesive bonds is discussed in chapter 3 in terms of the energy release rates.

Chapter 1

Thermoviscoelastic Constitutive Relation for a Class of Polymers

1.1 Introduction

In the past, most of the constitutive models proposed for polymers and glasses were constructed as phenomenological theories, and only few are based on the analysis of phenomena occurring at the molecular level [1]. Due to the lack of computational power, most of the previously thermoviscoelastic stress analyses were based on relatively simple constitutive models.

The earliest model assumes thermorheologically simple material response to temperature (horizontal shift of the relaxation modulus curve with temperature) and the general linear viscoelasticity for isothermal stressing in shear [2]. Dilatation is governed by a thermal expansion and an elastic response to hydrostatic stress, and the time shift factor is a function of the current temperature only as obtained empirically. This model is used by Lee et al. [2] in the study of residual stresses in a glass plate cooled symmetrically from its outer surfaces and also by Heymans [3] for thin films coated onto glass substrates.

In an improvement to that earlier model, the time shift factor was made to depend not only on the current temperature but also on an internal variable called the "fictive" temperature T_f, *i.e.*, $a_T = f(T, T_f)$, to take into account the time and temperature-dependent behavior of the coefficient of thermal expansion of glass [4, 5]. The internal variable T_f is used to quantify the effect commonly referred to as the volume or structural relaxation effect. The model assumes that the relaxations of both shear and isotropic stresses are governed by the same time shift factor. Furthermore, the thermal strain

is expressed as a time convolution integral over the thermal history. This improved model has been used extensively in many practical manufacturing problems such as glass annealing and tempering through the studies of Narayanaswamy [5], Gardon and Narayanaswamy [4]. Scherer and Rekson [6] generalized the model further and applied it to a cooling problem of a glass-to-metal sandwich seal.

In polymers the interstitial volume between polymer chains (free volume) is found to play an important role in the relaxation behavior . Following from observations on volume changes resulting from swelling experiments, the time shift of viscoelastic functions depends on the current free volume which in turn depends on the histories of temperature, pressure, and solvent concentration [8, 9].

Recently, Losi and Knauss [10] have addressed a new constitutive model for amorphous polymers, also based on the free volume theory. In this case the time scale of the material relaxation is taken to be affected by the instantaneous free volume (through the time shift), the change of which is taken as a fraction of the total volumetric deformation. Since the free volume changes are a part of the total deformation, this model includes a coupling between the strain and stress fields and the internal time scale of the polymer.

In this chapter we will briefly review the work of Losi and Knauss. For a more detailed discussion of the subject, the reader is referred to [1]. In the sequel, the thermorheological material model for polymers in thermodynamic equilibrium states is first delineated. This development is followed by the extension of the above model to polymers in metastable equilibrium (glassy) states. This constitutive model employs a material parameter β_{f_0}; its value is calculated in section 1.4. Finally, a constitutive model which covers all (thermodynamic) regimes including the glass transition is addressed in section 1.5.

In the discussion below, we refer to the states well below the glass transition as being in the "glassy" regime while the states far above the glass transition are in the "rubbery" regime.

1.2 Thermorheological material model for polymers in thermodynamic equilibrium states

The constitutive relation for an isotropic thermorheological material under a non-isothermal process is given by

$$\sigma_{ij}(t) = \int_{-\infty}^{t} 2G(\xi(t)-\xi(\tau))\frac{\partial \epsilon'_{ij}(\tau)}{\partial \tau}d\tau + \delta_{ij}\int_{-\infty}^{t} K(\xi(t)-\xi(\tau))\frac{\partial \epsilon_{kk}}{\partial \tau}d\tau - \delta_{ij}\, p(t) \tag{1.1}$$

$$p(t) = \int_{-\infty}^{t} \Theta(\xi(t)-\xi(\tau))\frac{\partial T}{\partial \tau}d\tau, \tag{1.2}$$

where ξ is the internal (reduced) time and $\Theta(t)$ is a (possibly) time-dependent material function which accounts for the effects of temperature on the stress state. $G(t)$ and $K(t)$ are the time-dependent bulk and shear moduli measured at some reference condition, *e.g.*, $T = T_r$.

The basic postulate of thermorheological simple materials is that the changes in temperatures and pressures cause the relaxation function to be shifted to the right or left when plotted against log t. The relaxation functions at other fixed temperatures T and pressure can be directly obtained from the corresponding functions at the reference T_r and pressure by replacing t by ξ, providing that the functional relation between ξ and t is known [1]. That relation is usually called the time shift function and is considered a basic property of the material.

For polymers, the time-dependent moduli $K(t)$ and $G(t)$ are usually measured at some constant temperature above the glass transition, and they are characterized by a Prony-Dirichlet series of the form

$$K(t) = K_\infty + \sum_{i}^{M} K_i \exp^{-\frac{t}{\tau'_i}} \tag{1.3}$$

$$G(t) = G_\infty + \sum_{i}^{N} G_i \exp^{-\frac{t}{\tau_i}}. \tag{1.4}$$

The described constitutive model requires two additionally material property functions beside the (isothermally) bulk and shear relaxation moduli, namely, $\Theta(t)$ and the

[1] This phenomenon is referred in literature as the time-temperature superposition principle.

time shift function. We consider these two functions in detail next. All considerations apply to cases in which a polymer is initially in the rubbery regime and the sudden changes in temperature and/or pressure would not be high enough to force the polymer through the glass transition. In other words, upon a sudden change in environmental condition, the polymer will change to a new state which is also in the rubbery regime. The extension of this model to polymers at temperature below the glass transition is addressed in section 1.3.

1.2.1 Construction of $\Theta(t)$

In the absence of experimental data, $\Theta(t)$ is determined through a bound-estimate [1] by the following argument: The time-dependent nature of the viscoelastic volumetric response is a result of short-range rearrangements of the polymer chains, such as bond rotation or local readjustments of position, and also of long-range motion involving a drift of the entire chain. Since the long-range motions of polymer chains depends strongly on the deformability of the network which in turn depends on the macroscopic deformation of the solid, these motions are hindered when the macroscopic deformation is restrained. As a result, the stress state in this case is reasonably assumed to be history (time) independent. The function $\Theta(t)$ can be evaluated by considering the isotropic stress in a polymer which is initially in the rubbery regime and is subjected to a temperature change $\triangle T$ while its volumetric deformation is completely restrained ($\epsilon_{kk} = 0$). Since the resulting isotropic stress σ_{kk} in this case is time-independent as based on the previous argument, it follows that the function Θ is a constant and that

$$\sigma_{kk} = p = \Theta \triangle T. \tag{1.5}$$

Since the polymer in the rubbery regime ($T >> T_g$) is assumed to behave essentially linearly elastic with a rubbery value α_{l_V} and K_∞ (of equation (1.3)) as its volumetric thermal expansion coefficient and bulk modulus, respectively, its isotropic stress can also be obtained from linear elasticity as

$$p = K_\infty \epsilon_{kk} = K_\infty \alpha_{l_V} \triangle T. \tag{1.6}$$

By comparing (1.5) and (1.6) one finds that $\Theta(t) = \alpha_{l_V} K_\infty$, and the term $p(t)$ in equation (1.1) can, therefore, be simplified to a history-independent term equalling $\alpha_{l_V} K_\infty \triangle T$.

1.2.2 Time shift function

We now turn our attention to the time shift function. It is well known that the material viscosity is the governing factor in the relaxation behavior of a polymer. Higher viscosities retard the relaxation process while lower viscosities accelerate the creep process. The relaxation process therefore needs to be scaled in time by the instantaneous value of viscosity η. If the time shift factor a_T is defined as the ratio of the instantaneous viscosity to that measured in some reference condition, the time shift function is given as

$$\xi(t) = \int_0^t \frac{d\tau}{\frac{\eta}{\eta_0}} = \int_0^t \frac{d\tau}{a_T}. \tag{1.7}$$

Based on experimental observations, the time shift function for polymers will depend not only on thermal history but also on the pressure history [7]. An accurate constitutive model must, therefore, include the pressure-dependence of the time shift function.

Based on the hard sphere model for liquids, Cohen and Turnbull [11] suggested that the viscosity η is related to the free volume of the liquid, which is defined as the region accessible to the center of a molecule through a drifting motion without interaction with its neighbors, by

$$\log a_T = \log(\frac{\eta}{\eta_0}) = B(\frac{1}{f} - \frac{1}{f_0}) \tag{1.8}$$

where B is a material parameter, f and f_0 are, respectively, the fractional free volume content at current condition (time) due to temperature and hydrostatic stress changes and at the reference condition corresponding to the state of the polymer in which the time dependent viscoelastic moduli were measured. The above equation is commonly designated as the Doolittle equation since it was first obtained semi-empirically by Doolittle [12].

The effects of temperature and pressure histories on the relaxation time scale (or

viscosity) are indirect through the fractional free volume as proposed (elastically) by Ferry and Stratton [7].

$$f = f_0 + \alpha_f \triangle T + \beta_f \triangle \sigma_{kk} \tag{1.9}$$

where α_f, β_f are material parameters, $\triangle T$ and $\triangle \sigma_{kk}$ are temperature and isotropic stress (or pressure) changes with respect to the reference condition at f_0.

According to this model, an increase in temperature causes an expansion and therefore increases the free volume which in turns shifts the relaxation function to the left. On the other hand, high pressures effect a decrease in the free volume, with a shift of the viscoelastic spectra towards the glassy behavior. It also follows that high tensile stresses accelerate the creep process due to an increase in free volume, and they are known to cause the yield-like phenomenon in glassy polymers [13]. It should be recalled that equations (1.8) and (1.9) are derived primarily for polymers in the rubbery regime. The free volume obtained by equation (1.9) is called the (thermodynamic) equilibrium free volume and is denoted by f_∞.

For polymers in the rubbery regime, another approach, the molecular theory, claims that a change in the free volume can be assumed to be some constant fraction of the total deformation (inclusive thermal expansion/contraction), *i.e.*,

$$f = f_0 + \delta \ \triangle \epsilon_{kk}. \tag{1.10}$$

Since equation (1.10) replaces (1.9), δ must be related to β_f or α_f. Again, the assumption that polymers in the rubbery regime behave essentially linearly elastically gives

$$\triangle \epsilon_{kk} = \frac{\triangle \sigma_{kk}}{K_\infty} - \alpha_{l_V} \triangle T.$$

Using this in equation (1.10) and comparing the resulting equation with (1.9), it follows that

$$\beta_f = \frac{\delta}{K_\infty}. \tag{1.11}$$

We next show that β_f and K_∞ are related to the compliance of the free volume

which is defined as

$$C_{free} = \frac{\partial f}{\partial \sigma_{kk}}. \tag{1.12}$$

β_f is the compliance of the equilibrium free volume since $\beta_f = \frac{\partial f_\infty}{\partial \sigma_{kk}}$ by virtue of equation (1.9). One then has

$$\beta_f = \frac{\partial f_\infty}{\partial \sigma_{kk}} = C_{free}|_{(T \gg T_g)} = C^*_{free}. \tag{1.13}$$

The relation between K_∞ and C_{free} is obtained as follows. Since the viscoelastic behavior of the bulk modulus (or its compliance) as presented by equation (1.3) can be described by a mechanical model shown in Figure 1.1 with each of the spring-dashpot assemblies depicting one component of the spectrum while the series of the elastic springs rendering the asymptotic response, the asymptotic bulk compliance is, therefore, equal to the sum of the compliance of the free volume and that of the occupied volume as indicated in the mechanical analogue.[2] Thus

$$K_\infty|_{T \gg T_g} = \frac{1}{C^*_{free} + C_{occ}}. \tag{1.14}$$

Using (1.13), (1.14) and (1.11), it follows that

$$\delta = \frac{C^*_{free}}{C^*_{free} + C_{occ}} \tag{1.15}$$

$$= \frac{\beta_{f_0}}{1 + \beta_{f_0}}, \tag{1.16}$$

where β_{f_0} is a ratio of C^*_{free} to C_{occ} and is determined in section 1.4 below.

Equation (1.15) states that the contribution of the change in volumetric deformation to the change in fractional free volume ($\delta \triangle \epsilon_{kk}$) is similar to the contribution of the total displacement of a mechanical model consisting of two springs (occupied and free volumes) in series to the displacement of each individual spring.

[2] A major simplification is made here since the molecular rearrangements could modify the chain topology in such a way that a "trading" between free and occupied volume occurs, as would be the case when the regions where molecules partially overlap change in size without a macroscopic change in volume.

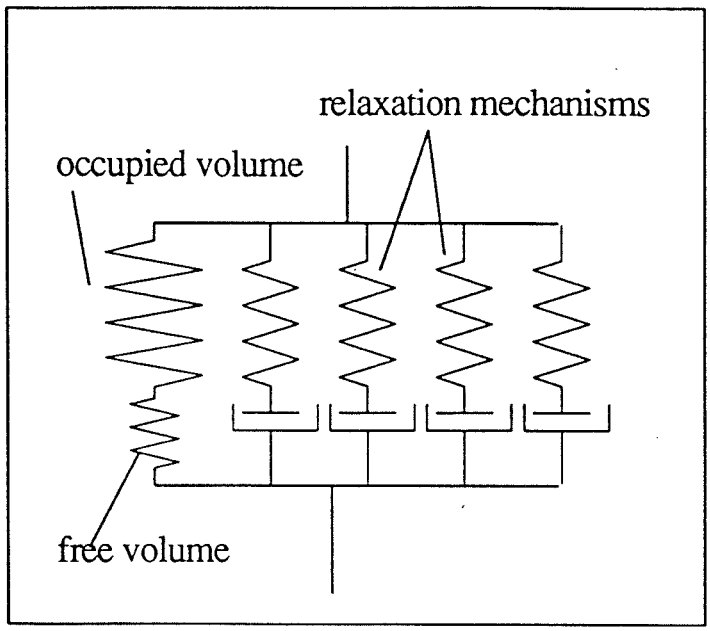

Figure 1.1: Mechanical analogue for nonlinearly viscoelastic bulk behavior (Losi, 1990).

1.3 Extension to polymers in metastable equilibrium states

The extension of the previous constitutive relation to polymers in metastable equilibrium state necessitates introducing the so-call frozen-in free volume which is addressed next.

1.3.1 Frozen-in free volume

To begin, we examine the viscoelastic behavior of the free volume. Upon sudden pressure or temperature changes, the free volume undergoes an instantaneous change followed by a time-dependent creep behavior which contributes to the evolution of the material towards an equilibrium state. The creep behavior can last from microseconds up to several years depending on the values of isotropic stress and temperature.

When the polymer is in the rubbery regime, the instantaneous change (as observed on a laboratory time scale) is the same as the asymptotic (equilibrium) change due to a very fast creep. The free volume change in this case is time-independent and can be predicted by equation (1.9) or equivalently by equation (1.10). The constitutive behavior of the polymer for this case is described by equation (1.1) with all parameters

as defined previously.

Conversely, when the polymer is in the glassy regime, the evolution of the instantaneous change towards the asymptotic (equilibrium) value occurs at a very slow rate such that the (thermodynamic) equilibrium change may not be attainable. The instantaneous change in this case is identified as a metastable equilibrium change (different from the true thermodynamic equilibrium change as observed in the former case). The metastable equilibrium is defined here as a state in which there is virtually no time-dependent change in the condition of the polymer, but the material is not at the thermodynamic equilibrium. The condition of metastable equilibrium typically occurs below the glass transition, *e.g.*, when the volume of vacancies is larger than the equilibrium free volume. The molecular interpretation of the metastable equilibrium is given immediately below.

According to the thermodynamic equilibrium description, as indicated in equation (1.9), the change in fractional free volume is proportional to $\triangle T$, and as a consequence a polymer can be cooled under the isobaric condition ($\sigma_{kk} = 0$) to a state with a null free volume. However, in reality, the total annihilation of the vacancies in the solid is not likely to occur due to the random thermal vibration of the polymer chains which is invariably present to varying degrees. The free volume therefore gradually decreases to a (constant) residual (or frozen-in) value for cooling to temperatures well below the glass transition.

The metastable equilibrium free volume is obtained by Losi and Knauss [1] from a stochastic analysis of the viscoelastic process and is given by

$$f_e = \frac{f_\infty}{1 - \frac{A}{2} e^{B(\frac{1}{f_e} - \frac{1}{f_0})}} \tag{1.17}$$

where f_∞ is given by equation (1.9). Equation (1.17) predicts that for every small values of f_∞ there is always a larger nonzero positive value of f_e, and that $f_e = f_\infty$ for sufficiently large f_∞.

For later discussion, it is also of interest to evaluate the compliance of the metastable equilibrium free volume. The compliances of the metastable equilibrium free volume is

computed through equation (1.12) with the aid of (1.13).

$$C_{free}|_{(T \ll T_g)} = \left(\frac{\partial f_e}{\partial f_\infty}\right)\left(\frac{\partial f_\infty}{\partial \sigma_{kk}}\right) = C^*_{free}\,\phi(f_e). \tag{1.18}$$

$\phi(f_e)$ in the above equation is obtained by differentiating equation (1.17) with respect to f_∞ and has the following form

$$\phi(f_e) = \frac{1}{1 - \frac{A}{2}[1 - \frac{B}{f_e}]\exp(\frac{B}{f_e} - \frac{B}{f_0})}. \tag{1.19}$$

$\phi(f_e)$ is near unity for sufficiently large value of f_e but vanishes as the latter becomes small. The compliance of the free volume therefore vanishes at states well below the glass transition.

1.3.2 The constitutive model for polymers in the glassy regime

We develop now the constitutive model for polymers in the glassy regime when they can achieve at best a metastable equilibrium condition. Losi and Knauss gave two modifications to the previous constitutive model for polymers in the glassy state. First, the metastable equilibrium free volume should be used in place of the thermodynamic equilibrium free volume in all of the previous results since the prediction for time shifts based on the Doolittle equation, *e.g.*, equation (1.8), and the (thermodynamic) equilibrium free volume (f_∞) fails to conform to experimentally measured values at temperatures below the glass transition. Second, since the compliance of the metastable equilibrium free volume is different from that of its thermodynamic equilibrium counterpart, the asymptotic bulk modulus (K_∞) is, therefore, also different in the two regimes.[3]

In the previous section it has been stated that the compliance of the metastable equilibrium free volume vanishes for small values of f_e (cf. equation 1.18). This lack of free volume compliance affects the asymptotic bulk modulus of the polymer (in the glassy regime) which is denoted here as $\hat{K}_\infty$. With the aid of the mechanical analogue

[3] As a consequence a correct asymptotic bulk modulus must used in the evaluation of the function $p(t)$ for the glassy regime.

mentioned in section 1.2.2, $\hat{K}_\infty$ is related to the compliances of the (thermodynamic) equilibrium free volume and the occupied volume fractions by

$$\hat{K}_\infty = \frac{1}{C_{free}|_{(T \ll T_g)} + C_{occ}} = \frac{1}{C^*_{free}\,\phi(f_e) + C_{occ}}.$$

Using (1.14) and the definition of β_{f_0} (as the ratio of C^*_{free} to C_{occ}) in the immediately above equation, it follows that

$$\hat{K}_\infty = K_\infty \frac{1+\beta_{f_0}}{1+\beta_{f_0}\phi(f_e)}. \tag{1.20}$$

The change in the fractional free volume for the present case is still assumed to be some fraction of the total volumetric deformation (cf. equation 1.10) but with δ (as given by equation 1.15) being computed based on the (correct) metastable equilibrium free volume compliance, *i.e.*,

$$\delta = \frac{C_{free}|_{T \ll T_g}}{C_{free}|_{T \ll T_g} + C_{occ}} = \frac{\beta_{f_0}\phi(f_e)}{1+\phi(f_e)\beta_{f_0}}. \tag{1.21}$$

Equation (1.21) is applied to both the glassy regime ($T \ll T_g$) as well as the rubbery regime ($T \gg T_g$) since it reduces to (1.16) for sufficiently large value of f_e.

1.4 Evaluation of β_{f_0}

In this section, we want to calculate β_{f_0} defined previously in term of experimentally measurable quantities α_{l_V} and $K(t)$.

The basic event of the glass transition is observed to be a kinetic phenomenon under ordinary experimental conditions. This kinetic phenomenon is attributed to a (possible) nonequilibrium state of the polymer at temperatures below glass transition temperature. It is interesting that although T_g is a function of the experimental time scale, the value of the change of the thermodynamic variables (such as C_p and α) across the glass transition is not. This suggests that there is an underlying thermodynamic transition[4] [14]. Losi and Knauss showed that the nonequilibrium effect dominates over the consequences of

[4]If the glass transition is characterized as a thermodynamic transition, the discontinuities of the thermodynamic variables must satisfy certain relations.

the thermodynamic transition [10]; they obtained β_{f_0} by neglecting the presence of a second-order transition at T_g, *i.e.*, $\dfrac{\partial^2 U}{\partial V \partial T}$ is assumed to be continuous across the glass transition (U is the internal energy of the system). From thermodynamics,

$$\left(\frac{\partial U}{\partial V}\right)_T = \sigma_{kk}.$$

Since far above or well below the glass transition the polymer behaves essentially linearly elastic, the values of $\left.\dfrac{\partial^2 U}{\partial V \partial T}\right|_{T,V}$ are, at both ends of the glass transition

$$\left(\frac{\partial^2 U}{\partial V \partial T}\right)_{T_g \gg T_g} = \left(\frac{\partial \sigma_{kk}}{\partial T}\right)_V = \alpha_{l_V} K_\infty \tag{1.22}$$

$$\left(\frac{\partial^2 U}{\partial V \partial T}\right)_{T_g \ll T_g} = \alpha_{g_V} \left(\hat{K}_\infty + \sum_i K_i\right). \tag{1.23}$$

The initial assumption that $\dfrac{\partial^2 U}{\partial V \partial T}$ is continuous across glass transition then determines β_{f_0} which is given by

$$\beta_{f_0} = \frac{\alpha_{l_V}}{\alpha_{g_V}} - 1 - \sum_i \frac{K_i}{K_\infty}. \tag{1.24}$$

1.5 The complete model for all thermodynamic regimes

So far the constitutive model is proposed for cases in which upon environmental changes, the polymer does not pass through the glass transition. Furthermore, there is no time-dependent evolution of the instantaneous free volume change due to either extremely slow or very fast creep. The constitutive relation, which applies to all regimes including the glass transition and takes into account the time dependent behavior of the free volume, is still described by equation (1.1) with the time shift function given by (1.8). However, the time scale of the material relaxation is taken to be affected by the current free volume f (through the time shift) which is

$$f(t) = f_i + \int_0^t \delta(f(\tau)) d\epsilon_{kk}(\tau), \tag{1.25}$$

where f_i is the fractional free volume content in the initial, unperturbed state.

In the computations of the current free volume f and the thermal pressure $p(t)$ of equation (1.1), the parameters $\delta(f)$, $\hat{K}_\infty$, $\phi(f)$, and β_{f_0} are defined by equations (1.21), (1.20), (1.19), (1.24) with f in place of f_e, respectively.

Chapter 2

Thermoviscoelastic Stress Analysis

2.1 Introduction

Adhesive bonding offers certain advantages over many of the conventional joining methods such as spot welding, brazing welding and over the use of discrete fasteners. Besides potentially beneficial economic aspects adhesive joining is prone to lead to lower stress concentrations and thus offers the prospect of reduced failure through fatigue and fracture damage. Investigations into the strength of adhesively bonded structures typically deal with a plethora of scientific and engineering questions, ranging from the need to understand the nature of the (chemical) bond between the joined solids, the distribution of the forces transmitted through the joint and the dependence of the latter on the structural geometry (test configuration). Of particular importance in pursuing the physio-chemical characterization of the interface strength is a sufficiently detailed knowledge of the stresses and deformations at and near the interface(s), for an imprecise knowledge of these conditions will invariably lead to improper interpretations of mechanical tests for the purpose of developing physio-chemical bonding concepts.

One of the least addressed and understood phenomenon in this context is the generation of residual stresses, which are invariably present to varying degrees. Adhesive bonds are typically formed by heating the polymeric adhesive to above the glass transition temperature while pressing the adherends together, and then cooling them under sustained pressure to room or use temperatures. Because the polymer is rate and temperature sensitive, and in particular sensitive to the rate of thermal changes, the cooling history has a potentially significant effect on the strength of the joint through the generation of residual stresses that depend on the manufacturing history. These stresses

can be so large as to cause the failure of the adhesive bond without the addition of any or with only minimal forces across it.

It is the purpose of this work, presented in two chapters (chapters 2 and 3), to examine the development of residual stresses in a geometrically reasonably realistic situation, and to explore the corresponding decrease of the bond strength in terms of an associated energy release deficit. This chapter addresses the problem of the (computational) stress analysis, which is a prerequisite for the energy analysis relegated to the next chapter.

Previous investigations of the residual stresses in an adhesive bond were limited because of (a) the lack of a suitable description of the mechanical behavior of polymers and (b) a powerful computational tool; these two elements are now available. An "early" thermoelastic analysis by Carson and Sapetta for an aluminum-epoxy joint suggested that at temperatures of about 100^0C below the glass transition temperature the joint should readily fail solely because of the high residual stresses [15]. Weitsman calculated (approximately) thermally residual stresses in a symmetric double-lap joint based on both linearly elastic and viscoelastic models for the adhesive, using variational methods [16]. For an infinite joint configuration, he found an optimal cooling path for achieving the lowest residual stresses which did not necessarily involve temporally linear cooling [17]. However, the viscoelastic constitutive description for the polymer employed in these analyses was much simpler than that used here; also the transient (spatial) temperature distribution in the sandwich was assumed to be uniform throughout the cooling history, thus excluding a (possibly) severe effect of the bending response of the metal components on the final stresses as discussed here for the finite bond configuration.

While progress can be made to determine residual stresses in bonded joints through the experimental process of trepanation with suitably chosen sections and defoliation, such investigations, while representing important experimental tools, deal only with after-the-fact situations and tend to provide a more limited understanding of the influence of various processing parameters on the final stress state. It is desired, therefore, to formulate a generic analytical problem, which, through its solution process demon-

strates the important aspects of what controls the build-up of these deleterious stresses. A necessary prerequisite to such an analysis is the existence of a constitutive description for the polymer which incorporates its dependence on the rates of mechanical deformations and on the thermal history. A model for this characterization has been offered by Knauss and Emri [8, 9] and by Losi and Knauss [10]; while further investigations into its generality are in progress, we consider it at this time a viable material description for the present purposes, because it has already provided very realistic simulations for a considerable range of physical test situations [9, 18]. This nonlinear model is not trivially applied to any arbitrary polymeric material, because a considerable amount of characterization testing needs to be available. Some of these tests are not even in the standard repertoire of the current mechanical characterization of polymers (*e.g.*, volume compliance measurements). For this reason we employ here, for demonstration purposes, the properties of a material modelled after polyvinylacetate (PVAc), which has a glass transition temperature of about 30^0C, lower than typical structural adhesives. One can largely compensate for this shortcoming by making all deliberations relative to the glass transition temperature. Moreover, PVAc is an uncrosslinked polymer for which truly long term behavior is liquid-like; thus very long time considerations would underestimate the very long term residual stresses relative to thermosetting adhesives. Discussion of this consequence is included in section 2.5.1.2.

In the sequel the thermomechanical problem is first delineated, comprising specification of geometries and the formulation of the transient thermal problem. This development is followed by a description of the finite element and concurrent thermal analysis in section 2.3, and section 2.4 presents the (plane strain) stress results for specific geometries, *i.e.*, aluminum-polymer sandwiches of both finite and infinite extents. The implications of these results to adhesives made of other polymer systems and under other processing conditions are discussed in section 2.5.

2.2 Problem formulation

We consider the two-dimensional problems of two (aluminum) adherends of infinite and of finite extent, bonded by a thin layer of adhesive polymer as indicated in Figure 2.1 (for the infinite domain $l \rightarrow \infty$). The infinite geometry is used as a precursor for the

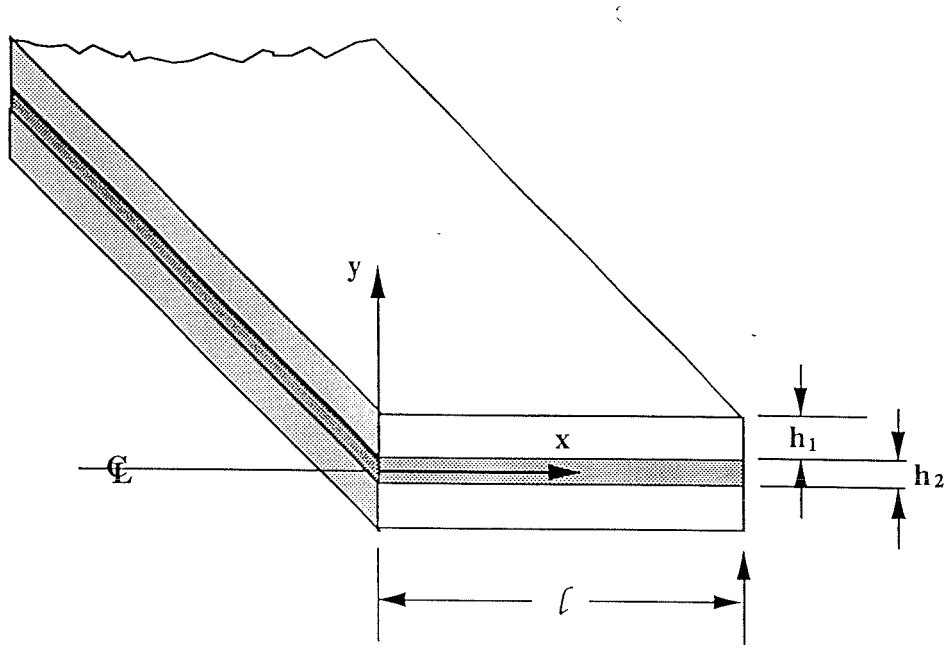

Figure 2.1: Geometry and reference frame.

finite one since it is simpler to understand and its solution corresponds to the "far field" solution for the finite configuration. The whole assembly is initially at a uniform temperature T_i above the glass transition and the outside or large flat surfaces of the adherends are cooled to below the glass transition according to the cooling history

$$\begin{aligned} T &= T_i + \frac{(T_f - T_i)}{t_R} t \qquad 0 < t \leq t_R \\ &= T_f \qquad\qquad t > t_R, \end{aligned}$$

where T_f and t_R are the final temperature and the "cooling" time, respectively. For reasons of simplicity, the edges of the sandwich are considered to be thermally insulated. The heat flow and spatially varying temperature distribution is determined subjected

to these thermal boundary conditions; all exposed surfaces are traction free.[1] The thickness of each aluminum plate is held at 1.6 cm ($\sim$ 0.5 inch) in this study while the thickness of the polymer is allowed to vary between 0.32 mm to 1.6 mm. The initial and final temperatures of the sandwich are 60^0C and -5^0C, respectively, with the glass transition temperature of the polymer (PVAc) being 29^0C.

The constitutive behavior of PVAc is characterized by the nonlinearly viscoelastic model employed previously for thermoviscoelastic stress analyses by Losi and Knauss. This model is based on the assumption that in addition to the thermally induced change in free volume, the mechanically (stress) generated change in (free) volume affects the time dependence of the polymer. This model has been described briefly in chapter 1. The material parameters for PVAc is listed in appendix A. The material properties of the aluminum are also listed there.

The shear modulus of PVAc, shown as the solid line in Figure 2.2, was obtained from the creep compliance as measured by Heymans [3] while its time-dependent bulk modulus was extracted from data by McKinney and Belcher[2] [19] and is shown (also as the solid line) in Figure 2.3.

Within the framework of the small deformation theory and by ignoring the thermo-mechanical coupling term in the Helmholtz free energy, a thermomechanical boundary value problem (without a heat source) must satisfy the following governing equations with appropriate initial and boundary conditions:

$$k \bigtriangledown^2 T = \rho C_p(T) \frac{dT}{dt} \tag{2.1}$$

$$\sigma_{ij,j} = 0 \tag{2.2}$$

$$\epsilon_{ij} = \frac{1}{2}(u_{i,j} + u_{j,i}) \tag{2.3}$$

[1]Normally during the bond formation, the large flat surfaces of the adherends are not traction free but under a nonuniform and (probably) time dependent pressure field. Because of the already large number of variables accounted for in the analysis we exclude this "pressure" boundary condition.

[2]The original data gives a very short relaxation time and an unreasonably low T_g of 17^0C either because of the molecular weight was very low or because of plasticization by the pressurizing medium. The original time-dependent bulk modulus curve is, therefore, shifted by 2.5 decades towards longer relaxation times to approximate a T_g of 29^0C for the bulk behavior. The consequence of additional approximations are considered at the beginning of section 2.4 and in section 2.5.1.1.

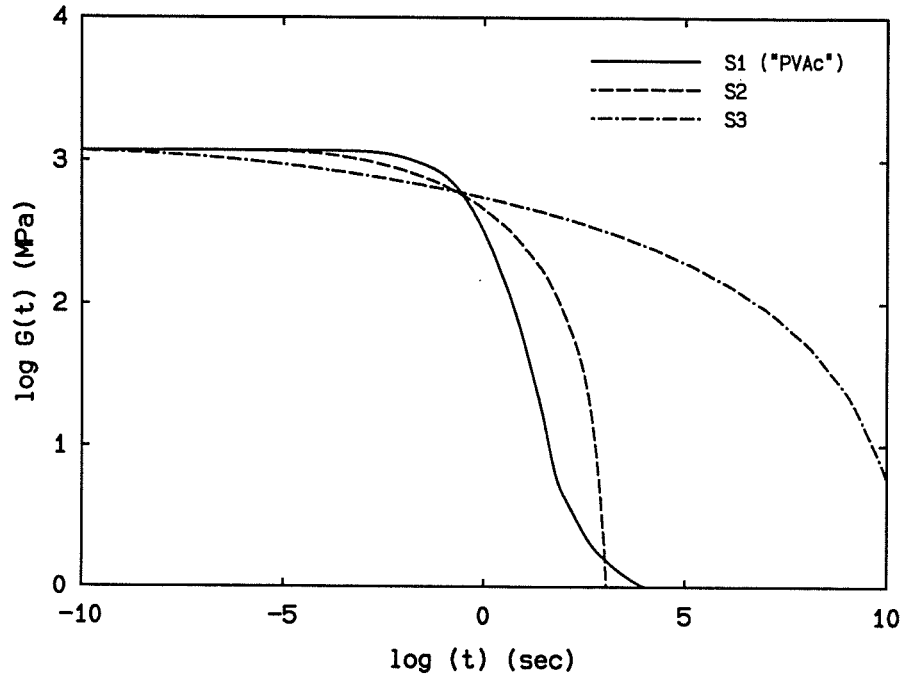

Figure 2.2: Shear moduli of various representative materials, referenced to a temperature of 11^0C above T_g. The dashed curves refer to studies described in section 2.5.1.

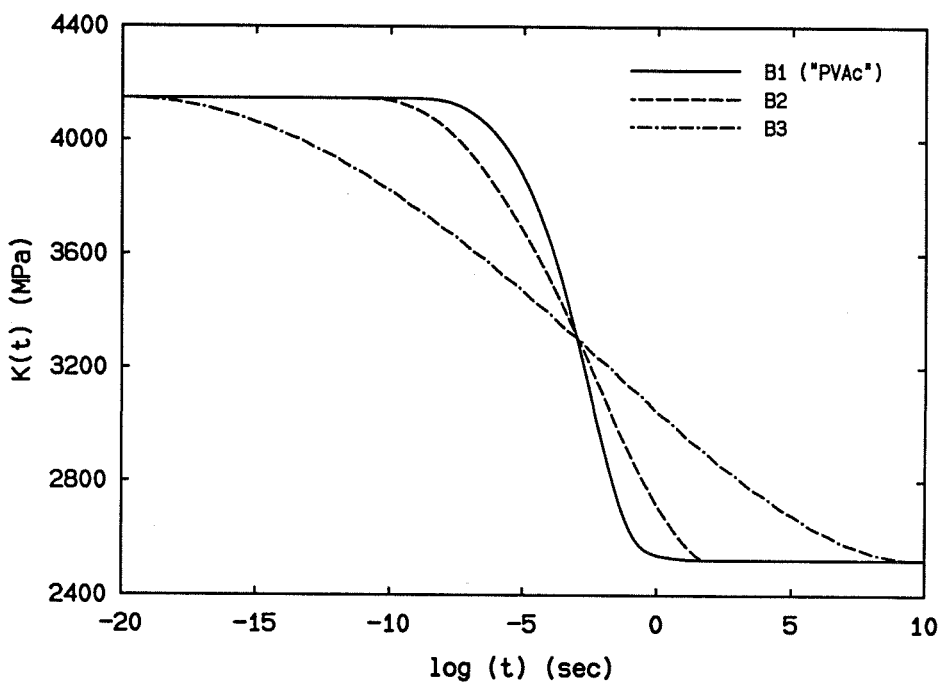

Figure 2.3: Bulk moduli of various representative materials, referenced to a temperature of 11^0C above T_g. The dashed curves refer to studies described in section 2.5.1.

$$\sigma_{ij} = \mathcal{F}(\epsilon_{ij}, T), \tag{2.4}$$

where $\mathcal{F}$ is the thermomechanical response functional of the material of the body (chapter 1), k and $C_p(T)$ are the thermal conductivity coefficient and the temperature dependent heat capacity, respectively; ρ is the density; σ_{ij}, ϵ_{ij} and u_i denote the (nominal) components of stress, strain and displacement under assumption of small deformation. As a result of the omission of the thermomechanical coupling term, the energy equation reduces to the heat conduction equation. Even though the equations look explicitly uncoupled, they are, in fact, coupled because C_p in equation (2.1) depends on the volumetric strain such as in the case of the nonlinearly viscoelastic model for polymers.[3]

2.3 Computing algorithm and discretization

The simultaneous solution of the equilibrium equation coupled with the problem of heat flow deserves special consideration. Also, the efficient partition of the whole geometry into finite elements warrants discussion. Both of these topics are addressed briefly in the sequel. A more detailed description of the finite element modelling the thermoviscoelastic boundary value problem is given in appendix B.

2.3.1 Computing algorithm

The fully coupled thermomechanical problem is often solved by what is known as a staggered algorithm based on an isothermal mechanical phase followed by a heat conduction phase. That algorithm is more efficient and convenient than the monolithic or simultaneous solution scheme, in which the time-stepping algorithm is applied to the full problem of evolution, because the latter scheme usually leads to an impossibly large and non-symmetric system. However, the staggered scheme is at best conditionally stable [20, 21, 22]. In spite of this potential drawback, we use the staggered algorithm. Because the thermomechanical response of the polymer depends on the volumetric strain through the time shift factor, the stresses and strains must be determined iteratively

[3]The heat capacity of the polymer is discontinuous at the glass transition which corresponds to a critical fractional free volume of 0.65 percent for PVAc.

during an isothermal phase. The iterative procedure may fail to converge unless the time step $\triangle t$ is sufficiently small. However, if convergence is achieved within each time step, the resulting temperature and displacement fields do not evolve in an unstable manner. This conditionally stable (staggered) scheme has not posed any numerical difficulty in our computations, possibly because of the omission of the explicit coupling term in the energy equations.

We use 4-node quadrilateral isoparametric elements. Because the long term (rubbery) bulk modulus is several orders of magnitude larger than the long term (rubbery) shear modulus in many polymers, the adhesive is nearly incompressible in the long time or rubbery regime. Isoparametric elements are known to behave poorly in such cases due to the locking phenomenon which can have a serious effect on the stress solutions unless special formulations are used [23, 24, 25].

We employ, therefore, the reduced integration scheme [25], in which the volumetric strain is segregated and treated with a reduced quadrature while the remaining deviatoric term is integrated by full quadrature. Further, the thermomechanical response function (or material property) is always evaluated based on the volumetric strain history at the reduced quadrature point. Thus it is assumed that the material property of an element is uniform. This scheme eliminates mesh locking (see appendix B). Both the nonlinearly viscoelastic model as well as the staggered (thermal) scheme were implemented in a finite element code, FEAP[4], as used by Losi and Knauss [18], however modified here to include the reduced integration scheme.

2.3.2 Discretization

Due to (double) symmetry, only one quarter of the (finite) geometry needs to be considered. The infinite sandwich is modelled as a strip with one side being fixed in the axial (x) direction to reflect the symmetrical condition and the other side being restrained such that the displacements (in x direction) of all nodes along that side are independent of the thickness coordinate. That model will give the correct vanishing shear stress τ_{xy}

[4]This code was originally developed by R. L. Taylor of U.C. Berkeley [26].

in the sandwich without considering a large finite element mesh. A typical mesh used in modelling an infinite sandwich consists of 100 elements (layers) across the adherend (aluminum) thickness and 10 - 50 elements across the polymer thickness.

Due to the stress singularity at the intersection of the free edge and the interface [27], a mesh of at least 5000 nodes had to be employed to obtain results sufficiently refined and acceptable to us.

2.4 Results and discussion

In this section the computation of stresses are detailed with the objective to interprete them quantitatively and to deduce from them a cooling rate that is optimal in some sense for achieving low residual stresses. To this end we examine the effects of the cooling rate applied to the surfaces (or t_R) on residual stresses for the two geometries of an infinite and a finite dimensioned sandwich with $h_1 = 1.6$ cm, and h_2 varying from 0.32 to 1.6 mm; these results are then discussed further in light of other process conditions as well as of other polymers in section 2.5. Since cooling stresses continue to change with time after thermal equilibrium has been reached (see Figure 2.4 for a typical response), the stresses presented in the next two sections warrant discussion.

The time required for the adherend to achieve thermal equilibrium, as determined from the first term of the series solution of Carslaw and Jaeger [28], is about five seconds longer than the "cooling time" without the polymer. The thermal equilibrium time for the sandwich is about 10 to 20 seconds longer than that value, depending on the polymer layer thickness.[5] However, in that time frame the stresses have not reached their maximum values; an explanation for this response is given immediately below.

The (final) fractional free volume f for PVAc modelled here is about 0.6 percent for all cooling rates considered and for the final temperature at or below -5^0C. By using this value for f in equation (1.8) of chapter 1, the relaxation times increase by

[5]Since the thermal conductivity coefficient of the aluminum is relatively high ($k = 237.1\ \frac{Watt}{mK}$) and since the thicknesses of both polymer and adherend are small ($h_1 = 1.6$ cm, $h_2 = 0.32 - 1.6$ mm), the thermal equilibrium time for the sandwich is very short, only about 15 seconds in step cooling ($t_R = 0.02$ sec).

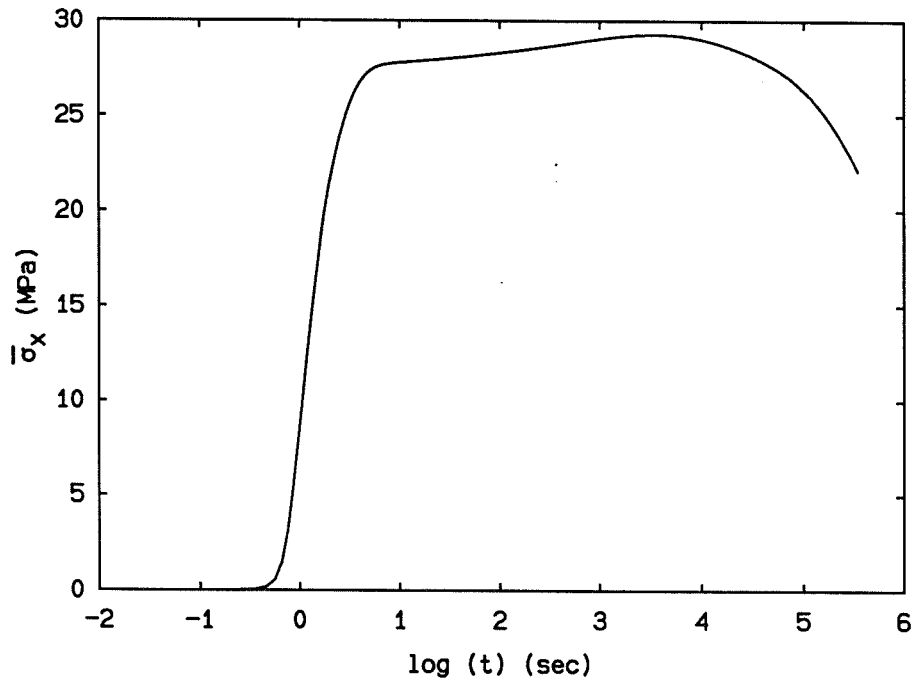

Figure 2.4: A typical history of the thickness-averaged cooling stress $\bar{\sigma}_x$ in the polymer. In this example, the time required for thermal equilibrium is about 15 seconds (quench cooling).

a factor of 10^6 relative to that at the reference temperature $T_r = 40^0C$. Since the relaxation times, especially those for the bulk modulus, at the reference condition are very short, we expect that mechanical relaxation is not necessarily "frozen" at the final temperature. In fact, the (shear) stress relaxation occurs over times on the order of days while the thermal volume creep in the current description is on the order of hours because the (shortest) bulk relaxation time of the model solid is shorter than that corresponding to the shear behavior by a factor of 10^4. Thus the effect of the thermal volume creep dominates that of the stress relaxation for a short time immediately after thermal equilibrium and becomes less important for longer times.[6] As a result, the stresses keep increasing for a short time after thermal equilibrium prevails in the sandwich, then decrease (relax) at a slow rate. Thus, for demonstration purposes, all stress solutions presented in this chapter refer to the (timewise) maximum stresses.

[6]In the absence of experimental data for $\Theta(t)$, the thermal pressure $p(t)$ is assumed to be history (time) independent (see chapter 1); as a consequence, the thermal volume creep (or the viscoelastic thermal expansion behavior) of the polymer resembles to its creep bulk compliance.

This delayed stress rise is increasingly suppressed as the distribution of bulk relaxation times shifts to longer times. Our calculations (not detailed here) show that when the relaxation times for the bulk behavior are on the same order of those for shear behavior (by log-shifting the time dependent bulk modulus curve 4 decades to longer times), the cooling stresses reach their maximum values at the time of thermal equilibrium.

In connection with these remarks, we wish to make the following observation on the viscoelastic characteristic of a "frozen" polymer. As outlined in chapter 1, the free volume of the cooling polymer will decrease and finally reach a (constant) residual value (of about 0.6 percent) if the final temperature is sufficiently low. In that case the polymer is in a metastable equilibrium (glassy) state and is assumed to behave essentially in a linearly elastic manner. The metastable equilibrium state is defined here as that state in which there is virtually no time-dependent change in the condition of the polymer, but the material is not at thermodynamic equilibrium. Since the bulk relaxation times of the model solid (PVAc) are very short as pointed out earlier, the use of glassy properties, especially the glassy thermal expansion coefficient, to characterize a polymer in a metastable equilibrium state may not always be justifiable. This decision is strongly impacted by the bulk relaxation spectrum relative to that in shear.

2.4.1 Infinite bonded plates

We consider first a sandwich, infinite in the x- and z-directions so that all displacements are functions of y only. The only nonzero stress component is then the normal stress σ_x ($\sigma_y = \tau_{xy} = 0$). The distribution of this stress across the polymer thickness is given in Figure 2.5 for different layer thicknesses and for step cooling ($t_R = 0.02$ sec). To exhibit the effect of the cooling rates on the residual stresses, the thickness-averaged σ_x stress, $\bar{\sigma}_x$, is presented in Figure 2.6, for $h_2 = 0.32$, 0.80, and 1.6 mm, as a function of t_R.

In (sub)sections below we discuss first the form of the (residual) stress profile as exemplified in Figure 2.5 and then examine the applicability or validity of thermoelastic- as opposed to the thermoviscoelastic-analyses as often practiced in engineering design. This discussion necessitates introducing the concept of the glass transition temperature

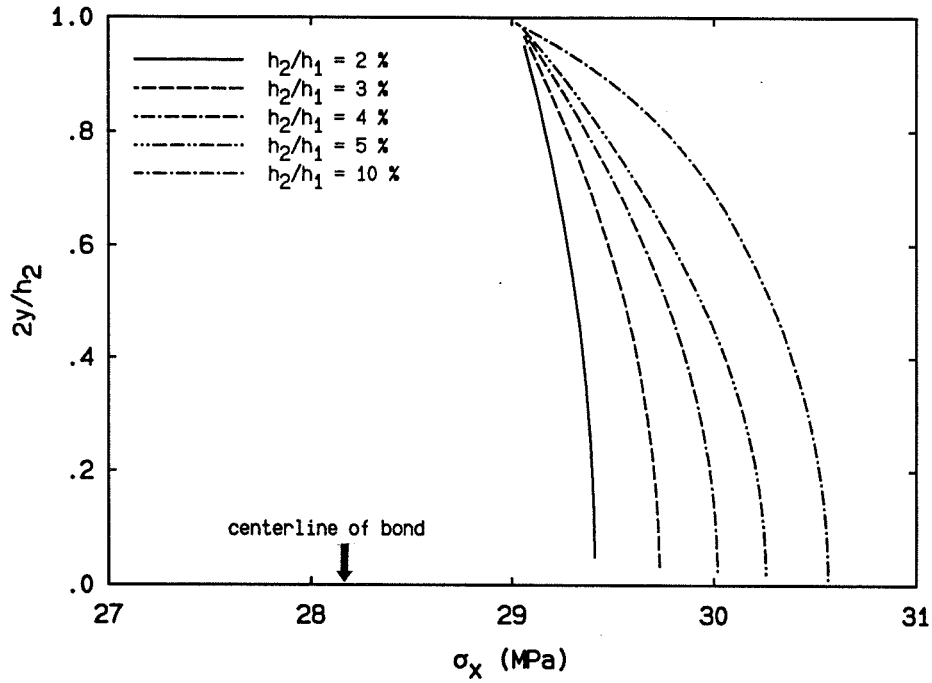

Figure 2.5: Residual stress σ_x across polymer thickness in an infinite sandwich for step cooling ($t_R = 0.02$ sec). (Note that the thermoelastic analysis yields an uniformly stress distribution with a magnitude of 11.3 MPa for all polymer thicknesses).

and the so-called stress-free temperature, especially in the context of cooling rate effects on the glass transition.

The major factors for the build-up of the residual stresses are the following: At any time during cooling, temperature changes on the surface will precede those in the interior. Thus temporary temperature differences exist between points near the surface and in the interior. Furthermore, the thermal expansion coefficient varies across the sandwich since the adherend and the polymer are different materials and the thermal expansion coefficient of the polymer is temperature-dependent. The displacement continuity in the (infinite) sandwich is then responsible for the development of the residual stresses.

2.4.1.1 Residual stress profile

It is well known from previous work [2, 18, 29, 30] that a homogeneous viscoelastic body cooled from an outer boundary contains residual tension in the interior and residual

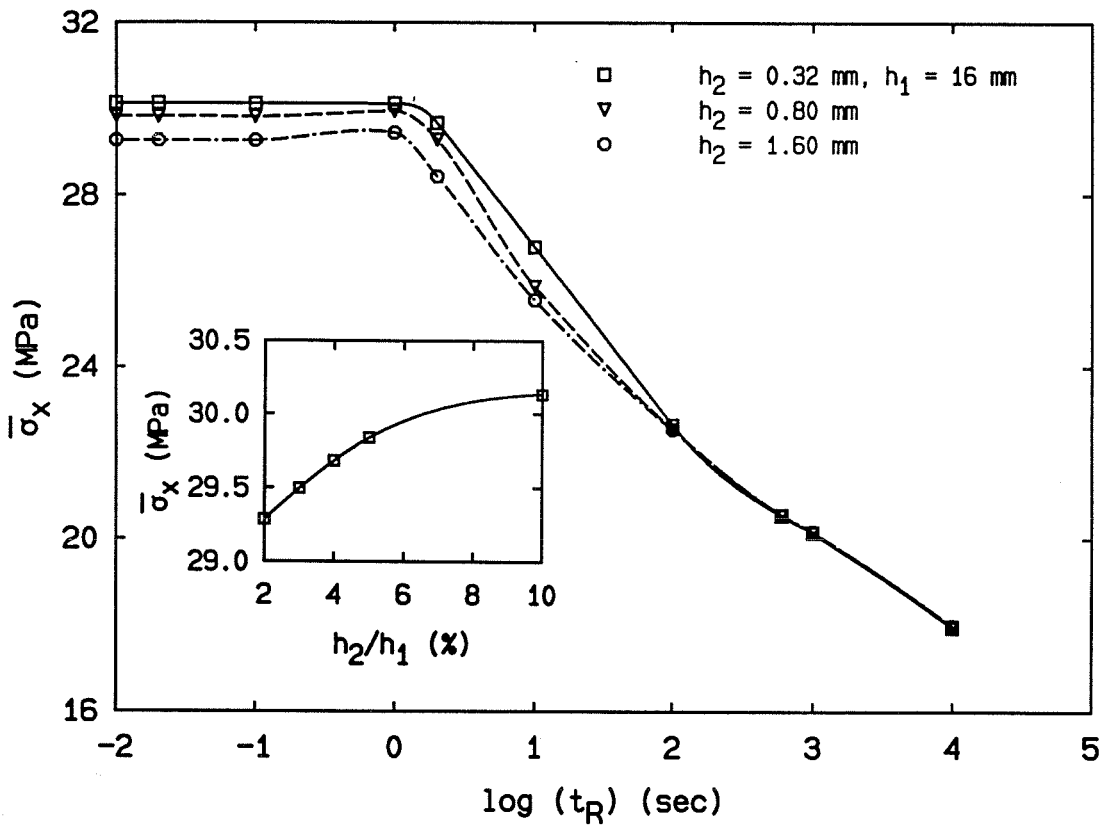

Figure 2.6: Average residual stress $\bar{\sigma}_x$ in the polymer of an infinite sandwich for different cooling times. The inset figure illustrates the crossplot of $\bar{\sigma}_x$ as a function of $\frac{h_2}{h_1}$ for quench cooling ($t_R = 0.02$ sec).

compression in the surface layers, a stress field that is desired to inhibit fracture from a surface. This stress behavior results from the early cooling and hardening of the surface before the interior has had a chance to cool and contract. The situation is similar here in that the stress at the center of the polymer layer is higher than near the adherends. The σ_x near the interface is not compressive, however, because the metal adherends contract to a lesser degree and thus superpose an overall tension on the polymer. A thicker polymer interlayer results in a larger transient temperature gradient across its thickness and as a consequence in a larger deviation from an uniform stress distribution. These trends are clearly evident in Figure 2.5.

2.4.1.2 The glass transition temperature and its dependence on cooling rate

When the polymer is cooled across its glass transition, its thermodynamic state changes from the rubbery to the glassy state. A common definition of the glass transition temperature is in terms of the (interpolated) location of the change in slope of the specific volume-temperature trace when the measurement is made under a very slow and constant rate of temperature change. If such a measurement is performed at a constant but higher cooling rate, the fractional free volume at the glass transition is higher, instead of being at its critical value.[7]

Alternatively, the glass transition is sometimes assumed to occur at some critical value of the fractional free volume [31]. This critical fractional free volume is chosen to be the same as that at which the discontinuity of the heat capacity occurs.[8] For the model material employed here this critical free volume is 0.65 percent. Thus we define the (alternate) glass transition temperature $\hat{T}_g$ here as that temperature at which the fractional free volume of the polymer reaches 0.65 percent while the temperature falls from T_i to $\hat{T}_g$. Unlike the previous definition of the glass transition temperature, this one gives a quantitative way to characterize the "onset" of the sudden changes

[7] As a result the glass transition temperature appears to be higher for higher cooling rates.

[8] The discontinuity of the heat capacity has been considered indicative of a glass transition as a thermodynamic property [31].

in mechanical properties of the polymer under a more general thermal (mechanical) history. We thus denote the glass transition temperature of the homopolymer measured at an infinitesimally small rate of cooling by T_g, which is notably different from $\hat{T}_g$ as defined in terms of a critical free volume.

The effect of the cooling rates on $\hat{T}_g$ is considered next. The glass transition temperature $\hat{T}_g$ of the polymer (in a sandwich configuration) is a decreasing function of the cooling rate since a higher cooling rate results in a smaller volume contraction for a given temperature change. A direct consequence (of this quantitative result) is that a higher cooling rate induces a smaller time shift (see section 2.4.1.6 for consequences). It also follows that $\hat{T}_g < T_g$.

2.4.1.3 The stress-free temperature and its dependence on cooling rate

We next turn our attention to the stress-free temperature. Since the long term shear relaxation modulus of a polymer is very small (or zero as in the case of thermoplastic materials such as PVAc) there should exist a minimum temperature above the glass transition at which the sandwich is essentially still stress free. Let us define this stress-free temperature T_0 as the lowest temperature at which no (significant) stresses arise as the temperature drops from T_i to T_0. It is assumed that stress relaxation is fast enough for the stresses to be completely relaxed down to this temperature.

For a low cooling rate, the thermal strain mismatch (the difference in thermal strains of the two materials) is low because of a gradual temperature gradient and the stresses are generated at a sufficiently slow rate so that none survive viscous relaxation even at relatively low temperatures.[9] It thus follows that the lower the cooling rate the lower the stress-free temperature.

[9]The time shift factor a_T is higher for low cooling rates; however, the cooling time also increases and its magnitude relative to the temperature-shifted relaxation times is larger for the lower cooling rate. As a consequence the (rate dependent) thermal expansion coefficient of the polymer increases with the cooling times while its stiffness decreases. This stiffness reduction is observed to be more significant than the effect of the higher (rate dependent) thermal expansion coefficient for $t_R > 10$ sec (see section 2.4.1.6).

2.4.1.4 Evolution of the stress σ_x

With the definitions of $\hat{T}_g$ and T_0 in mind, one divides the cooling history of the polymer as it passes from T_i to T_f into three phases. In the first ("liquid") phase, $T_i > T > T_0$, the polymer behaves essentially as an incompressible liquid and any stress developed during this phase will relax immediately to zero. The second ("viscoelastic") phase occurs for $T_0 > T > \hat{T}_g$. In the last ("glassy") phase, $\hat{T}_g > T > T_f$, the polymer is assumed to be essentially linearly elastic, so that the stress increment in this phase can be evaluated in a thermoelastic manner. Since both $\hat{T}_g$ and T_0 depend on the cooling rate as mentioned in sections 2.4.1.2 and 2.4.1.3, any assumptions regarding $\hat{T}_g$, T_0 and the omission of the contribution of stresses developed during the viscoelastic phase to the residual stresses must be made with care. In addition, T_0, T_g and $\hat{T}_g$ are not necessarily identical. It should be emphasized that even though the temperature range of the glassy phase is smaller than $|T_f - T_g|$ since $\hat{T}_g < T_g$, the residual stresses computed from the fully thermoviscoelastic analysis may not be conservative since (a) the stress contribution from the viscoelastic phase of the cooling may not be ignored and (b) for the present model material (PVAc), the "frozen" polymer still exhibit some time dependent characteristic at temperatures below $\hat{T}_g$ ($f = 0.65\%$) as mentioned in the introduction of section 2.4. The second statement seems to be contradictory with experiences as pointed out immediately below. Since the value of the change of the shear modulus across the glass transition is several orders larger than that for the thermal expansion, one normally assumes, at least for a problem of a sandwich under a (spatially) uniformly temperature change, that the thermoelastic analysis with the glassy modulus and glassy thermal expansion coefficient for the polymer would yield the highest residual stresses. We show now that this assumption is not necessarily realistic for the model solid. If the bulk relaxation times are short relative to the shear relaxation times, one can visualize a situation in which the thermal transient time[10] is shorter than the shear relaxation times but still longer than those for the bulk behavior. The magnitude of

[10]The thermal time scale is governed by both the cooling time t_R and the thermal diffusion time (see appendix C).

the (time dependent) shear modulus of the polymer in that case is on the same order as (not several orders smaller than) the glassy shear modulus while its (rate dependent) thermal expansion coefficient is close to the rubbery thermal expansion coefficient. The residual stresses from the thermoviscoelastic analysis for this example are, therefore, not necessarily bounded by the thermoelastic results.[11]

2.4.1.5 Thermoelastic analysis

When both the adherend and the polymer are considered to be linearly elastic, the residual stress in the polymer is given by [12]

$$\sigma_{x_2} = \frac{2E_1h_1E_2(\alpha_1 \triangle T_1 - \alpha_2 \triangle T_2)}{2h_1E_1 + h_2E_2} \tag{2.5}$$

with E, α, and $\triangle T$ denoting the elastic modulus, the thermal coefficient of expansion and the temperature change; subscripts 1 and 2 refer to the adherends and the polymer, respectively.

The thermoelastic analysis as often used in engineering design evaluations assumes that the temperature distribution in the sandwich is spatially uniform throughout history and that T_0, $\hat{T}_g$ and T_g may be considered to be identical, so that residual stresses are accumulated only as the result of the temperature dropping below the glass transition. However, as discussed above, these assumptions are not necessarily realistic. The thermoelastic counterpart problem consists then of treating the polymer as (glassy) elastic below T_g $(= T_0 = \hat{T}_g)$ and as not being endowed any more with time dependent response.

The residual stress in the polymer is, therefore, estimated by using equation (2.5) with $\triangle T_1 = \triangle T_2 = T_f - T_g$. If we assume, for exemplary purposes, that $T_i = 60^0C$ and

[11] The stiffness of the polymer decreases more significantly with the cooling times than its (rate dependent) thermal expansion coefficient increases, its residual stresses are, therefore, reduced for longer cooling times as stated in footnote 9; however, the magnitude of this stiffness reduction is only slightly greater than the increase in the (rate dependent) thermal expansion coefficient. Thus the stress computed from the fully thermoviscoelastic analysis still can exceed the thermoelastic prediction when the (rate dependent) thermal expansion coefficient is close to the rubbery value.

[12] For plane strain, $\frac{E}{1-\nu^2}$ and $(1+\nu)\alpha$ are used in places of E and α.

that $T_f(= -5^0C)$ is reached after the relatively long time of 7 hours, a full thermoviscoelastic analysis yields a thickness-averaged stress $\bar{\sigma}_x$ in the adhesive of 17 MPa; on the other hand, a simple thermoelastic analysis with $\triangle T_1 = \triangle T_2 = -34^0C$ yields only a stress of 11.3 MPa, an underestimation of 35%. Thus, as was found before by Losi and Knauss [18], thermoelastic analysis renders typically nonconservative stress estimates.

2.1.4.6 The effect of cooling rates on residual stresses

The dependence of the stress on the rate of cooling ($\propto 1/t_R$) is illustrated in Figure 2.6 for $h_2 = 0.32$, 0.8 and 1.6 mm. The same characteristic behavior holds also for other thicknesses considered (*e.g.*, $\frac{h_2}{h_1} < 15\%, h_1 = 0.5 - 7$ cm, $h_2 = 0.1 - 1.6$ mm)[13]. For $t_R < 1$ sec the stresses are essentially insensitive to the cooling rate. Around $t_R = 1$ sec there appears a small maximum with a monotonic decrease for longer cooling times. For present discussion purposes we consider thus $t_R = 1$ as a "critical cooling time."

The magnitude of the transient stress in the polymer depends on both the local rate of strain as well as on the rate of change of the time shift factor with respect to temperatures. A higher cooling rate yields higher rates of strains because of larger associated temperature gradients and shorter times to reach thermal equilibrium. Without considering the effect of cooling rates on the time shift factor, one should experience that a higher cooling rate results in higher residual stresses.

In reality, the dependence of the residual stresses on the cooling rate is more complicated and is harder to assess since the time-dependent volume contraction of the polymer depends on the time-dependent mechanical behavior and on the transient temperature gradient, which in turn depend on the history of volume contraction. However, in the range $t_R > 1$ sec the above simple concept prevails as evidenced in Figure 2.6.

It remains to discuss the near-constancy of the stress for short times t_R. Histories of the thickness-averaged transient stress in the polymer for different values of t_R are given in Figure 2.7 where the curves for cooling times of $t_R < 0.1$ sec collapse onto

[13] Four more geometries have been considered in this study, and the stress results are given in appendix C in terms of the governing dimensionless parameters.

essentially the same trace as implied by Figure 2.7 for step cooling. This response is, no doubt, to a considerable degree due to the decreasing rate dependence of the polymer as one enters the glassy domain. However, some rate dependence should normally still be present. This remaining rate dependence has, however, a counterbalance. As mentioned in section 2.4.1.2 and above in this section, a high cooling rate yields high strain rates but produces a smaller time shift (toward glassy behavior) for the viscoelastic functions due to a smaller volume contraction. The effect of an increase in the strain rate due to higher cooling rates on residual stress is thus offset by a slower change in stiffness under rapidly transient temperatures. The same impression is gained from a plot of the thickness-average stress against the (dropping) temperatures. For cooling times equal to and shorter than 1 sec all traces are the same as shown in Figure 2.8.

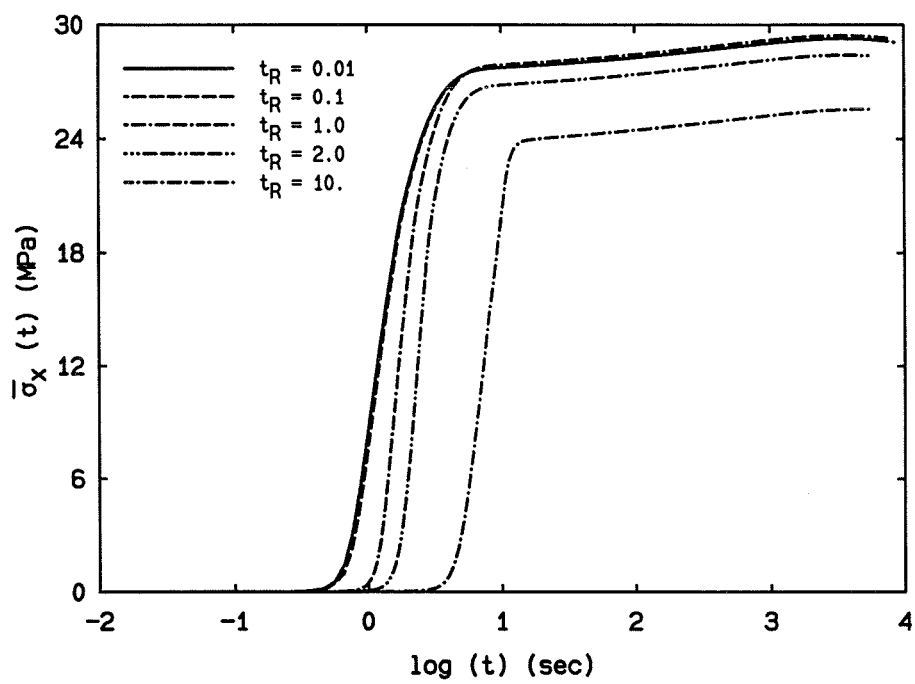

Figure 2.7: History of the average transient stress $\bar{\sigma}_x$ in the polymer of an infinite sandwich for different cooling times.

The strongest lesson learned from this examination is thus that there exists a "critical" cooling time below which the residual stresses maintain essentially constant but maximum values. With longer cooling times these stress values decrease monotonically,

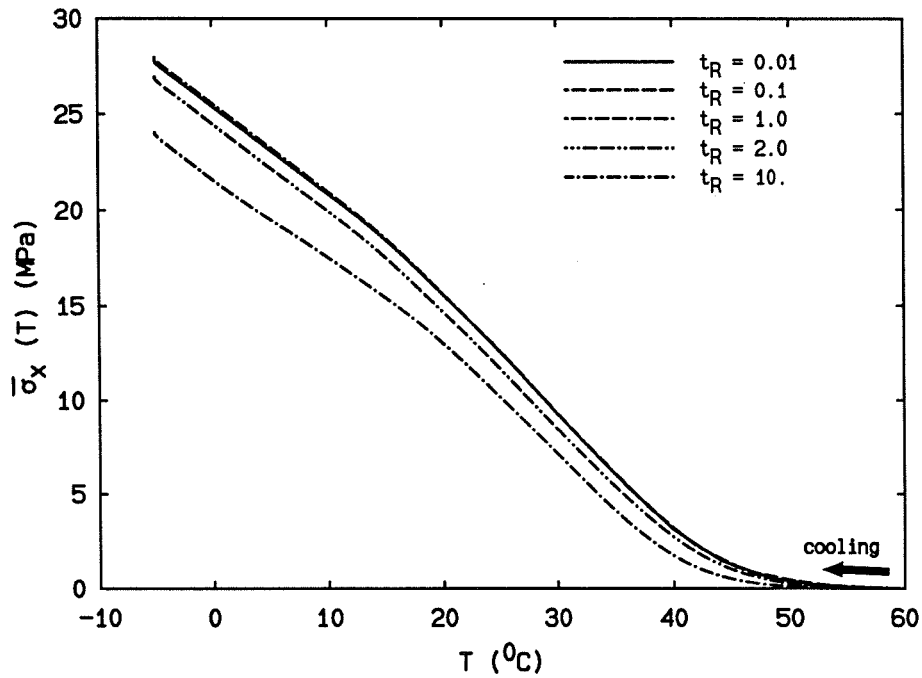

Figure 2.8: Average transient stress $\bar{\sigma}_x$ in the polymer of an infinite sandwich versus temperatures for different cooling times.

reduction on the order of 50% below those obtained in a "quench" process requiring cooling times on the order of a day. There appears to be no other critical cooling time which would clearly demarcate an economically favorable trade-off between the magnitude of the residual stresses and the time (and cost) consuming process of cooling.

2.4.1.7 Sensitivity to changes in thickness ratio

Because cooling histories, and thus strain rates, are influenced by the thickness of the adherends and the polymer layer via the thermal diffusion time scale, it is of interest to examine the effect of different ratios $\frac{h_2}{h_1}$. Figure 2.6 contains data for three such ratios (given in the inset) which span a realistic range for this parameter as encountered in engineering. It is interesting to note that this parameter does not have a markedly strong influence on the magnitude of the residual stresses. That statement is accentuated further by the inset figure which illustrates a cross plot of the primary plot to allow for some potential extrapolation to additional thickness ratios. The inset figure applies to $t_R = 0.02$ and represents the response for supercritical cooling ($t_R < 1$ sec); for $t_R > 1$

sec the dependence decreases, essentially vanishing for $t_R > 100$ sec. The influence is thus minor for relatively fast cooling and essentially absent for slow cooling.[14]

2.4.1.8 Optimal cooling rate

One objective in the production of an adhesive bond is to achieve low residual stresses within a minimum cooling time. However, since the residual stresses in the bond are, in general, a decreasing function of the cooling time t_R, one has to accept a trade off between the magnitude of the residual stresses and the cooling time. Since there is no appreciable change in the residual stress for any change in the cooling time above $t_R \approx 600$ to 10^3 sec as shown in Figure 2.6, an acceptable cooling time from the practical point of view may be around 600 to 10^3 sec.

2.4.1.9 Residual stresses and ultimate strength

The maximum residual stress computed for the thicknesses of the polymer layer considered is about 30 MPa. Since the ultimate strength of the model material (PVAc) at $T \sim 23 - 24^0C$ varies from 30 MPa to 50 MPa depending on its molecular weight,[15] it is clear that residual stresses can contribute significantly to adhesive failure. This statement is especially alarming if one considers that the interfacial bond strength is usually significantly below that of the polymer itself. Observations to that effect have been offered before in connection with composites by Pagano [33]. An additional consideration enters when one recalls that the strength of a polymer is, roughly speaking, a decreasing function of temperature. As a consequence it may happen that during cooling the intermediate stresses may exceed the temporarily low material strength so that the polymer bond may fail during the formation process. This possibility is often suppressed by the addition of external compressive stresses, which, in the case of adhesive bonding, are believed to be added to enforce a good mechanical bond, rather than for reasons of counteracting intermediate material failure. Finally we remark that even

[14] At long cooling times, a thicker adhesive yields a slightly lower residual stress, which shows the same trend as the result from the thermoelastic analysis (cf. equation 2.5).

[15] These are apparently the only available strength data for PVAc [32].

if the residual stresses are insufficient to cause failure immediately upon cool down, the strong possibility exists that failure occurs at a later time due to the time dependent nature of the polymer properties.

2.4.2 The finite case

We consider next the case when the lateral extent of the plate is finite, *e.g.*, $l = 16h_1$ which induces non-zero σ_y and τ_{xy} stresses and changes σ_x from the case for the infinite domain. The stress field for this problem is complicated by the singularities where the interfaces and the free edge meet. σ_y is self equilibrated since there are no surface forces acting on the plate. By Saint-Venant's principle, σ_y and τ_{xy} decay gradually away from the free edge and the solution for the infinite sandwich applies on the remaining "interior." The evolution of the stresses τ_{xy} and σ_y are further complicated by the bending of the adherend under the transient temperature gradient and because of the early incompressible state of the polymer. For an elastic adhesive, this bending does not contribute to the residual stresses of the adhesive owing to its time and rate invariant properties. However, for the nonlinearly viscoelastic material employed here, the stiffness is a decreasing function of temperature and the polymer is quite soft in the time frame when the adherends bend, but becomes much stiffer at the time when they attempt to return to their straight configuration. Since the "early" bending of the adherend is substantial during fast cooling, one may expect that it can have a large effect on the ultimate values of σ_y and τ_{xy}.

We carry out calculations for two polymer thicknesses: 0.32 mm (2% of the adherend thickness) and 0.80 mm (5%). The residual stresses across the sandwich thickness at different stations along the length for $h_2 = 0.32$ mm and for step cooling ($t_R = 0.02$ sec) are given in Figures 2.9 - 2.14. The tractions along the interface are of primary interest since they drive the potential bond failure. These stresses are presented in Figures 2.15 and 2.16 for $h_2 = 0.32$ mm and in Figures 2.17 and 2.18 for $h_2 = 0.8$mm, for various values of t_R. We also include there results from the thermoelastic analysis (for a finite sandwich plate) with the (questionable) assumption of a stress-free temperature

at $T_g = 29^0$ and based on glassy properties, which are designated as those corresponding to $t_R \rightarrow \infty$[16].

Apart from the corner singularity both σ_y and τ_{xy} exhibit maxima along the interface. If one examines this maximum as a function of the cooling time one finds a result that is similar to that corresponding for the infinite domain, in that below a certain cooling time (now only 0.2 sec) the stress remains at a maximum and drops to lower values as the cooling time increases from this "critical value." The location of the maximum shifts to different positions as the cooling time changes.

One notes that the tractions are significantly different for supercritical cooling (quenching) and for subcritical (slow) cooling. The tractions in the (pronouncedly) subcritical cooling ($t_R > 10$ sec) decay away from the "singular corner" such that the (spatial) oscillation has, practically speaking, disappeared. For the thicknesses of the polymer layer, the interface stresses σ_y and τ_{xy} exhibit a solution that is typical of the familiar "beam on elastic foundation" (a damped oscillating response). A simple analytical model for a finite sandwich plate has been developed for qualitative comparison. The detail derivation of that closed form approximation model is given in appendix D. The analytical result for τ_{xy} are in fair agreement with the thermoelastic results from finite element analysis. However, there is a substantial difference in σ_y between the two methods. The simple beam model tends to spread the distribution of σ_y over the whole length.

As shown in Figures 2.15 - 2.18, the edge effect can extend over a distance of several (total) sandwich thicknesses and not several thicknesses of the polymer layer. This effect is clearly the result of bending the plate rather than considering the end effect as a local perturbation over the domain on the order of the polymer thickness. The stresses at the center line ($x = l/2$) are, within 5%, the same as those obtained from the infinite sandwich configuration. We also observe that, as was true for the infinite plate, thermoelastic results are nonconservative.

[16]These thermoelastic analyses are also carried out by way of the finite element method.

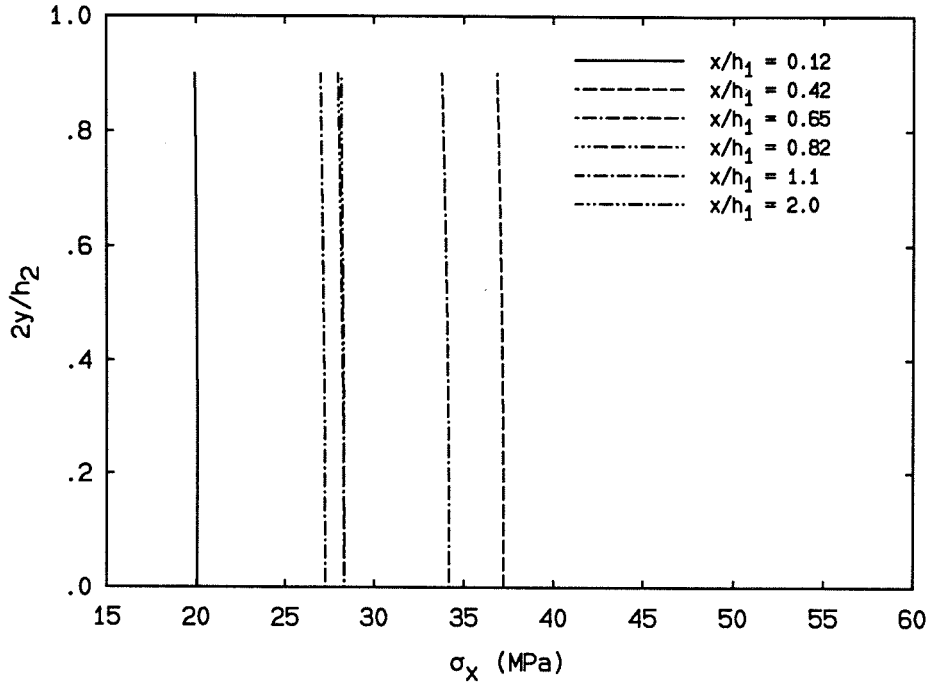

Figure 2.9: Normal stress σ_x across polymer thickness in the finite sandwich for step cooling and for $h_2 = 0.32$ mm.

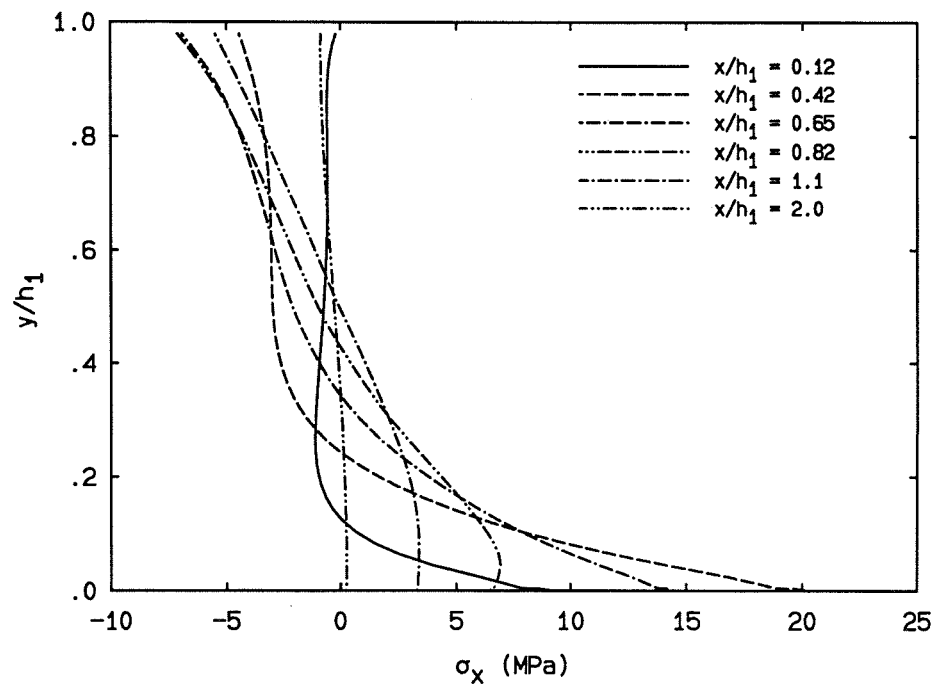

Figure 2.10: Normal stress σ_x across adherend thickness in the finite sandwich for step cooling and for $h_2 = 0.32$ mm.

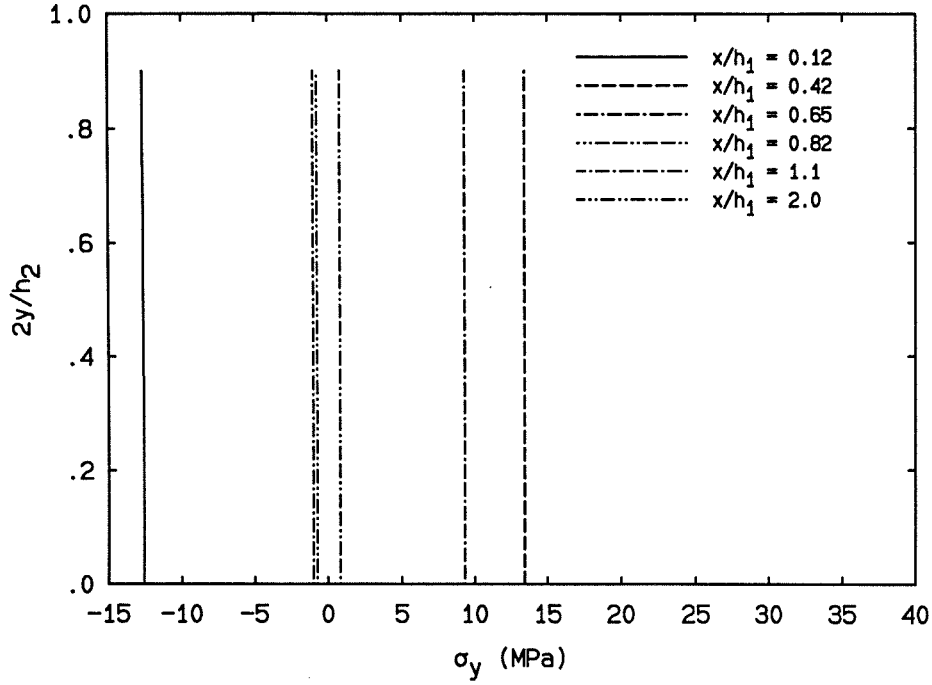

Figure 2.11: Normal stress σ_y across polymer thickness in the finite sandwich for step cooling and for $h_2 = 0.32$ mm.

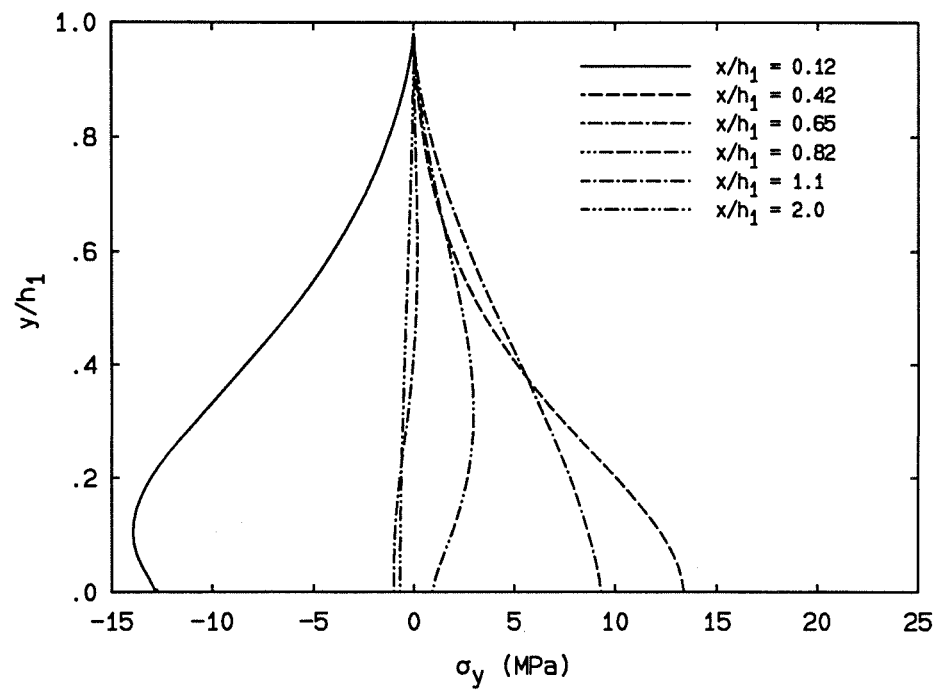

Figure 2.12: Normal stress σ_y across adherend thickness in the finite sandwich for step cooling and for $h_2 = 0.32$ mm.

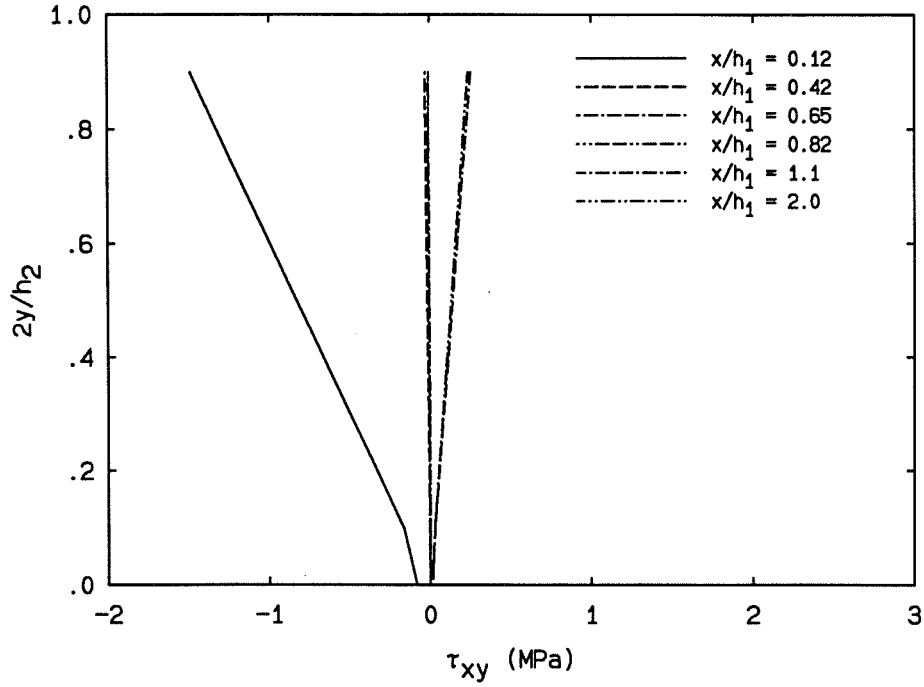

Figure 2.13: Shear stress τ_{xy} across polymer thickness in the finite sandwich for step cooling and for $h_2 = 0.32$ mm.

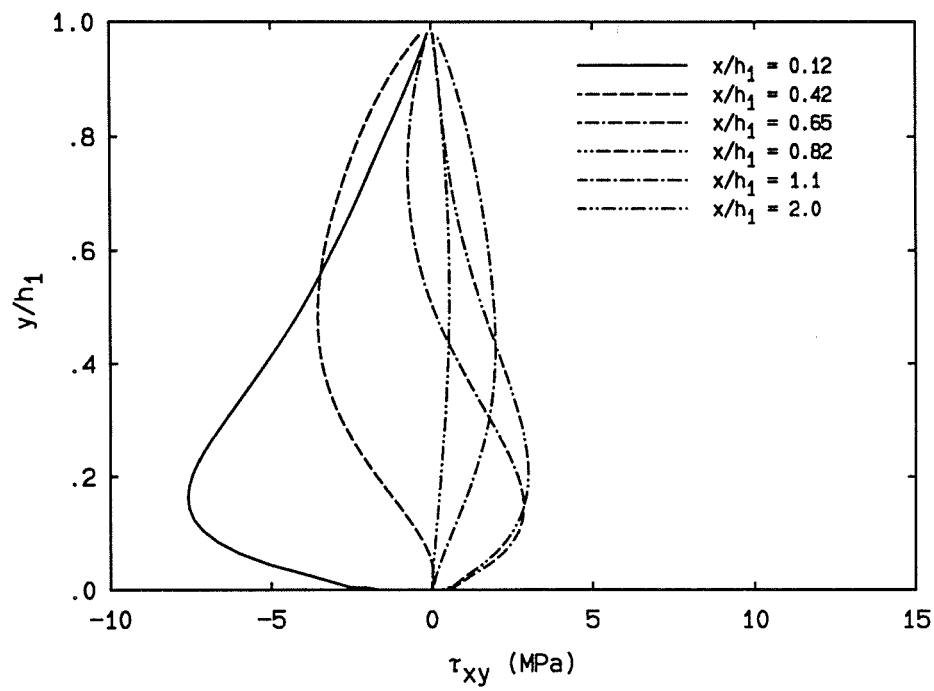

Figure 2.14: Shear stress τ_{xy} across adherend thickness in the finite sandwich for step cooling and for $h_2 = 0.32$ mm.

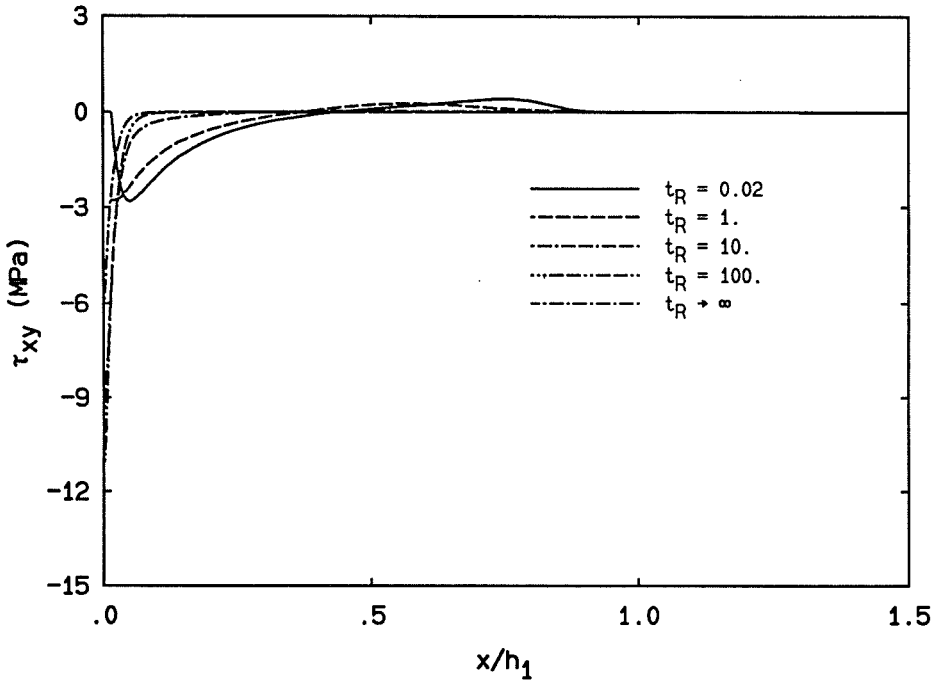

Figure 2.15: Interfacial shear stress τ_{xy} for different cooling times ($h_2 = 0.32$ mm). $t_R \to \infty$ designates value from the thermoelastic analysis.

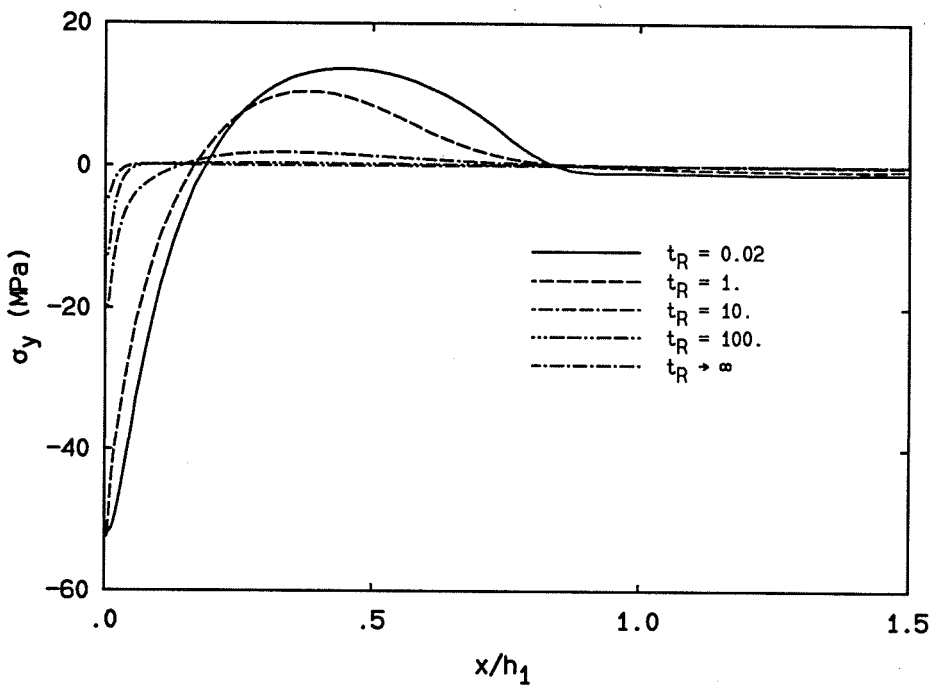

Figure 2.16: Interfacial normal stress σ_y for different cooling times ($h_2 = 0.32$ mm).

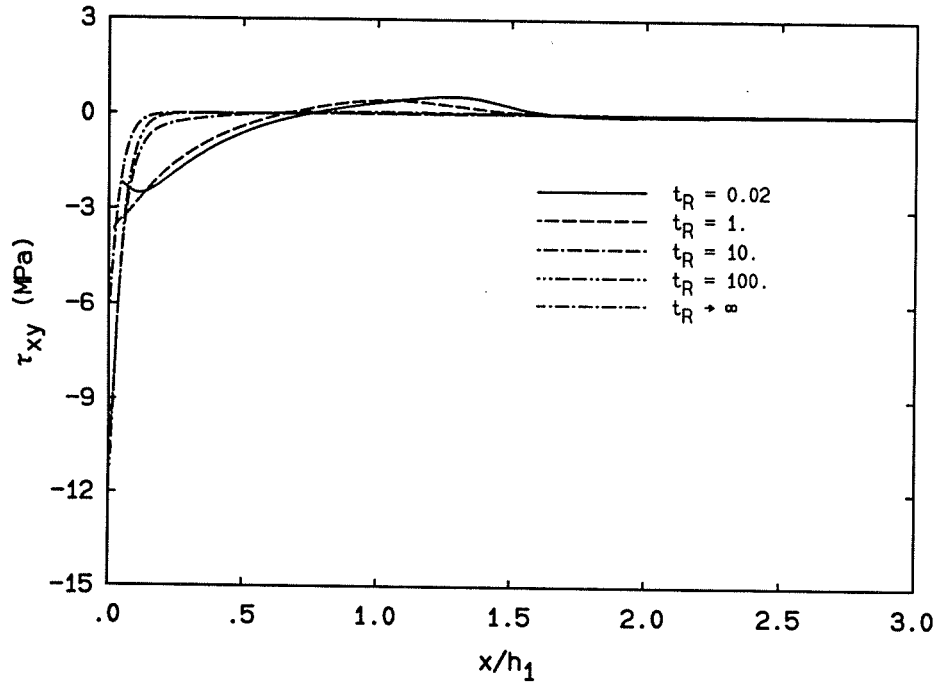

Figure 2.17: Interfacial shear stress τ_{xy} for different cooling times ($h_2 = 0.80$ mm).

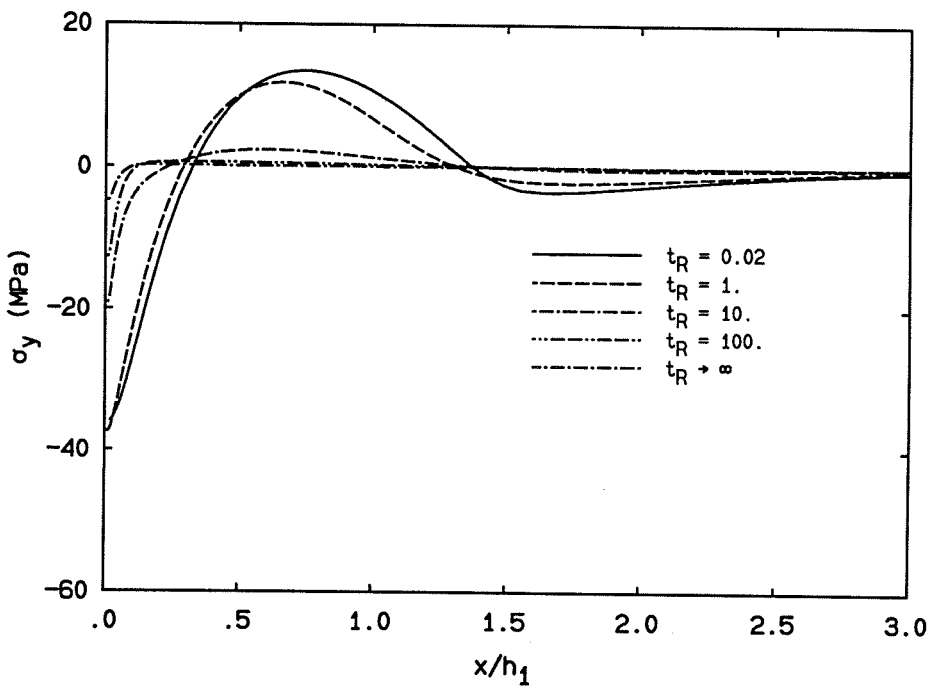

Figure 2.18: Interfacial normal stress σ_y for different cooling times ($h_2 = 0.80$ mm).

2.5 Generalizations

Because the foregoing numerical analyses address specific geometries and material properties it is of interest to be concerned with the implications of this study for bond systems of greater generality. The basic difficulty in this regard is that one deals basically with two time scales, one of which is coupled with the geometry. The first of these is prescribed by the rate of relaxation, modified by the temperature at any point, and the second is governed by thermal diffusion, which in turn is strongly coupled to the geometry of the structure. Of concern is thus the influence of different relaxation behavior, changes in the thermal history both with respect to magnitude and cooling rate, as influenced also by the geometry. We consider some of these aspects here, being well aware that a totally encompassing study transcends the scope and extent of this presentation.

2.5.1 Effect of different polymer properties

The question that motivates us in this section concerns the variation of the previous results when different polymer properties are involved. We continue to operate under the assumption that the thermoviscoelastic behavior is normalized primarily with respect to the glass transition, and that all thermal excursions should be referenced to that property. Also, the magnitude of the polymer stiffness as measured by, *e.g.*, the glassy modulus may be normalized by that parameter. It is of interest, though, to examine the effect which polymers possessing different time dependence (relaxation or creep rate) have on residual stresses. This characteristic may be exemplified by the log-log slope of the relaxation modulus or creep compliance. This slope typically ranges from 0.5 to 1.1 for most amorphous polymers [34]. We are particularly interested in the effect which changing of the relaxation behavior relative to the heat conduction time has on the residual stresses. This topic is discussed in the next section, followed by a brief summary of the influence of the nonvanishing long term shear moduli.

2.5.1.1 Influence of the relaxation times

In the previous sections, we have discussed the consequences of a large difference in the time scales of the shear and bulk relaxation behavior. Before considering other polymer systems, we will re-examine some of these consequences in more detail here. For the present, we continue to employ the shear and bulk moduli of PVAc in the thermovisocelastic analysis but with each modulus being log-shifted differently towards longer or shorter times. Figure 2.19 shows the average residual stress in the polymer layer for different bulk relaxation times, with the shear relaxation modulus providing the reference. It is clear that the residual stress decreases with the bulk relaxation times. Again this (stress) behavior is the result of the smaller time-temperature shift for viscoelastic functions and also of the smaller (rate dependent) thermal expansion coefficient. Similarly, we illustrated the effect of the shear relaxation times relative to the bulk relaxation times and to the thermal transient time on residual stresses in Figure 2.20 (but with the bulk relaxation modulus being the reference). Since the shear relaxation behavior has a "direct" effect on the residual stresses, significantly stress reduction is observed when the shear relaxation times decrease by a factor of 10^4 ($\bar{\sigma}_x = 0.12$ MPa). It also notes that for this case the shortest relaxation time of the (time dependent) shear modulus is on the same order of magnitude as that for the (reference) bulk relaxation modulus.

To cover a wider range of viscoelastic properties, we consider two additional shear relaxation moduli as well as two bulk moduli. Each additional relaxation modulus possesses the same short and long term moduli as the model solid ("reference material"), but exhibits different relaxation rates. They are compared with the reference material in Figures 2.2 and 2.3. We note that the extent of the transition region for the bulk modulus, especially that for B3, is exaggerated; this is done with the intention to illustrate more forcefully the importance of the time-dependent bulk behavior in establishing residual stresses. All other properties such as the thermal expansion, the thermal diffusion behavior, and the "material parameters" governing the time-temperature shift as

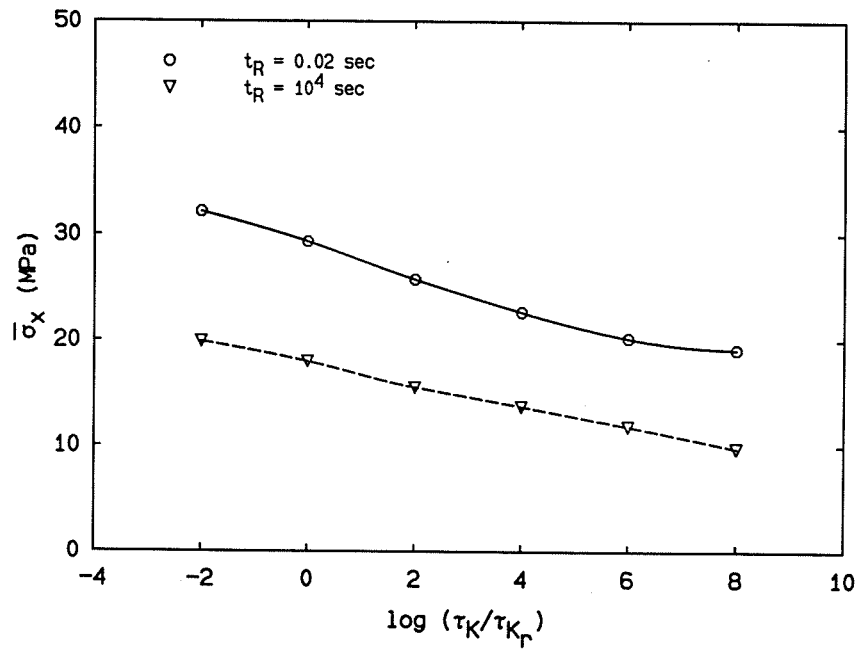

Figure 2.19: Average residual stress $\bar{\sigma}_x$ in the polymer of an infinite sandwich for different bulk relaxation times ($h_2 = 0.32$ mm). τ_{K_r} denotes the bulk relaxation time of the reference solid ("PVAc").

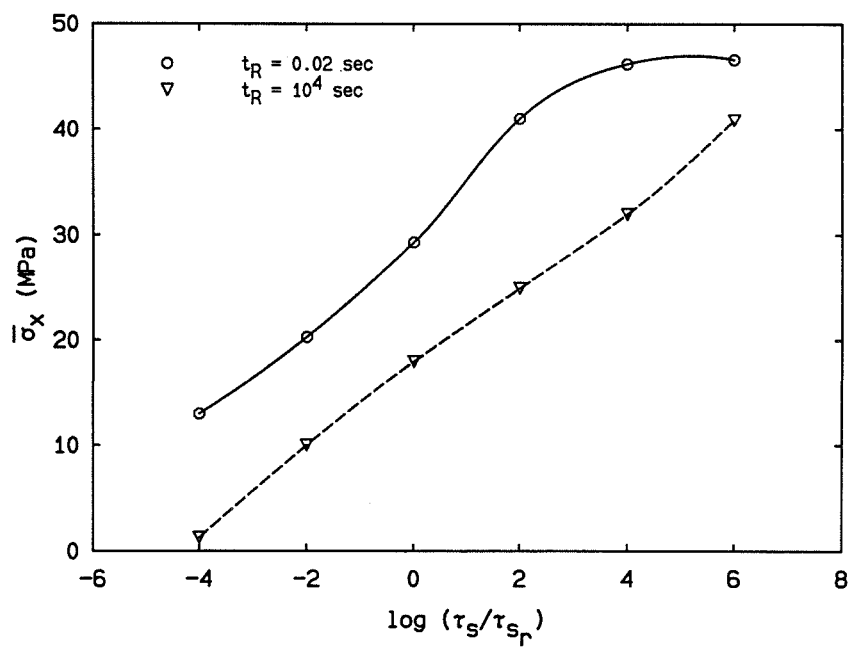

Figure 2.20: Average residual stress $\bar{\sigma}_x$ in the polymer of an infinite sandwich for different shear relaxation times ($h_2 = 0.32$ mm). τ_{s_r} denotes the shear relaxation time of the reference solid ("PVAc").

defined in free volume theory are assumed unaltered.

Figures 2.21 shows the effect which different viscoelastic properties have on the magnitude of residual stress as a function of the cooling time t_R. Since different combinations of shear and bulk moduli are considered, we adopt the notation of BI SJ for the material model which has a bulk modulus of BI and a shear modulus of SJ. It is clear that the character of these (selected) examples closely follow the result for the "reference" material as illustrated in Figure 2.6. However, the log-log slope of (primarily) the shear modulus is reflected in a different slope in the portion of the curve beyond the "critical" cooling time.

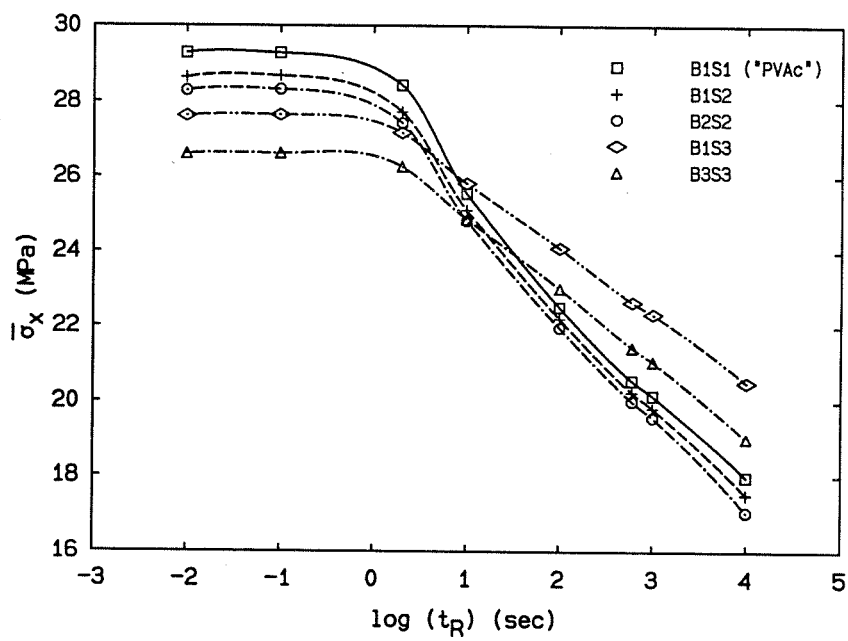

Figure 2.21: Average residual stress $\bar{\sigma}_x$ in the polymer of an infinite sandwich for different cooling times and for different viscoelastic properties ($h_2 = 0.32$ mm)

The (normal) stress relaxation behavior of the polymer is determined primarily by the (isothermal) shear relaxation modulus and also by the time-temperature shift which is influenced by the bulk modulus via free volume. For a qualitative discussion, we can define a characteristic relaxation time $\bar{\tau}(T)$ of an isothermal relaxation process at temperature T as the time required for the modulus to relax to the mean value between

the short and long term moduli. All shear moduli considered here have approximately the same characteristic relaxation time at the reference temperature ($T_g + 11^0C$) as well as for the bulk moduli; but the shear relaxation times are longer than those for bulk moduli by a factor of $10^{2.5}$. The characteristic relaxation times of the bulk moduli B1, B2, and B3 are very short at the reference temperature (on the order of 10^{-3} sec). For all cooling times, the thermal diffusion time scale is always longer than the characteristic bulk relaxation times ($\bar{\tau}_b$) of the three moduli at most transient temperatures. As a consequence a solid with B1 as its bulk modulus will produce a larger time-temperature shift than those with B2 or B3 since it yields a larger volumetric deformation for the same temperature change. In addition, the (rate dependent) thermal expansion coefficient of the former solid is also highest among the three materials (even though its viscoelastic properties have been shifted further towards the glassy regime during cooling) since the longest relaxation time of B1 is short relative to the thermal transient time and is shortest for the three moduli. Thus when one compares residual stresses of material models having the same shear modulus but with different bulk modulus such as B1S2 with B2S2 and B1S3 with B3S3, it is clear that for all cooling time t_R the stress is always higher for the material with B1, as illustrated in Figure 2.21.

On the other hand, if the time-temperature trade-off is the same for the comparison materials (same bulk relaxation modulus), the effect of different shear behaviors on the residual stresses is not as simple as in the previous case since the characteristic shear relaxation times are much longer than the bulk relaxation times so that their magnitudes relative to the diffusion time scale are more important. In a quench process, the relaxation behavior for the two solids with S2 and S3 as their shear modulus occurs at respectively shorter times than for that with S1. As a consequence the relaxation process at shorter times allows a relatively more rapid stress relaxation to take place at the higher temperatures, thus allowing the solid to reach a lower stress state before the freezing-in process begins.

From Figure 2.21 one notes that the residual stress for quenching appears to decrease

with the log-log slope of the (shear) relaxation modulus. We believe that in reality this lowering of the residual stresses in a quench process is the result of the diffusion time scale being shorter than the characteristic shear relaxation times of the three materials but still longer than their bulk relaxation times, as discussed above in this section.

Figure 2.22 shows the results of the same computations, executed for the same three materials B1S1, B2S2 and B3S3 except that the shear and bulk functions have been log-shifted to longer times by two decades. One observes that now the relaxation behavior has been slowed relative to the thermal time scale, which results in a uniform raising of the residual stress level over those observed in Figure 2.21 (particularly noticeable in the "quench region"). Since the bulk relaxation times of the three materials have increased, the diffusion time scale in a quench process may become shorter than these relaxation times, so that the effect of the different bulk behaviors on the residual stresses counterbalances that of the different shear behaviors. However the former effect is not strong enough to reverse the observed trend for the residual stresses of the three materials under "quench" cooling. In this context the reader is reminded that the ratio of the cooling time to the (characteristic) relaxation time can be also affected to a limited extent by the thickness of the sandwich, *i.e.*, the geometry.

2.5.1.2 Influence of the long term shear moduli

The shear moduli of all representative materials considered so far eventually vanish for long time, *i.e.*, $G_\infty = 0$. Not all polymers exhibit that characteristic. In fact, G_∞ typically ranges from zero to a value of several orders smaller than the glassy modulus, depending on the concentration of cross-links or the degree of entanglement coupling in uncrossed-linked polymers. For linear polymers of low molecular weight, the rubbery plateau region may span a very short time scale so that the polymer can be characterized by a mechanical model with $G_\infty \doteq 0$.

In order to extend the previous stress results to the case of nonvanishing G_∞, we compare residual stresses for material B1S1 and its counterpart with $G_\infty = 0.2$ GPa,[17]

[17]It should be recognized that this value of G_∞ (about 20% of the glassy value) may be large by

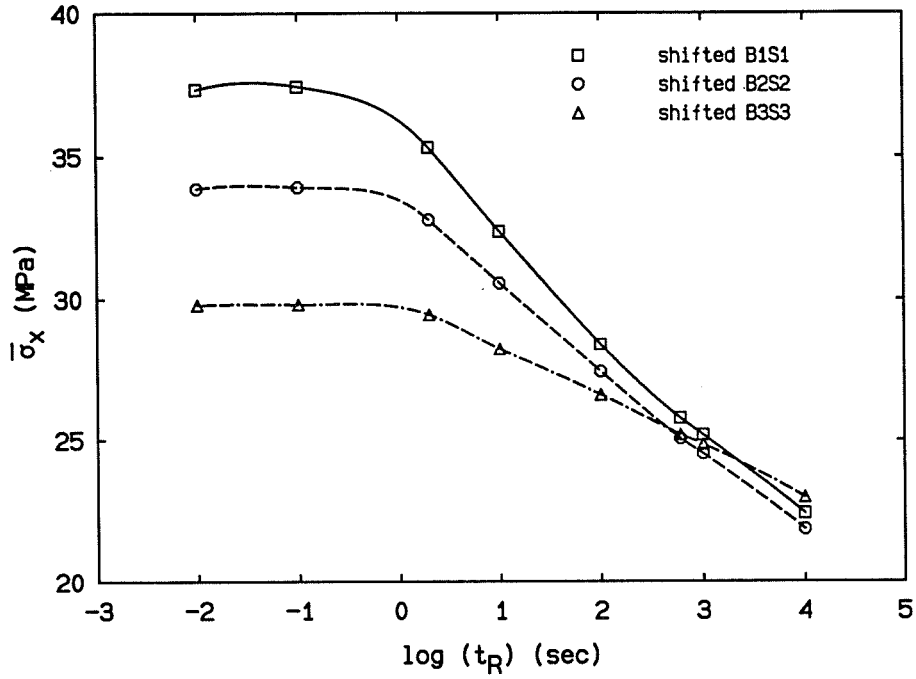

Figure 2.22: Average residual stress $\bar{\sigma}_x$ in the polymer of an infinite sandwich for different cooling times and for materials B1S1, B2S2, and B3S3 with their moduli shifted 2 decades towards longer time ($h_2 = 0.32$ mm).

i.e., B1S1c (the glassy shear modulus for S1c is also higher than that for S1 by 20%), for various cooling rates in Figure 2.23.

The uniaxial relaxation modulus of material B1S1c has a glassy value of 3.71 GPa (compared to 3.22 GPa for B1S1) and a rubbery value of 0.58 GPa. The uniaxial relaxation modulus of B1S1c is therefore approximately the same as that of B1S1 but is translated along the ordinate by an amount equal to 0.58 GPa. As a result, a similar (vertical) transposition (but by a different amount) is expected in the curve of $\bar{\sigma}_x$ vs $\log(t_R)$ for B1S1c relative to that for B1S1. This transposition is calculated to be about 20% of the stress for B1S1 from quench cooling. Moreover, as in their uniaxial relaxation responses, the difference in $\bar{\sigma}_x$ between B1S1c and B1S1 at short t_R (high cooling rate) is slightly less than that at long t_R (low cooling rate).

The amount of vertical translation of the curve of "$\bar{\sigma}_x$ versus t_R" for material B1S1c can be estimated based on a simple linear analysis which assumes that any additional

normal polymer standards.

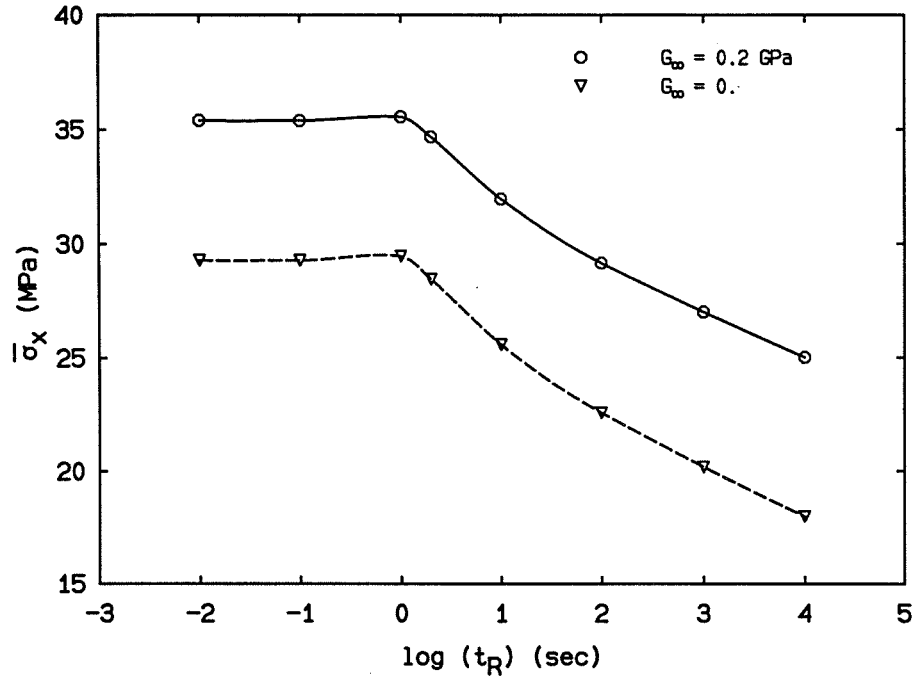

Figure 2.23: Average residual stress $\bar{\sigma}_x$ in the polymer of an infinite sandwich for various cooling times and for materials B1S1 and B1S1c ($h_2 = 0.32$ mm).

transient stresses generated in association with the nonvanishing E_∞ would not change the relaxation behavior of the polymer. The additional residual stress $\triangle\bar{\sigma}_x$ due to E_∞ is calculated from equation 2.5 (with appropriate modifications for plane strain). However, the time-dependent thermal strain of the polymer must be used in place of $\alpha_2 \triangle T_2$ in the equation. The thermal strain of the polymer is computed as the sum of the glassy and rubbery components, *e.g.*,

$$\epsilon_{t_2} = (1+\nu_g)\alpha_g(T_g - T_i) + (1+\nu_\infty)\alpha_l(T_f - T_g).$$

In this manner the vertical translation (addition) is calculated for B1S1c to be 8.3 MPa while the result from the thermoviscoelastic analysis gives a value of 6.1 MPa at $t_R = 0.02$ sec and 7 MPa at $t_R = 10^4$ sec.

2.5.2 Effect of the temperature range

In the previous discussion only a single temperature range (of 65^0C) across the glass transition was investigated. We now remark briefly on the effects which different thermal

change have.

One notes first that raising the initial temperature markedly above the glass transition has very little influence, since during cooling towards the glass transition the polymer is in a state of very rapid relaxation. Computations to that effect indicated that no change resulted if the initial temperature was 30^0C higher than the glass transition temperature. On the other hand, extending the cooling history to temperatures further below the glass transition temperature requires consideration of the two ranges for the supercritical (quenching) and subcritical cooling rates (slow cooling) (see Figure 2.24).

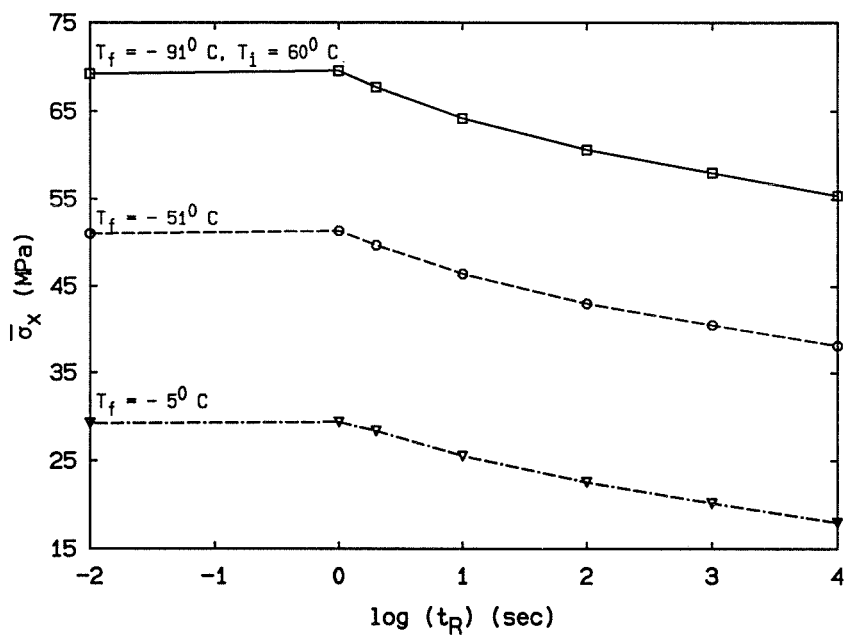

Figure 2.24: Average residual stress $\bar{\sigma}_x$ in the polymer of an infinite sandwich for various cooling times and for different temperature ranges ($h_2 = 0.32$ mm).

In the case of supercritical cooling the cooling time is small compared to the thermal diffusion time, so that when the "final" temperature T_f is reached at the outer surfaces, the polymer is not yet "hard," but becomes so only during the subsequent holding of the surfaces at that temperature. For further discussion we refer to Figure 2.25 where the thermal surface temperature history is depicted for a situation identified by subscript

"1" as conforming to the data recorded in Figure 2.6. We now consider matters when the temperature is lowered to $T_{f_2} < T_{f_1}$. In general there will be two effects: one is due to the magnitude of the temperature change and the other a (possible) change in the rate of cooling and straining. As discussed earlier, in this range of the thermal response variation the rates of strain have no significant effect. On the other hand the stress will be, to a first approximation, proportional to the magnitude of temperature drop, so that the stress levels can be scaled from the computed values by the ratio $\frac{T_i - T_{f_2}}{T_i - T_{f_1}}$ to estimate the stresses achieved through a larger temperature differential.

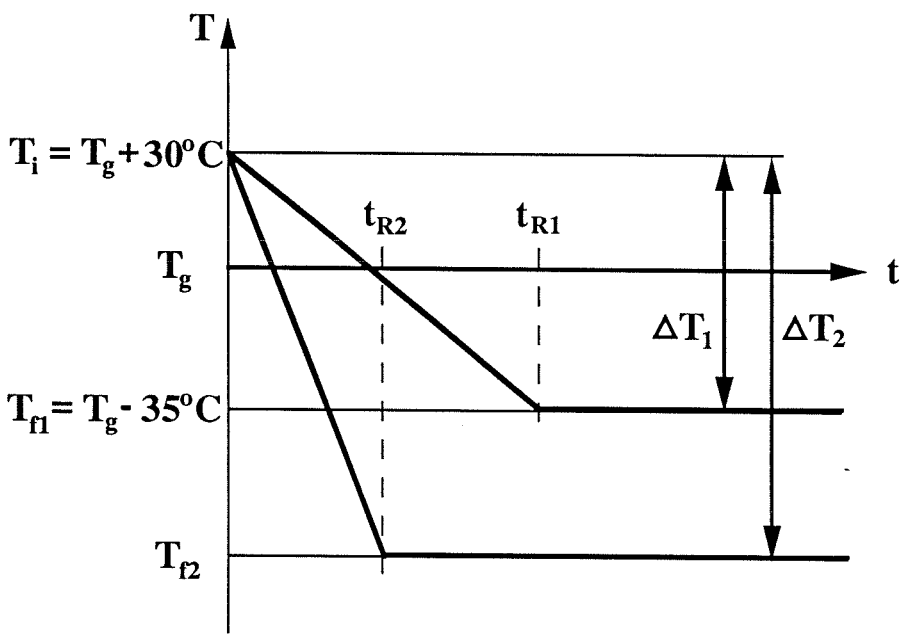

Figure 2.25: Different surface cooling histories.

For long (pronounced subcritical) cooling times uniform temperature distributions across the plate thickness prevail throughout the thermal history. However, the present study indicates (not detailed here further) that there is no (final) temperature below the glass transition or a "glassy state" such that further cooling would merely increase the stress level in a thermoelastic manner, with the coefficient of thermal expansion corresponding to the glassy value. This is a direct consequence of the short relaxation times of the bulk behavior as explained earlier throughout the chapter. In fact, if the

bulk relaxation modulus is shifted logarithmically 4 decades toward longer times, the residual stresses are sensitive to the cooling history for a temperature range spanned mostly by $T_g - 54^0C < T < T_g + 30^0C$.

It should be emphasized that lowering the final temperature from 34^0C below T_g to 80^0C and 120^0C below T_g increases the thickness-averaged stress $\bar{\sigma}_x$ by 75 % and 135 %, respectively, for quench cooling, and by 115 % and 210 % for pronouncedly long cooling times.

2.5.3 Special remark for the finite sandwich

The above generalizations are made based on results for an infinite sandwich. However, for a finite plate, one needs to consider additionally the effect of the transient, thermally induced bending response of the metal components arising from the supercritical (quench) cooling. Therefore, we carry out also computations for a finite sandwich with select cases for different polymer properties and temperature ranges.

In sections 2.5.1 and 2.5.2, the dependence of the residual stresses on the (viscoelastic) polymer properties and on the temperature ranges are examined in light of the relative time scale of thermal response and thermoviscoelastic relaxation/creep in the vitrification process. The interface stresses σ_y and τ_{xy} arising from the bending response of the adherends are also affected by the relative magnitudes of these two time scales, but at greater intensities.

The influence of different polymer properties on the interface stresses τ_{xy} and σ_y is shown in Figures 2.26 - 2.29 for a plate with $h_2 = 0.32$ mm, and for two short cooling times, *i.e.*, $t_R = 0.02$ and 2 sec. The maxima of the interface stresses σ_y and τ_{xy} for materials B1S1, B1S2, and B1S3 follow the behavior similar to that of $\bar{\sigma}_x$ for the infinite plate, but with a larger variation for different viscoelastic properties, especially when one compares the (stress) results for B1S1 with those for B1S3. Further, while the infinite plate solutions yield the highest values in $\bar{\sigma}_x$ for B1S1c compared to B1S1, B1S2 and B1S3, the present calculation (for the finite configuration) shows that the maxima of the interface stresses for B1S1c are the next lowest among the four materials. This

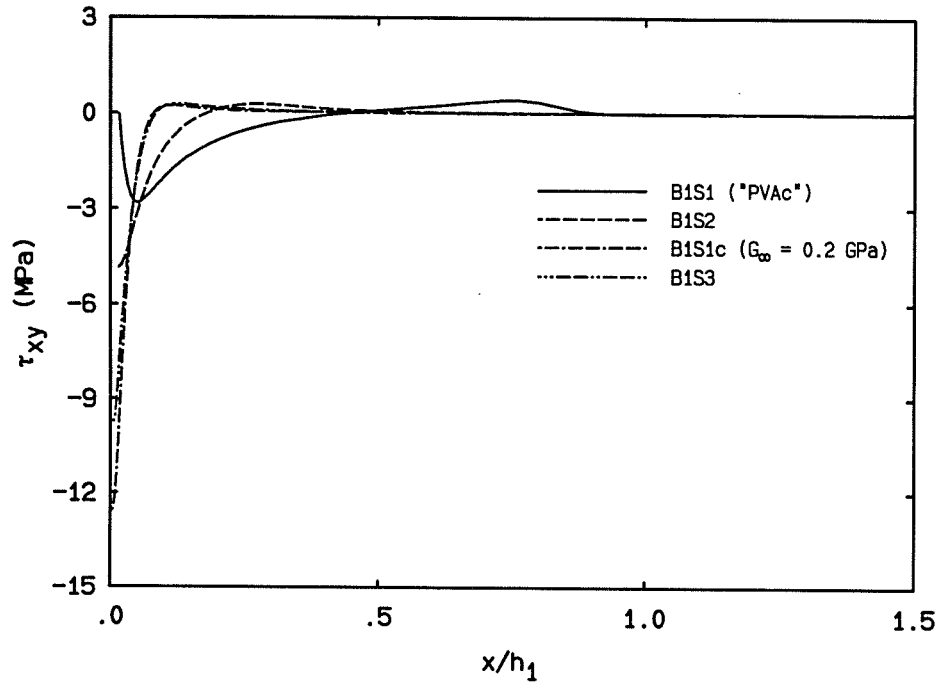

Figure 2.26: Interfacial shear stress τ_{xy} for different polymer properties and for step cooling ($h_2 = 0.32$ mm).

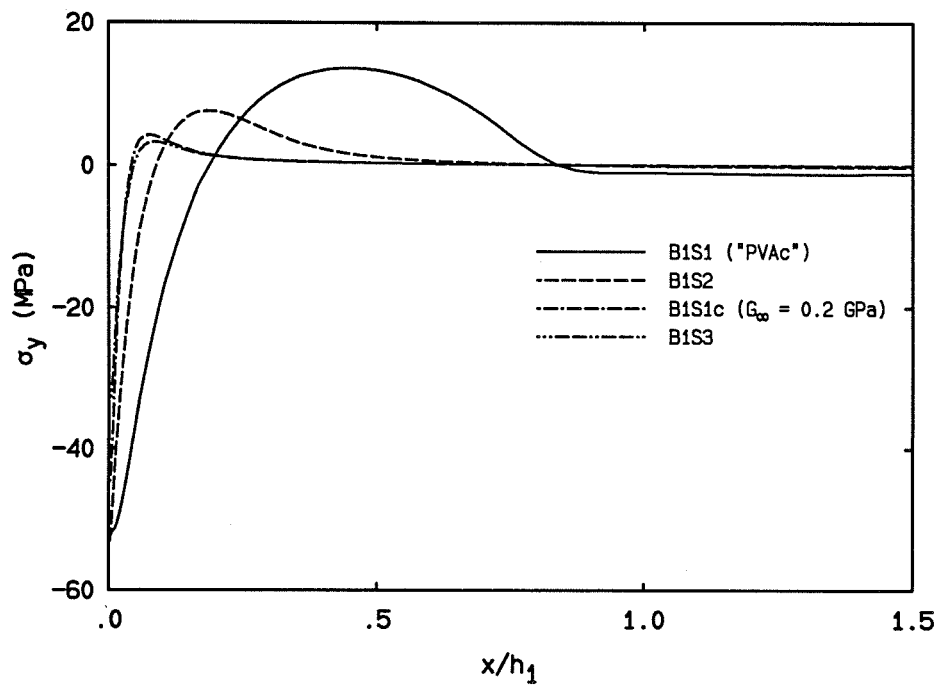

Figure 2.27: Interfacial normal stress σ_y for different polymer properties and for step cooling ($h_2 = 0.32$ mm).

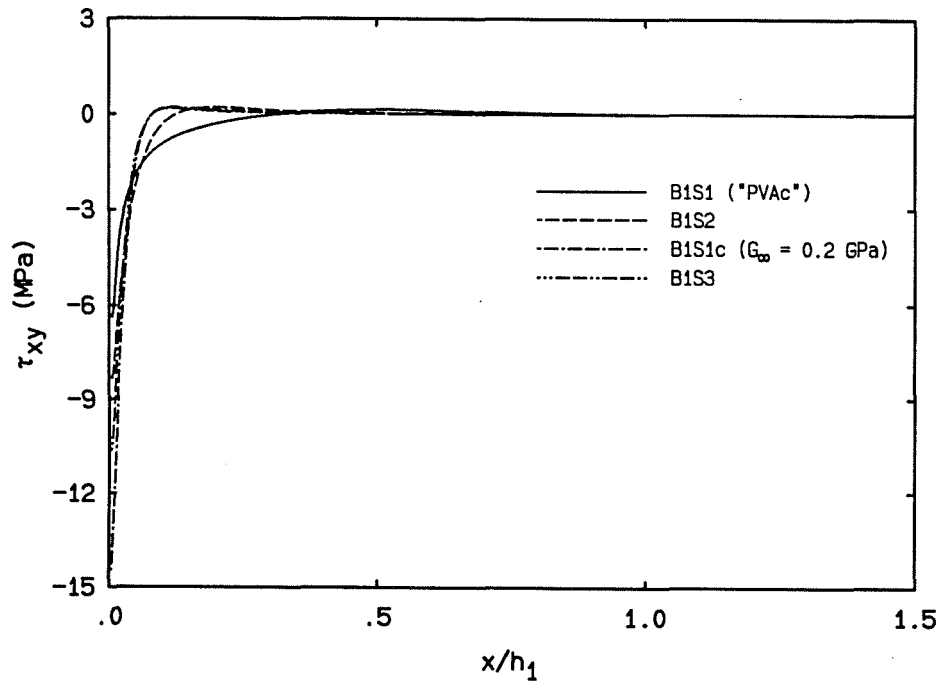

Figure 2.28: Interfacial shear stress τ_{xy} for different polymer properties and for $t_R = 2$ sec ($h_2 = 0.32$ mm).

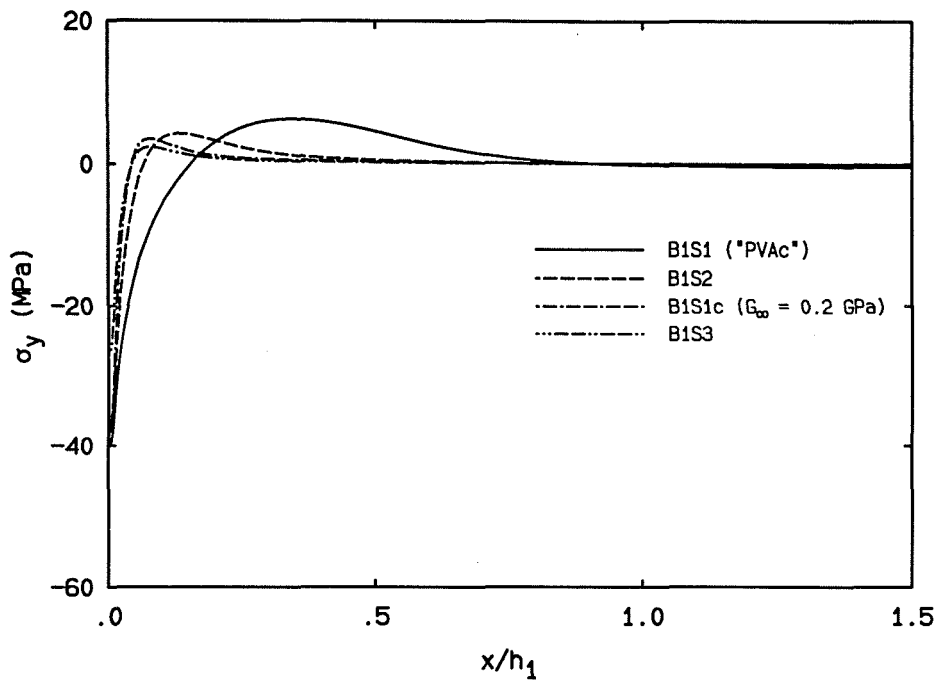

Figure 2.29: Interfacial normal stress σ_y for different polymer properties and for $t_R = 2$ sec ($h_2 = 0.32$ mm).

is attributed to the fact that the time dependent Poisson ratio of some materials considered here does not approach the compressibility limit ($\nu \doteq 0.5$) at most transient (high) temperatures because of the nonvanishing G_∞ (as for B1S1c) or because of the large extent of the longest shear relaxation time (as for B1S3) so that the polymer is less severely strained during the early bending of the adherends as detailed below following the presentation of (stress) results for different thermal changes.

The effect of different thermal changes on the interface tractions is shown in Figures 2.30 and 2.31 for $h_2 = 0.8$ mm and for quench cooling ($t_R = 0.02$ sec). It is interesting to note that the maxima of the interfacial normal stresses σ_y yield essentially the same value when they are scaled by their own thermal change; however, this characteristic does not hold for the interfacial shear stresses τ_{xy}. In fact, the "odd" stress spike in τ_{xy} for a temperature range of 151^0C ($T_f = -91^0C$ and $T_i = 60^0C$) raised our concern of the sufficiency of the mesh used for that extremely high cooling rate. For this reason, a similar computation (for $\triangle T = 151^0C$) was executed for a second grid with a very refined mesh in the area of stress spike; however, the results based on the new grid are essentially identical to those recorded in Figures 2.30 and 2.31. In contrast, a parallel computation for material B1S1c shows no similar stress spike (cf. Figures 2.32 and 2.33). The "spikes" in Figure 2.30 for τ_{xy} are, therefore, truly indicative of a phenomenon which is, as becomes apparent later, associated with the (lengthwise) "abrupt" change in the polymer properties and related to the incompressibility condition of the polymer in the rubbery regime.[18]

[18]The numerical inaccuracy tied to the incompressibility condition may attribute, in part, to this phenomenon.

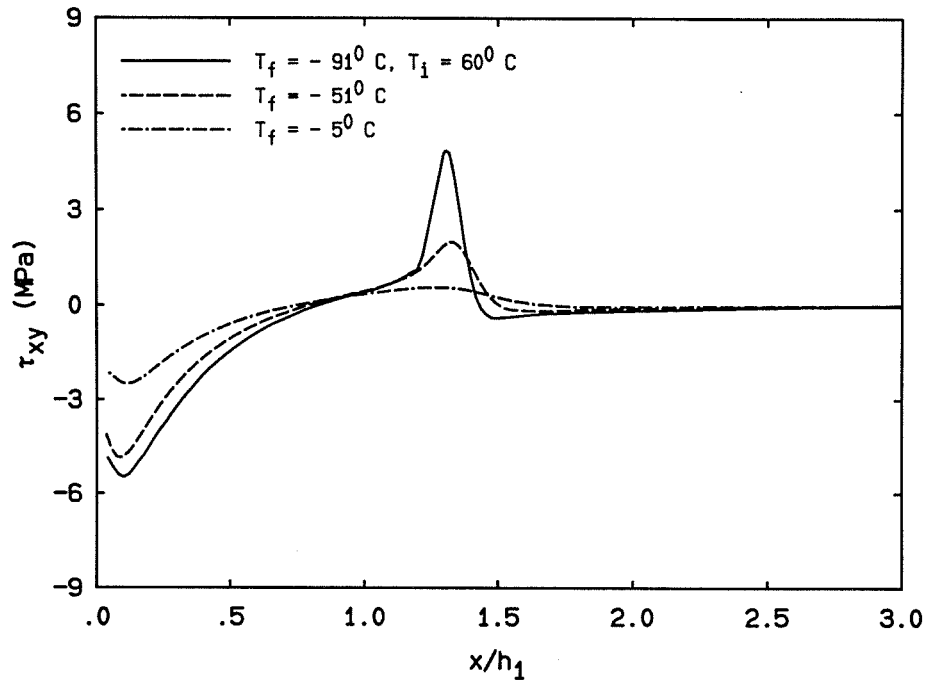

Figure 2.30: Interfacial shear stress τ_{xy} for different temperature ranges and for step cooling ($h_2 = 0.80$ mm).

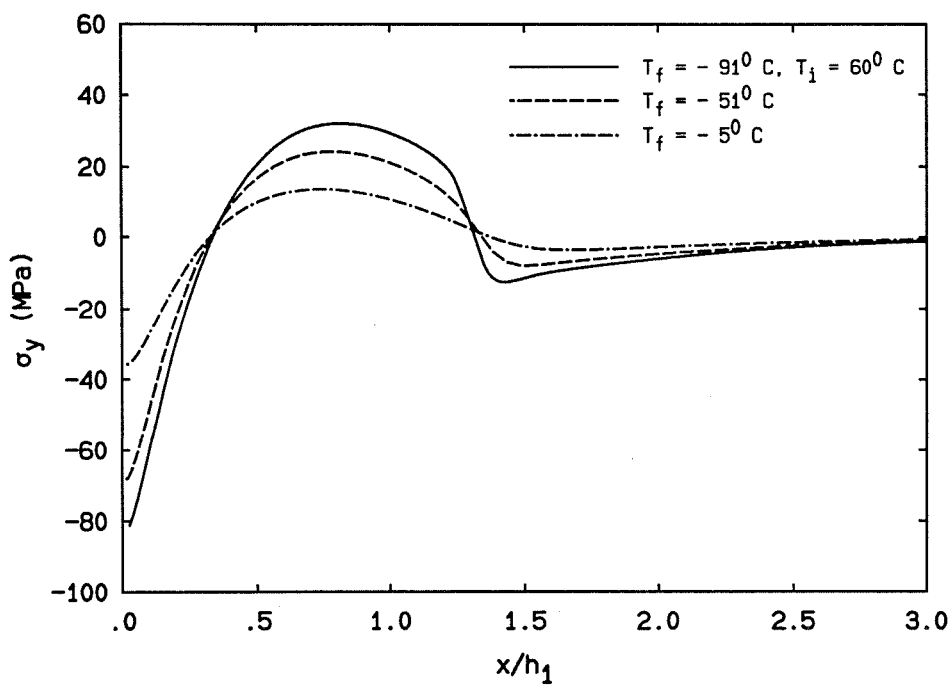

Figure 2.31: Interfacial normal stress σ_y for different temperature ranges and for step cooling ($h_2 = 0.80$ mm).

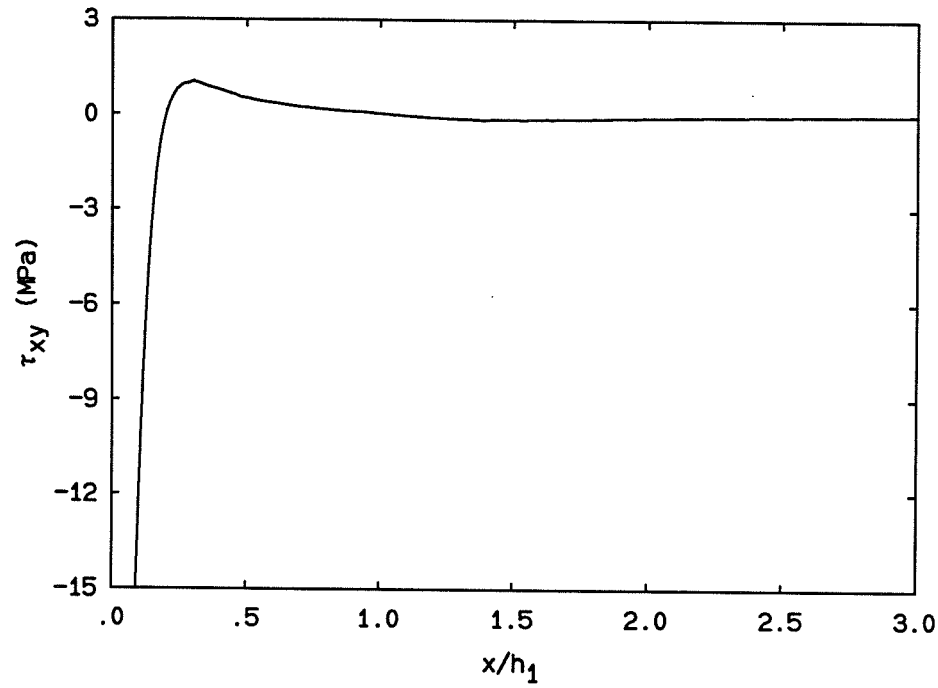

Figure 2.32: Interfacial shear stress τ_{xy} for $|\triangle T| = 151^0C$ and for material B1S1c under step cooling ($h_2 = 0.80$ mm).

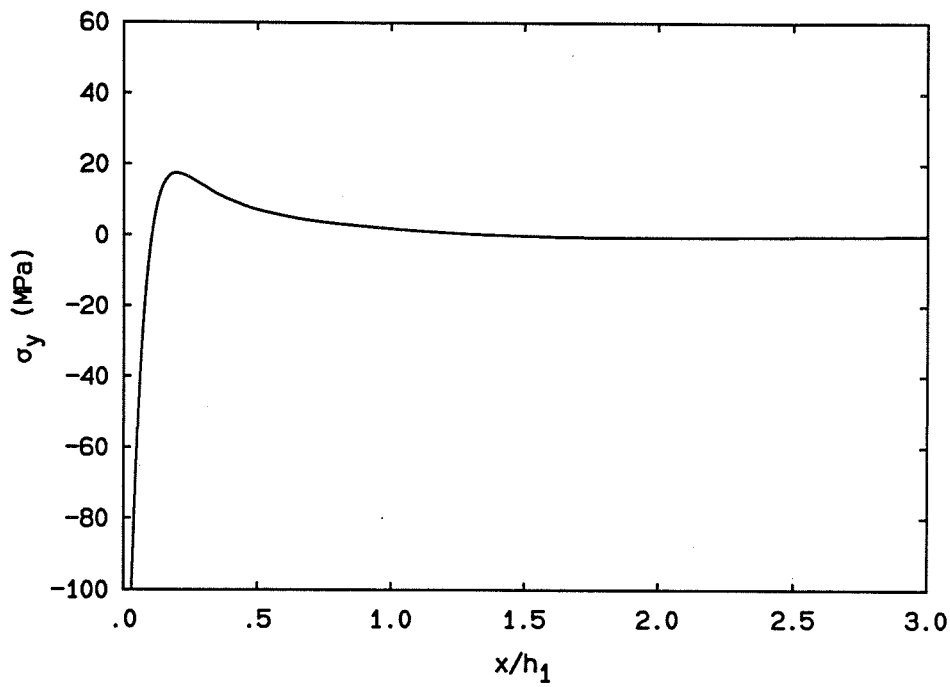

Figure 2.33: Interfacial normal stress σ_y for $|\triangle T| = 151^0C$ and for material B1S1c under step cooling ($h_2 = 0.80$ mm).

It remains to explain how the incompressibility condition of the polymer in the rubbery regime causes the large local strain and stress spikes in the polymer layer for quench cooling. The evolution of the interface stresses τ_{xy} and σ_y for $h_2 = 0.8$ mm, $t_R = 0.02$ sec and $|\triangle T| = 151^0C$ are given in Figures 2.34 and 2.35 for B1S1 and in Figures 2.37 and 2.38 for B1S1c. For the nonlinearly viscoelastic model employed here, the (total) strain dilatation governs the time shift for the viscoelastic functions; its evolution is, therefore, indicative of how the polymer properties would change during cooling. For that reason, the distribution of the strain dilatation $(\epsilon_x + \epsilon_y)$ along the interface is plotted for various times in Figures 2.36 and 2.39 for materials B1S1 and B1S1c, respectively. For short time, as the adherends bend apart due to the transient temperature variation across their thickness, they drag along with them the polymer which is still at the initially high temperature. Since the length of the adherends is 16 times longer than its thickness, the bending curvature is small so that only portions of the plate near the free edges curve while its remaining "interior" remains essentially straight. As a result, the polymer response varies along the length of sandwich (cf. Figures 2.36 and 2.39) since (a) the polymer properties depend on both the temperature change and the mechanically (stress) induced strain dilatation according to the free volume theory and (b) the normal strain ϵ_y (thus σ_y) is a function of the coordinate x. The interfacial normal stress σ_y is tensile near the free edges and is at its maximum (apart from the corner singularity) at a distance away (cf. Figures 2.35 and 2.38) even though the (normal) strain is highest near the free edge. This behavior arises because the high tensile strain near the free edges also induce fast stress relaxation there. Since all exposed surfaces of the sandwich are stress free, σ_y must be self equilibrated; σ_y becomes compressive and gradually tends to zero on the remaining length.

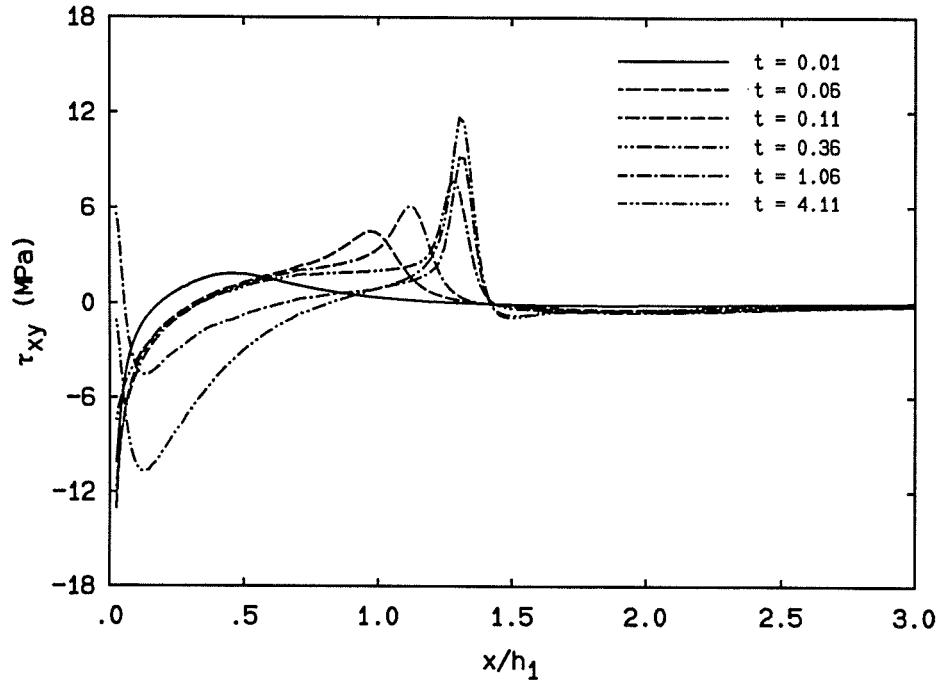

Figure 2.34: Evolution of interfacial shear stress τ_{xy} for B1S1 ("PVAc") and for $|\triangle T| = 151^0C$ ($h_2 = 0.80$ mm).

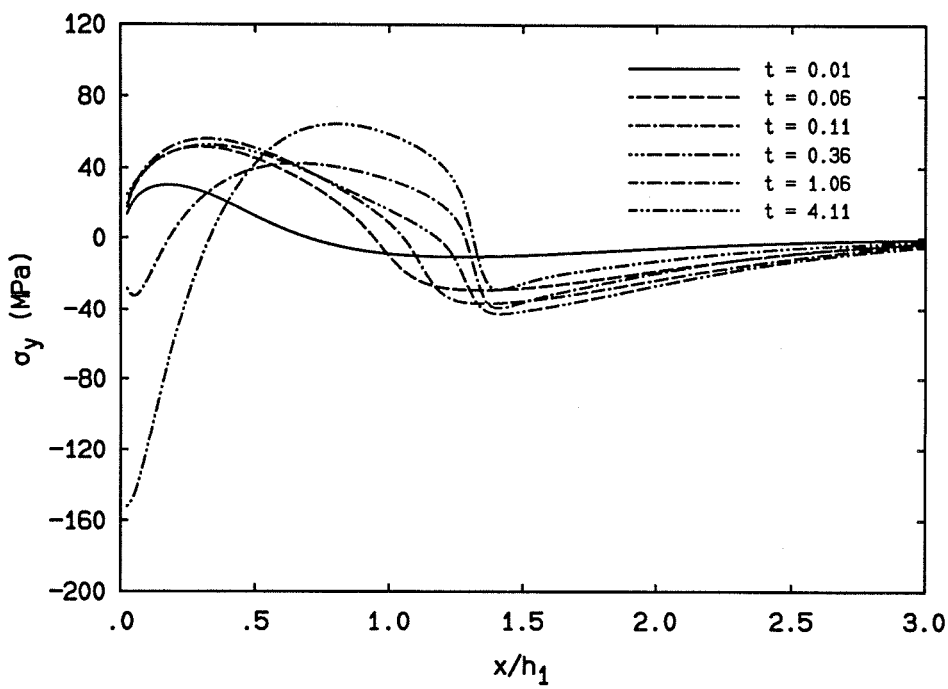

Figure 2.35: Evolution of interfacial normal stress σ_y for B1S1 ("PVAc") and for $|\triangle T| = 151^0C$ ($h_2 = 0.80$ mm).

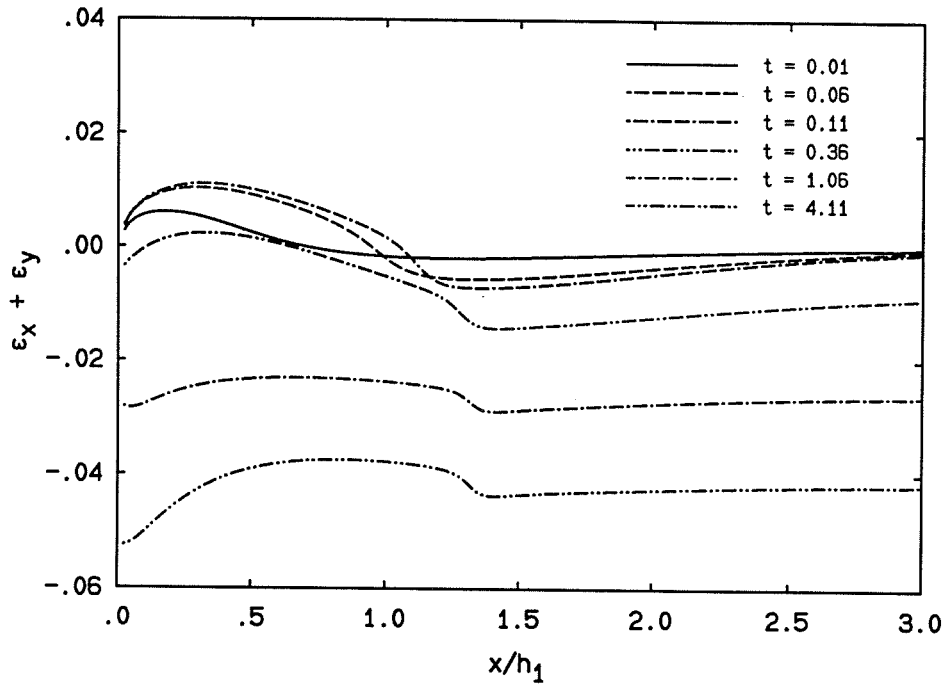

Figure 2.36: Evolution of strain dilatation plotted along the interface for B1S1 ("PVAc") and for $|\triangle T| = 151^0C$ ($h_2 = 0.80$ mm).

The interfacial shear stress τ_{xy} is the consequence of two effects. First, since the "Poisson response" of the adherend and the polymer are different, the (Poisson) contractions of these two components in the x direction under the interfacial normal stress σ_y are also different, so that the axial (x) displacement continuity across the interface is responsible, in part, for the interfacial shear stress. Secondly, since both the interfacial normal stress σ_y and the polymer properties vary along the length of the sandwich, the polymer is strained nonuniformly in the normal (y) direction, causing another source for the shear stress. It should be emphasized that the first effect is mainly due to the material mismatch between the polymer and the adherend while the second effect is attributed to the inhomogeneous normal stress σ_y and inhomogenous material response within the polymer layer. For short times τ_{xy} is negative near the free edge and becomes positive at a distance away; this behavior is primarily due to the Poisson response mismatch mentioned above: The polymer at the interface contracts more (in the x direction) than the metal counterpart under tensile (normal) stress σ_y

and expands further under the compressive stress. The inhomogenous normal stress σ_y and polymer properties cause an additional negative shear stress field which superposes on the previously described shear stress distribution; however, this (additional) stress contribution is small compared with the (previously discussed) Poisson ratio effect since the polymer is still at the initially high temperature during this stage of cooling so that it remains in the near-rubbery regime under applied stress σ_y.[19]

For long times, as the sandwich approaches thermal equilibrium, the adherends gradually return to their original straight position while the polymer experiences its own thermal change and becomes "frozen" (hard). Since the polymer is stiffer during the release of the initial strains reacting to the bending response, σ_y reverses to be compressive near the free edge. However, σ_y is still tensile over a "relatively" long length in order to satisfy the stress equilibrium, especially when the (reversely) compressive stress near the free edge is very large (cf. Figures 2.35 and 2.38). In contrast, τ_{xy} does not necessarily change to positive values near the free edge since the Poisson ratio mismatch between the two materials is not significant as the polymer enters the glassy state[20] (cf. Figures 2.34 and 2.37). Further since the thermal contraction of polymer is larger than that of the adherend, an additionally negative shear stress field is also generated near the free edge. In contrast, the thermal contraction mismatch within the polymer layer due to the inhomogeneous thermal properties (with a larger thermal expansion coefficient near the free edge) produces a (another) positive shear stress field. However, if the bending effect is highly localized as for B1S1c, the effect of the inhomogeneous thermal properties is likely to be "absorbed" by the singularity at the intersection of the free edge and the interface. On the other hand, when the bending response of the adherend affects a wide area, *e.g.*, over distance of several total thicknesses, as for B1S1, the effect of the inhomogeneous polymer properties is large and well separated from the "corner" singularity (cf. Figure 2.36), leading to the stress spike.

[19] Although the interior part of the polymer layer is under compressive stress σ_y, this stress is not high enough to push the material there towards the glassy regime.

[20] ν equals 0.37 for glassy PVAc and 0.33 for aluminum.

In summary, the incompressibility condition of the polymer in the rubbery regime affects the stresses in two ways: (a) it causes a larger Poisson ratio mismatch during the early bending of the adherends which leads to large shear strains in the polymer layer, especially at the interface near the free edge, and (b) it results in a large area affected by the bending response, thus separating the polymer layer into two regions with different material responses (cf. Figure 2.36) and leading to the stress spikes in τ_{xy}. It is thus apparent that the residual stresses are affected significantly by the cooling rate and the extent of the compressible, rubbery state of the polymer, in part, because of the bending response.

2.6 Conclusions

The residual thermal stresses in a simulated adhesive bond have been considered in the context of a nonlinear viscoelastic (free-volume) model for the thermoviscoelastic characteristic of a polymer. These stresses depend significantly on the surface cooling rates. In the case of the infinite sandwich, the residual (average) stress varies logarithmically with the cooling time t_R in a fashion similar to the variation of the relaxation modulus with time: Below a "critical cooling time," the residual stress is nearly constant while above it the residual stress drops with longer cooling times. Further, lowering the final temperature from 35^0C to 80^0C below T_g increases the residual stresses by 75 % for quench cooling and by 115 % for pronouncedly long cooling times.

The present study indicates that the thermoelastic analysis may not apply well to any range of temperatures depending on the relaxation times of the shear and bulk moduli relative to the diffusion time. It is particularly clear from these studies that the time dependent bulk response of the polymer has a significant influence on residual stresses and that, therefore, an accurate description of the time dependent bulk modulus is absolutely necessary for these types of problems.

Even though we are interested only in thermally induced residual stresses in adhesive bonds, the results from this study can apply, in a broad sense, to other manufacturing

processes such as the curing of fibrous composites and the cooling phase of polymer parts in injection molding and extrusion.

It needs to be stressed that the constitutive theory used here is strictly a small deformation model of nonlinearly viscoelastic behavior of polymers. Due to the initial bending of the adherend, a fast cooling may cause large strains in the polymer apart from the (corner) singularities. Since large strains will induce anisotropy due to the molecular orientation of the polymer which in turns affects the viscosity and time shift factor in addition to the nonlinear strain-displacement relation, future work should be based on a more advanced constitutive model where all of these effects are taken into account. Furthermore, only a linear cool-down from the initial temperature to the final temperature has been considered in the study. It has already been shown that the selection of an optimal cool-down path could reduce thermally induced residual stresses for epoxy resins [17]. Future work may, therefore, include a determination of such an optimal cooling history for a prescribed cooling time and a desired temperature range.

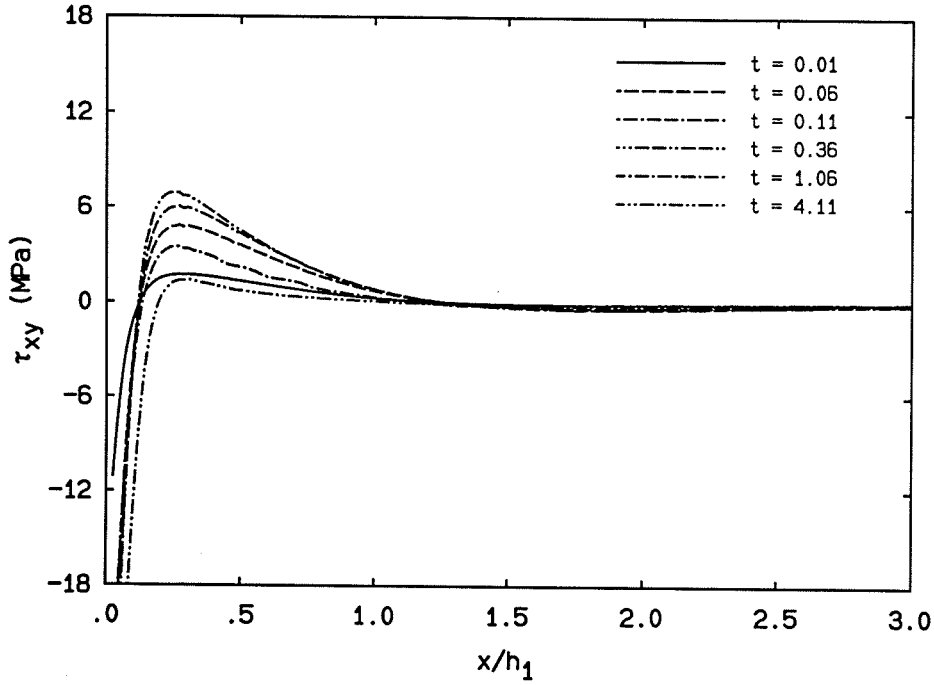

Figure 2.37: Evolution of interfacial shear stress τ_{xy} for B1S1c and for $|\triangle T| = 151^0C$ ($h_2 = 0.80$ mm).

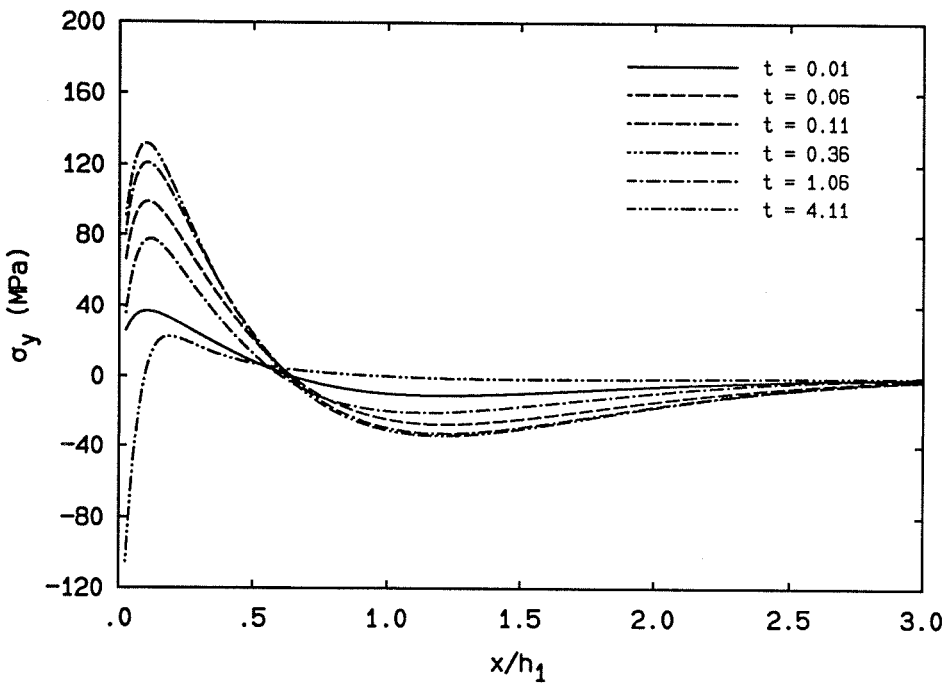

Figure 2.38: Evolution of interfacial normal stress σ_y for B1S1c and for $|\triangle T| = 151^0C$ ($h_2 = 0.80$ mm).

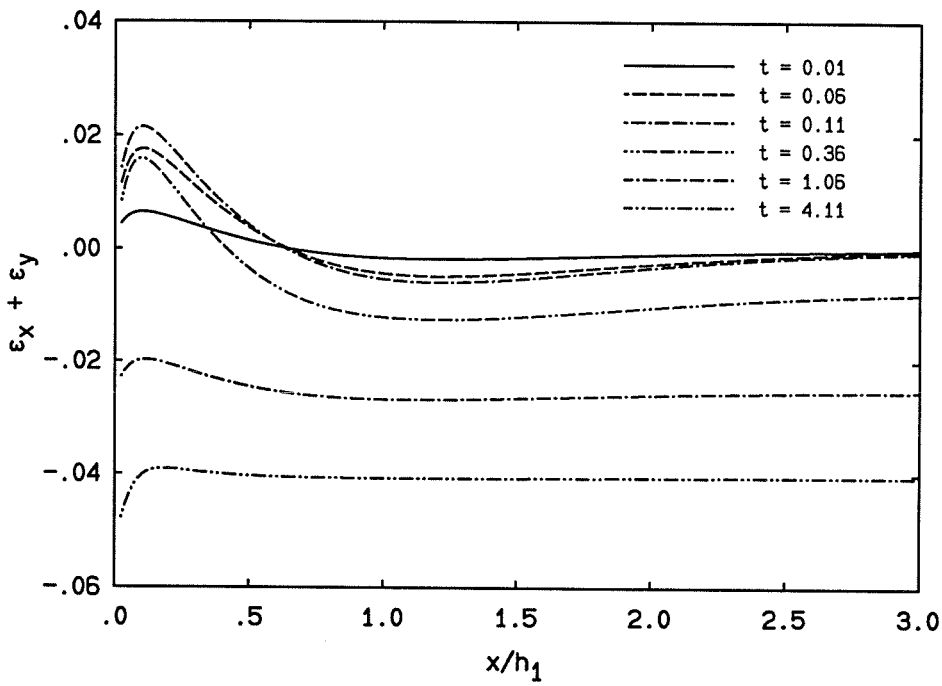

Figure 2.39: Evolution of strain dilatation plotted along the interface for B1S1c and for $|\triangle T| = 151^0C$ ($h_2 = 0.80$ mm).

Chapter 3

Fracture Analysis

3.1 Introduction

Adhesive bonds for structural purposes are typically formed through heating the adherends together with the interspersed adhesive layer under moderate pressure from a temperature above the glass transition of the polymer to the use temperature (substantially) below the latter. It is thus inevitable that, depending on the processing conditions, residual stresses are generated to varying degrees (see chapter 2). During use these residual stresses act in addition to those induced by the loading so that the final load carrying ability of the bonded joint may be materially impaired. In fact, it is believed that in many cases an apparent bond weakness observed in laboratory tests is primarily the result of residual stresses rather than an intrinsically weak chemical/mechanical interface connection.

Thus, understanding the failure/fracture behavior of adhesively bonded joints is important from two points of view. First, it is essential to be able to predict the onset and propagation of (interfacial) fracture for engineering design purposes. Second, in pursuing the understanding and evaluation of the physio-chemical aspects of bonding, it is mandatory that one be able to fully evaluate the relation between the past (formation) history of the bond and its strength, in terms of the surface chemistry or physics. Thus, an evaluation of the "bond strength" may attribute unfairly low strength to a particular interface chemistry, unless residual stresses are properly accounted for. Indeed, when the residual stresses induced during manufacturing are so high that the bond may fail under minimal or no loading at all, it would be inappropriate to assess the chemistry or surface physics as the culprit for the "apparent" residual "weakness."

Failure, and specifically fracture, of adhesive bonds is the result of the growth of one or several flaws, most often at or near an interface. In that situation it is advantageous to characterize the instability of crack propagation in terms of energy release rates, although the definite answer as to whether that characterization is the most efficient means from an engineering point of view is not yet clearly established: The uncertainty in this regard derives, in the general interface-near fracture process, primarily from unresolved issues concerning the nature of the stress field at the tip of an interface crack [38]. In case the crack advance is constrained to occur along the interface, which is the situation underlying the discussion in the sequel here, this issue is largely circumvented [38]. A major question remaining then concerns the role which the fracture topology, in interaction with friction or mode mixity play in the process of unstable crack advance [39]. In the following development we are, therefore, concerned only with the examination of the available energy for fracture and investigate the change in the residually stored energy with a small advance of the crack along an interface.

With this idea in mind we consider the effect of inhomogeneous stresses introduced during the thermal bond formation process. Because of the already large number of variables accounted for in this analysis we exclude the effect of pressure during the bond formation from consideration here, although this effect is within the scope of the analysis and material model employed here. We point out that the requisite material characterization, which involves thermal rate effects as well as other thermoviscoelastic responses of the adhesive polymer, is not generally practiced and thus an appropriate characterization is not available for even a limited number of materials. For this reason we draw on the computations of the residual stresses in a bonded joint, the adhesive for which has been modelled by a relatively simple polymer, Polyvinylacetate (PVAc), as outlined in chapter 2 delineating the stress analysis aspect of this problem. We expect that while the resulting values are not necessarily directly applicable to arbitrary commercial adhesives, the results are, nevertheless, indicative of the phenomena one needs to be concerned within this context.

Because adhesive bonds are typically used at temperatures considerably below the glass transition the fracture process occurs in what, in viscoelastic parlance, is called the "glassy state." As a consequence we assume that all stress changes related to fracture occur elastically, with the corresponding properties of the polymer being its glassy or short term ones. In addition, we follow linearly elastic fracture analysis concepts to determine then the energy release rate associated with crack advance along an interface, taking into account the special deformations of the adherend(s) that result from such an adhesion breakdown, namely crack closure away from the crack tip.

3.2 Problem statement

Consider a sandwich consisting of two aluminum plates ($E = 6.895 \times 10^{10}$ Pa, $\nu = 0.33$) joined by a polymer layer. The geometry is two-dimensional and considered to be in a state of plane strain, with the reference frame indicated in Figure 2.1 of chapter 2. The "length" of the sandwich is "l" ($l \to \infty$ for an infinite plate) and the adherend and polymer layer thicknesses are h_1 and h_2, respectively. In the bond formation process this polymer exhibits thermoviscoelastic properties that are sensitive to the rate of (thermal) strain and additionally to the rate of cooling through incorporation of free volume effects, which in turn are influenced by rate dependent and mechanically induced volume behavior. The details of this constitutive description have been discussed in chapter 1 and the (stress) results appropriate for the present problem are delineated in chapter 2. It suffices here to repeat from the Introduction that for the present fracture problem only the short term elastic (glassy) properties of the polymer ($E = 0.322 \times 10^{10}$ Pa, $\nu = 0.371$) enter the current considerations.

To examine the effect of residual stresses on the fracture of bonded joints, an "edge" crack is introduced into the polymer layer at or near the interface. The nature of the crack may be due to either a manufacturing flaw or to service loads. Because the sandwich is symmetric with respect to the midplane, only cracks located above the midplane (or plane of symmetry) need to be considered. The length of the crack is

semi-infinite in the infinite sandwich and has length "a" for the finite configuration. The two faces of the crack are assumed to be frictionless. It turns out that when the polymer is cracked parallel to the interface, the released surfaces tend to close but are then free to slide at the "free edge" while separating at the tip since the residual normal stress σ_y (cf. Figures 2.16 and 2.18 of chapter 2) is compressive near the free edge and tensile at some distance away. The solution algorithm for this "contact" (fracture) problem and the computation of the energy release rate are outlined in the next section.

3.3 Computing Algorithm

The iterative procedure for the solution of the contact (fracture) problem deserves special consideration. Also, the computation of the energy release rate warrants discussion. Both of these topics are addressed briefly in the sequel.

3.3.1 Iterative procedure for the contact problem

Since both the adherend and the polymer are considered to be linearly elastic for the present problem, the formulated problem can be analyzed within the context of linear fracture mechanics for dissimilar materials.

It is well known from previous work [40, 41, 42] that the linearly elastic asymptotic solution to the interface crack problem has various undesirable consequences for the predicted near tip field: crack faces can overlap and the stress components change sign alternately. Since our concern here is only with the (global) energy release rate without recourse to the detailed near tip stresses and displacement, this (near tip) contact zone is completely ignored in modelling the present problem. In addition, when tractions on the crack line are completely released, the crack surfaces interpenetrate over a small domain at the free edge; the residual normal stress σ_y (for the uncracked sandwich) is compressive there. It will be shown in section 3.4.2 that a significant error results if this interpenetration near the free edge is not modelled realistically as a region of crack closure. The crack surfaces are, therefore, modelled to be in contact but free to slide over the interpenetration domain near the free edge. Thus the basic difficulty for the

present problem consists of the determination of the stress and displacement fields which satisfy (a) the stress free condition on the open part of the crack and (b) the vanishing condition of the "relative" normal (y) displacement of the crack surfaces (which are free of shear stress) on the contact domain. It should be emphasized that the (boundary) conditions (a) and (b) prescribed on the crack surfaces depend on the displacements of these surfaces according to whether the surfaces are pressed together or separate in the (stress) unloading process. The present problem is, therefore, "geometrically" nonlinear and is solved by an iterative procedure. The discussion of this iterative procedure necessitates introducing an alternately crack surface loading problem; the connection between this alternate problem and the (original) residually stress crack problem is given immediately below.

Assuming that, for the immediate discussion, the solution of the present problem is already determined, *e.g.*, both the contact domain and the open portion of the crack are known, as shown schematically in Figure 3.1, the stresses of a residual stress crack problem (case A) can be obtained by superposition of the originally residual stresses (case B without a crack) and those of a crack surface loading problem (case C). The principle of superposition holds here because the adherend and the polymer both act in a linearly elastic manner for this consideration. The crack faces of case C are subjected to a shear traction over the whole crack length and a normal traction over the open portion of the crack, both of which are equal in magnitude but opposite in sign to those given for B over the appropriate length on the crack line. In addition, the "relative" normal displacements of the released surfaces in the contact area (or along the crack closure) are imposed to be zero. This superposition (a) leads to an iterative procedure in solving for the solution of case A as detailed in the next paragraph, and (b) asserts the equivalence between case A and case C for the energy release rate since the strain energy of case B is independent of the crack length and its $\frac{\partial U}{\partial a}$ is zero.

We outline next the iterative procedure. The open portion of the crack is first assumed. The stress solutions of the crack surface loading problem is obtained and is

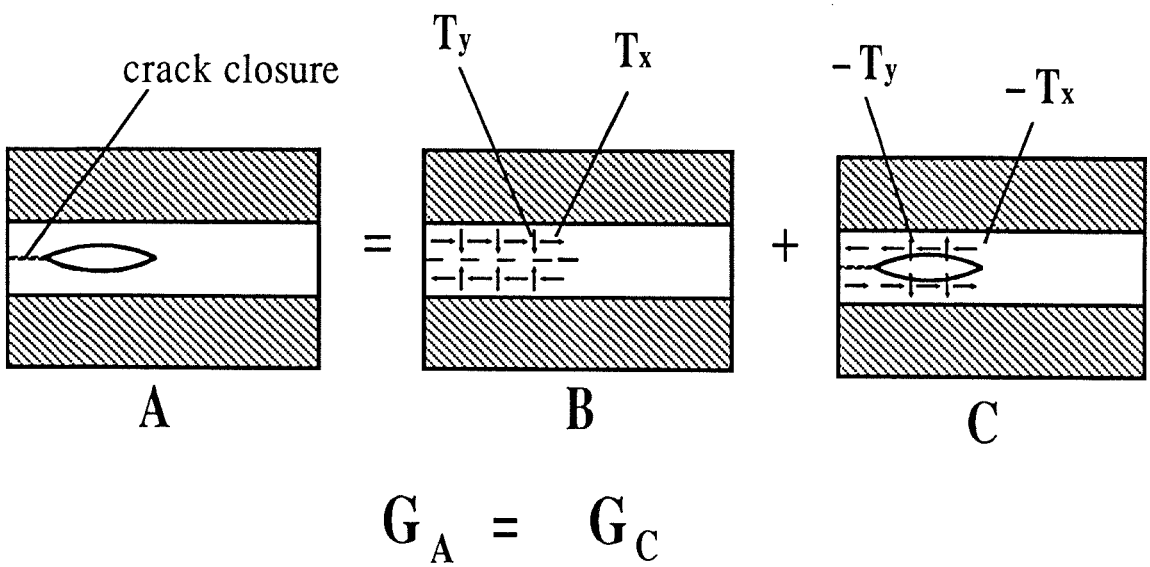

Figure 3.1: Schematic representation of superposition method for thermal stress crack problems.

then added to the corresponding original residual stresses. The superimposed iterated solutions must satisfy two conditions. First, the released crack faces must separate along an "open" portion; second, the superimposed normal traction (σ_y) must be compressive everywhere in the contact zone. If one of these two conditions is violated, another guess will be used, and the whole procedure is repeated until both conditions are satisfied.

3.3.2 Computation of the energy release rate

It was pointed out in the previous section that the energy release rate in a residual stress crack problem is identical to that in a crack surface loading problem. It suffices here to show the computation of the energy release rate in a crack surface loading problem. The computation of the energy release rate for a semi-infinite crack in an infinite sandwich can be accomplished in a closed form approximation via a bi-material cantilever plate model. The corresponding derivation is given in appendix E.

On the other hand, the energy release rate in a finite dimensioned sandwich is determined by way of the finite element method with the crack tip path (or area)

independent integral. Based on the mechanical energy balance and the local steady state condition at the crack tip, the energy release from a homogeneous body per unit crack advance (per unit thickness) is defined as, [43]

$$\mathcal{G} = \lim_{\Gamma \to 0} \int_{\Gamma} [W\delta_{ij} - \sigma_{ij} u_{i,1}]\, n_j d\Gamma, \tag{3.1}$$

where W is the stress work density. Γ is a small contour which is fixed in size and orientation with respect to the crack tip and translates with the crack tip. $\mathcal{G}$ must be independent of the shape of Γ as Γ is shrunk to zero. Moran and Shih [43] have shown that for a traction free crack in an homogenous elastic solid, $\mathcal{G}$ will be independent of Γ for all Γ without the condition $\Gamma \to 0$. In that case, $\mathcal{G}$ is equivalent to the well known path-independent J integral. They also established the following result for $\mathcal{G}$ for a surface loaded crack,

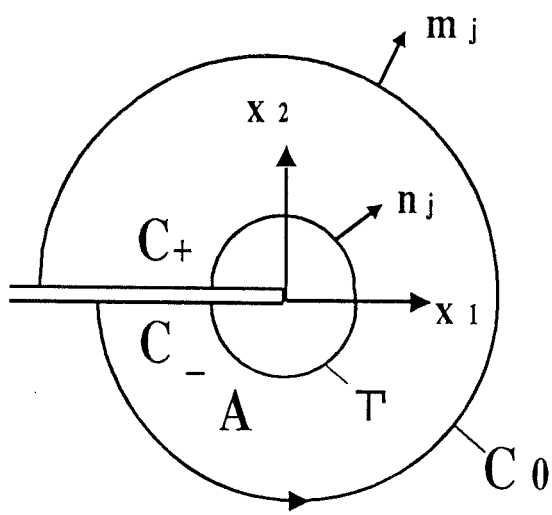

Figure 3.2: Conventions at crack tip. Domain A is enclosed by Γ, C_+, C_-, and C_0.

$$\mathcal{G} = \int_A \{\, [W\delta_{ij} - \sigma_{ij} u_{i,1}] q_{1,j} \;+\; [W_{,1} - (\sigma_{ij} u_{i,1})_{,j}] q_1 \,\} dA - \int_{C_+ + C_-} \sigma_{i2} u_{i,1} m_2 q_1 dC, \tag{3.2}$$

where q_1 is a weight function which has a value of unity at the tip and zero on the outer contour C_0 (c.f. Figure 3.2); m_2 is the unit outward normal vector; "A" is the area

enclosed by C_0, and C_+, C_- are paths along the crack faces. Even though all of the above results are restricted to cracks in a homogeneous, elastic solid, they are also valid for cracks parallel to the interface in a sandwich plate because the plate is homogeneous in the crack direction [45].

All energy release rates presented in this chapter (for a finite sandwich) are the average values of those evaluated via equation (3.2) for ten different outer contours C_0 with stresses and displacement from finite element analysis. Particular care must be exercised in the computation of $\mathcal{G}$ for a long crack. The stress gradient close to the corner of the interface and the free edge is very steep due to the singularity there (chapter 2). For cracks longer than $\frac{a}{h_1} > 3$, crack closure occurs over a smaller portion of the crack at the free edge and the effect of the end singularity grows stronger. Unless the mesh is very refined at the corner to enable capturing the steep crack surface loads, the difference in $\mathcal{G}$ from the inner and outer paths can be as much as 40% . In all of the calculations, the mesh is chosen so that the maximum difference in $\mathcal{G}$ for different paths enclosing the crack tip is 8%.

3.4 Results and discussion

In this section the computation of the energy release rates are detailed. We also illustrate several important results for assessing the durability of bonded joints such as the potentially failure (fracture) location in the adhesive polymer, the critical crack length for maximum energy release rate in finite bonded plates, and the effect of the cooling rates on the energy release rate. In the sequel, the energy release rates for an infinite sandwich is first delineated, followed by the results for the finite configuration.

3.4.1 Infinite configuration

We consider a semi-infinite crack in a sandwich, infinite in the x- and z- directions. As mentioned in section 3.3, the energy release rate for an infinite crack is determined via a cantilever plate model. The energy release rates for cracks in the polymer layer, at various locations from the midplane (plane of symmetry) are given in Figure 3.3

for different polymer thicknesses and for step cooling (t_R = 0.02 sec). These results indicate that for a fixed geometry and cooling history, the energy release rate is always maximum at the interface. The effect of the cooling rates on the energy release rate for an interfacial crack is shown in Figure 3.4. Similar to the residual stress, the (maximum) energy release rate is nearly constant below the critical cooling time and drops rapidly for any cooling time longer than the critical value. This behavior follows from the fact

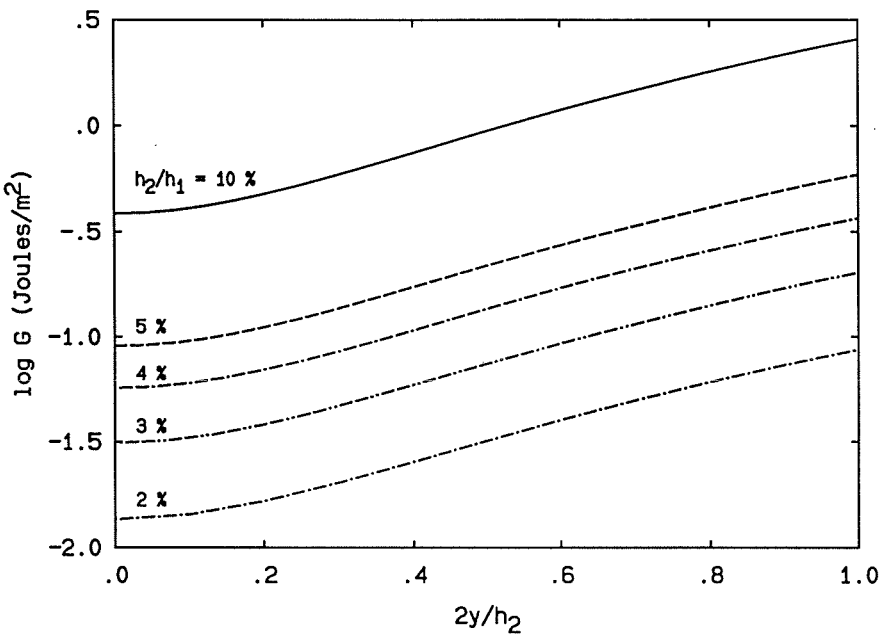

Figure 3.3: Energy release rate for a semi-infinite crack at various position from the midplane with residual stresses obtained for step cooling (t_R = 0.02 sec).

that (a) the energy release rate is proportional to the square of the residual stresses, (b) σ_x is the only nonvanishing stress component in the infinite plate and (c) the polymer layer is very thin so that the thickness-variation of σ_x from the average value $\bar{\sigma}_x$ is small and therefore has a small influence on the energy release rate. Also from Figure 3.4, it is clear that the energy release rate increases significantly with the polymer thickness even though the influence of polymer thickness on the residual stress is only minor (cf. the inset in Figure 2.6). That statement is accentuated further by the inset figure which illustrates a cross plot of the primary plot and applies to t_R = 0.02 sec (note that in

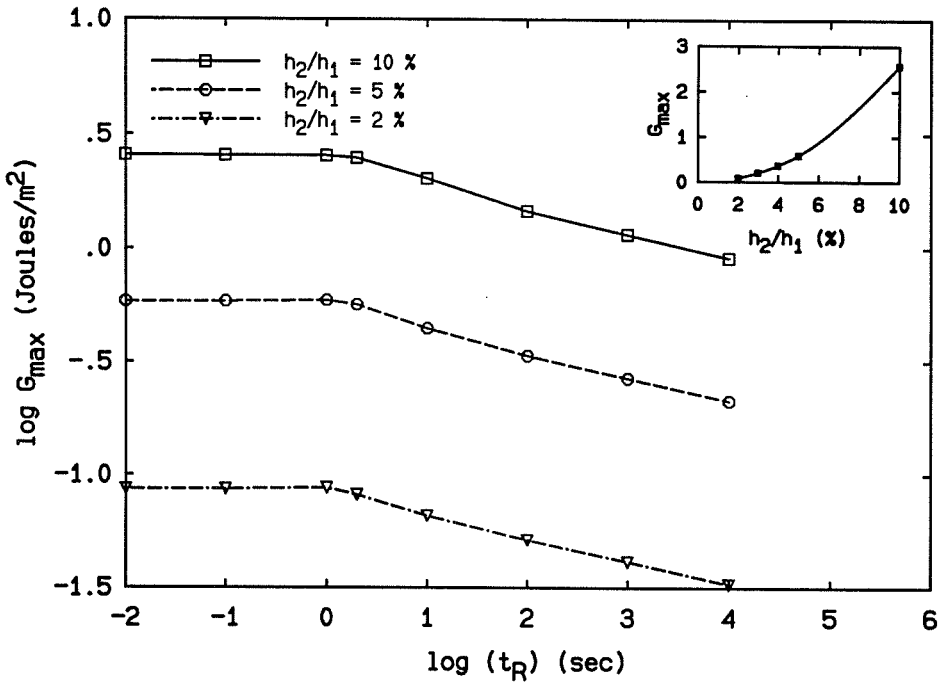

Figure 3.4: Energy release rate for a semi-infinite crack at the interface with residual stresses obtained for different cooling times.

the inset figure, the energy release rate, not the logarithm of the energy release rate, is plotted on the ordinate). The energy release rate is roughly proportional to the square of $\left(\frac{h_2}{h_1}\right)$.

We next explain the occurrence of the maximum energy release rate at the interface in terms of the cantilever plate model. The energy available for crack extension in each plate is proportional to the square of the applied bending moment.[1] Let M^* be the resultant moment due to residual stresses in each plate when the crack is at the midplane position. From Figure 3.5a, it is clear that with P defined in that figure and representing the net force acting on a cut across the sandwich

$$M^* = \frac{P}{4}(2h_1 + h_2).$$

For an interface crack, the two forces acting on the lower plate at (b) and (c) result in a couple M^* as indicated in the figure. The moment of the force P acting at (a) about

[1]The contribution from axial deformation (stretch) is small in comparison to that from bending and is neglected in the present discussion.

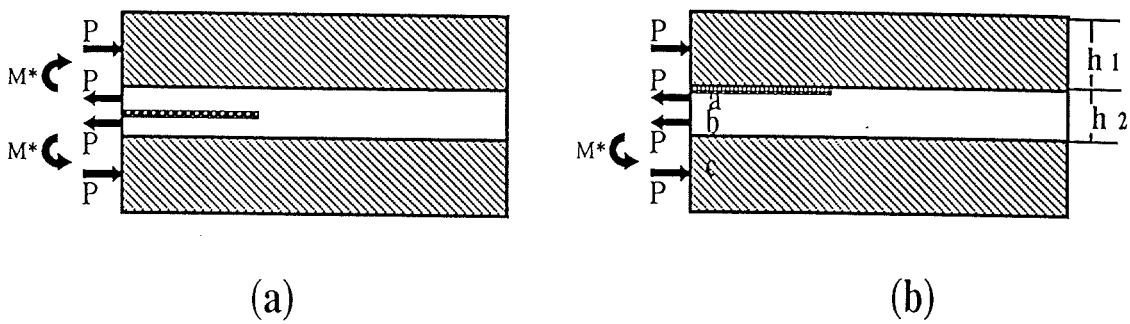

Figure 3.5: Geometry of a cracked sandwich. (a) Crack at the midplane position. (b) Crack at the interface.

the neutral axis of the lower plate also equals M^* since

$$M \text{ (due to force at (a))} = P(\frac{3}{4}h_2 + h_1 - y_0) \tag{3.3}$$

and from appendix E (equation (E.10))

$$y_0 = \frac{\frac{E_2'h_2^2}{2} + \frac{E_1'h_1^2}{2} + E_1'h_1h_2}{E_2'h_2 + E_1'h_1}$$

so that equation (3.3) becomes

$$\begin{aligned} M \text{ (due to force at (a))} &= \frac{P}{4}.\frac{E_2'h_2^2 + 3E_1'h_1h_2 + 2E_1'h_1^2}{E_2'h_2 + E_1'h_1} \\ &= \frac{P}{4}(2h_1 + h_2) = M^*. \end{aligned}$$

Therefore, as the crack location moves from the midplane position to the interface, the bending moment will vary from M^* to $2M^*$ for the lower beam and from M^* to 0 for the upper beam. As a result, the energy release rate of the sandwich will vary from $2M^{*^2}$ to $4M^{*^2}$[2].

[2]Our numerical calculations show that $\mathcal{G}$ varies between 0.1 and 0.59 $Joules/m^2$ as the crack location

3.4.2 A finite case

As illustrated in the previous section, the failure of an adhesive bond is more likely at the interface because (a) the energy release rate is maximum there and (b) the toughness is likely to be lowest there. Thus for demonstration purposes, we consider only the case of an interfacial crack for a finite sandwich ($l = 16h_1$). The energy release rate for an interfacial crack is given in Figure 3.6 as a function of crack length for different cooling times t_R and for a polymer thickness of 0.32 mm. Similar results but for a polymer thickness of 0.8 mm is given in Figure 3.7 (Note the difference in scale on the ordinate in the two figures). The last point on the curves of Figures 3.6 and 3.7 corresponds to the case $\frac{a}{l} = 0.5$. For low cooling rates, the value of $\mathcal{G}$ at $\frac{a}{l} = 0.5$ approaches the results for the semi-infinite crack. On the other hand, for supercritical cooling, it is higher since the energy contribution from the work done by the tractions acting on the crack faces cannot be ignored as in the analysis for the semi-infinite crack. The (maximum) energy release rate is a monotonically decreasing function of the cooling time (cf. Figure 3.8) and occurs at different (critical) crack lengths (cf. Figures 3.6 and 3.7). It is interesting to note that for each cooling rate, there is critical crack length for the maximum energy release rate. The tip of this critical crack length does not coincide with the location where the interfacial normal stress σ_y reaches its maximum. It should be emphasized that since the interface stresses τ_{xy} and σ_y are significantly different for the supercritical (quench) cooling and for the subcritical (slow) cooling (cf. Figures 2.15 -2.18), the maximum energy release rate is reduced by a factor of 300 as one passes from quench cooling to (pronouncedly) slow cooling, but this factor is still about a hundred times greater than that for the infinite plate. Finally, we remark that if the interpenetration near the free edge is allowed to happen, the energy release rates based on that unrealistic (crack) model are far below the corresponding values reported here. For $\frac{a}{h_1} = 1.025$, $h_2 = 0.8$ mm, and for step cooling, the energy release rate equals 72 $Joules/m^2$ if crack closure is taken into account and 0.7 $Joules/m^2$ if interpenetration

location changes from the midplane position to the interface, for $h_2 = 0.80$ mm and for quench cooling ($t_R = 0.02$ sec).

were not considered; the results are different by a factor of about a hundred. Modelling the present problem must, therefore, include crack closure.

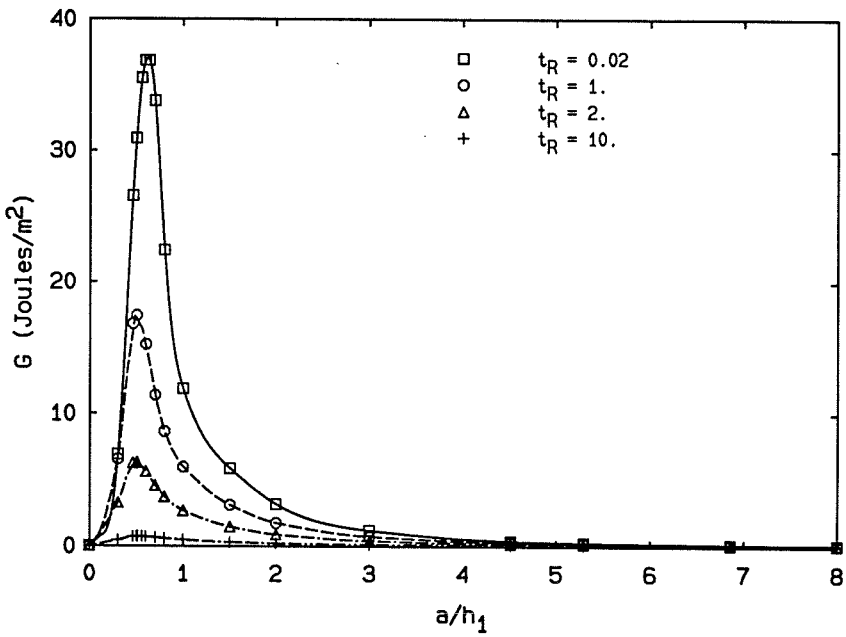

Figure 3.6: Energy release rate for an interfacial crack in the finite sandwich for different cooling times ($h_2 = 0.32$ mm).

3.5 Generalization

Because the foregoing numerical analyses are for specific geometries and material properties, it is of interest to be concerned with the implication of this study for bond systems of greater generality. In this regard, we examine the influences of the (viscoelastic) polymer properties and the temperature ranges on the energy release rate. In addition bonded plates used for structural purposes carry loads during their service life. It is, therefore, appropriate to examine also the combined effect of residual stresses and external loads on joint failure. We consider these aspects here in the sequel.

3.5.1 Influence of the polymer properties and temperature range

Different ranges of the cooldown temperature and different (viscoelastic) polymer properties result in alternate residual stresses. It is, therefore, appropriate to examine how

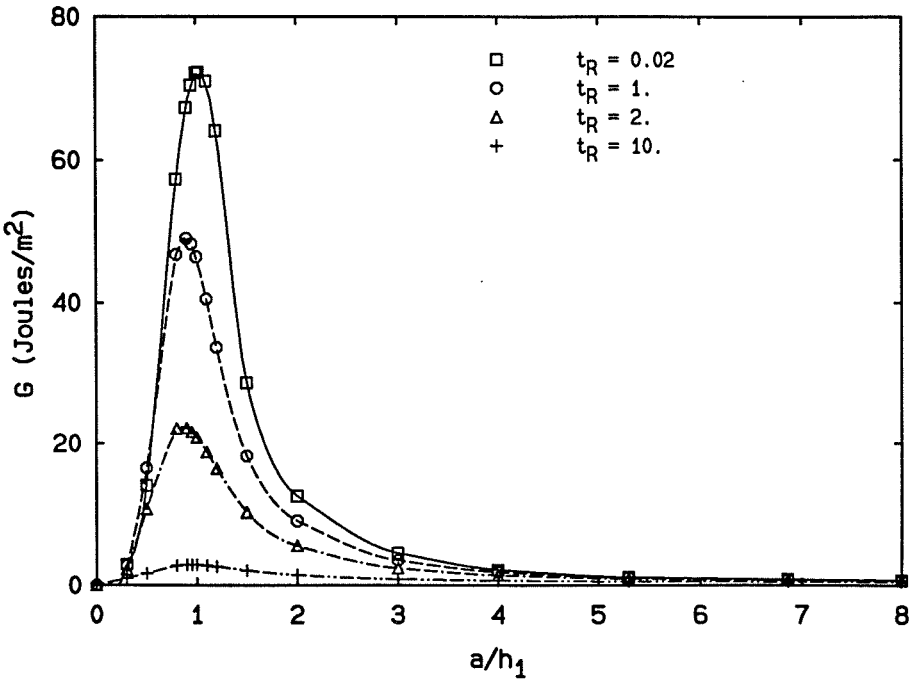

Figure 3.7: Energy release rate for an interfacial crack in the finite sandwich for different cooling times ($h_2 = 0.80$ mm).

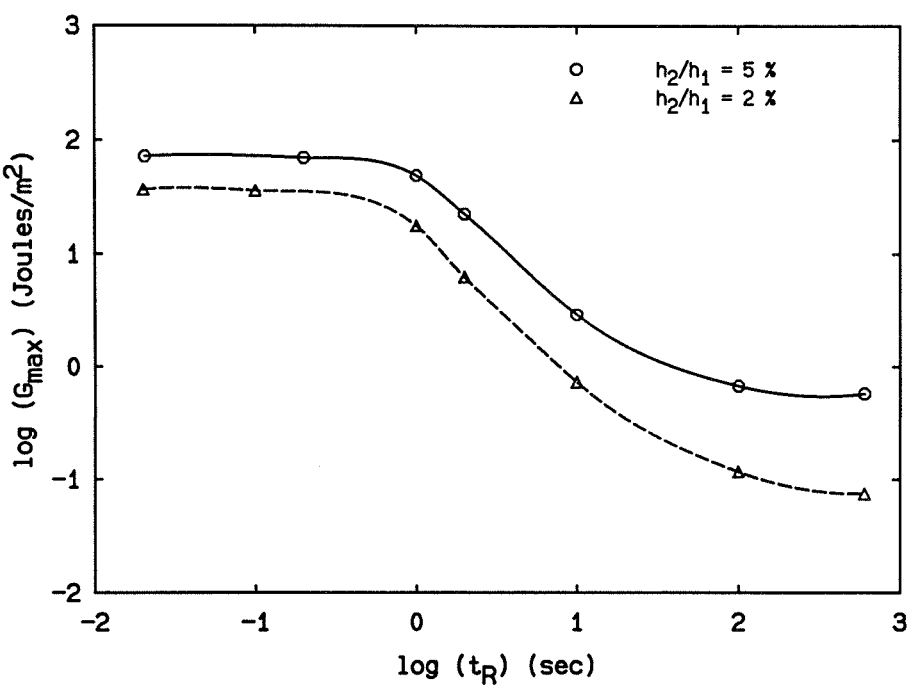

Figure 3.8: Maximum energy release rate for an interfacial crack in the finite sandwich for different cooling times.

these changes in stresses affect the bond durability or load carrying ability of the structure through the energy release deficit. It was illustrated in section 3.4.1 that the energy release rate for the infinite plate domain is roughly proportional to the square of the (thickness-averaged) stress $\bar{\sigma}_x$ so that its value for other temperature ranges (or polymer properties) can be scaled from the previously computed values recorded in Figure 3.4 by the ratio $\frac{\bar{\sigma}_{x_1}}{\bar{\sigma}_{x_2}}$ where $\bar{\sigma}_{x_1}$ and $\bar{\sigma}_{x_2}$ are the average stresses corresponding to the two temperature ranges (or to the two polymers) considered. We show, therefore, only the effect of different temperature ranges on the energy release rate for an infinite bonded joint ($h_1 = 1.6$ cm, $h_2 = 0.32$ mm) which is depicted in Figure 3.9. The inset in Figure 3.9 illustrates a cross plot of the primary plot at $t_R = 0.02$ sec to allow for some potential extrapolation to additional temperatures below T_g.

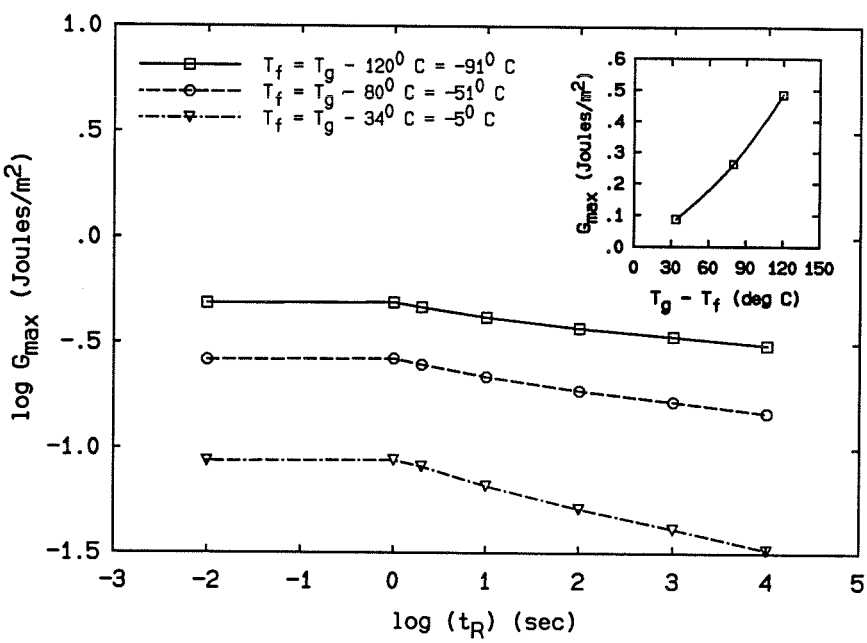

Figure 3.9: Maximum energy release rate for an infinite sandwich cooled through different temperature ranges ($h_2 = 0.32$ mm).

The residual stress state is more complicated for a finite sandwich; for this situation the energy release rate is not necessarily scaled by the square of the maxima of the interface stresses σ_y or τ_{xy}. For this reason, the energy release rates have been computed

for different (viscoelastic) polymer properties and for different temperature ranges, and the results are presented in Figures 3.10 - 3.12. It was pointed out in chapter 2 that residual stresses in a finite sandwich are affected significantly by the cooling rates and by the extent of the incompressible, rubbery state of the polymer which is governed by the longest shear relaxation time and by the long term shear modulus (G_∞). The energy release rate is, therefore, also affected significantly by these (processing) parameters. It is evident from Figures 3.10 - 3.12 that the (maximum) energy release rate follows a behavior that is similar to that of the maxima of the interfacial normal stresses σ_y (cf. Figures 2.27, 2.29, and 2.31). Moreover, it is apparent that the maximum energy release rate is roughly proportional to the square of $(T_f - T_i)$ only for $T_g - T_f > 80^0C$. An estimate of the maximum energy release rate for additional T_f by multiplying the (maximum) results recorded in Figures 3.6 and 3.7 by the square of the ratio of the temperature ranges yields a nonconservative value with an error larger than 20 %.

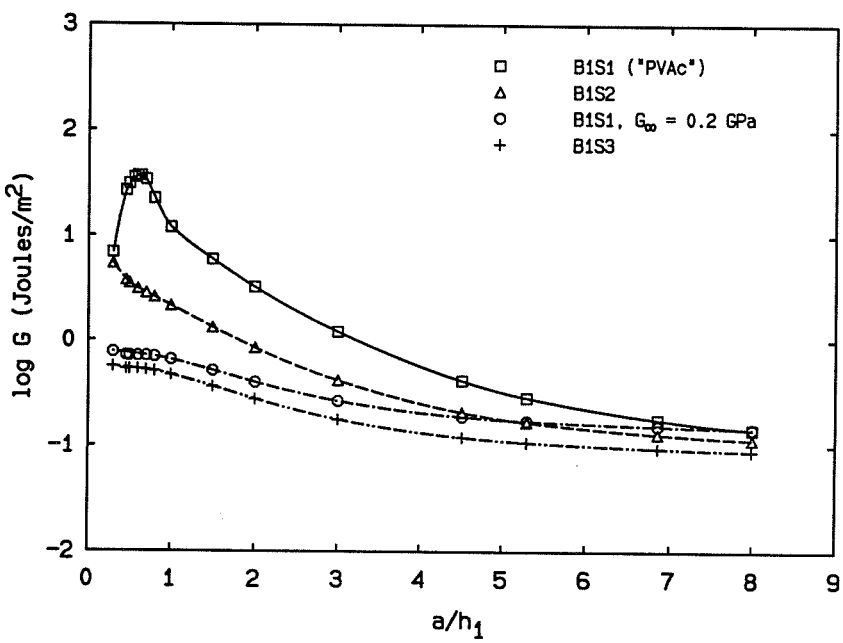

Figure 3.10: Energy release rate for an interfacial crack in the finite sandwich under step cooling and for different (viscoelastic) polymer properties ($h_2 = 0.32$ mm).

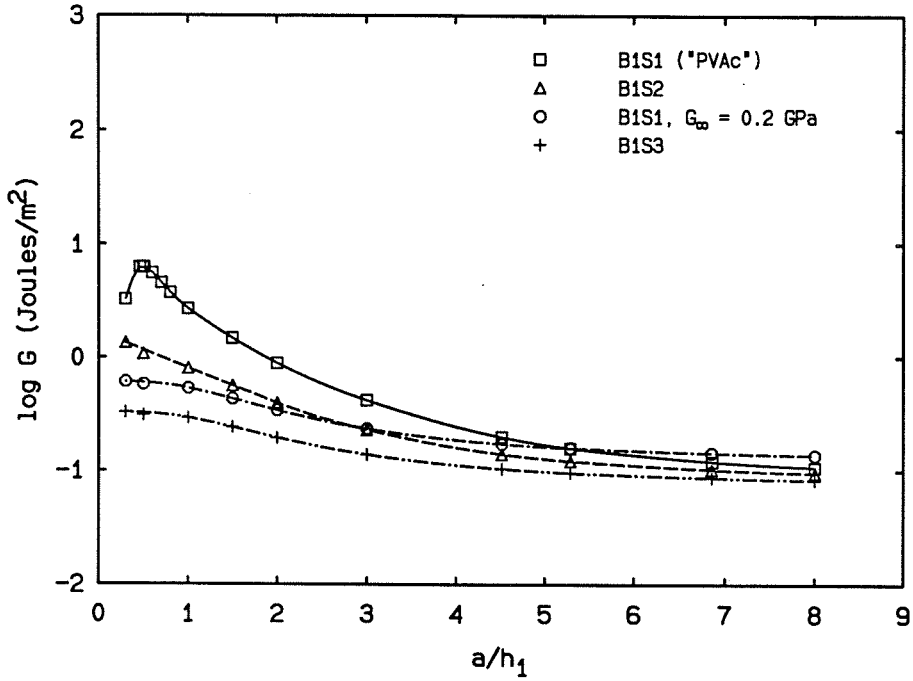

Figure 3.11: Energy release rate for an interfacial crack in the finite sandwich cooled at $t_R = 2$ sec and for different (viscoelastic) polymer properties ($h_2 = 0.32$ mm).

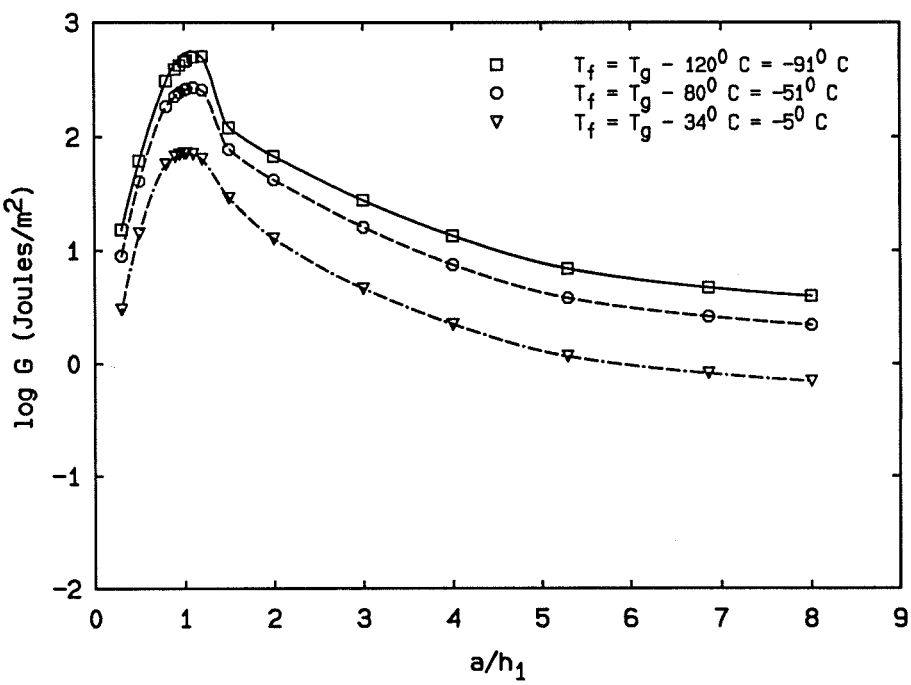

Figure 3.12: Energy release rate for an interfacial crack in the finite sandwich under step cooling and for different temperature ranges ($h_2 = 0.8$ mm).

3.5.2 Maximum energy release rates and fracture toughness

The maximum energy release rates obtained in this study are small compared to the $\mathcal{G}_{\text{crit}}$ for dry PVAc which is on the order of 4-10 $\frac{kJ}{m^2}$ [46]. However, experiments have shown that a transition region exists between the adherend and the bulk adhesive in which the physical and chemical properties of the polymer differ from the bulk material. Since $\mathcal{G}_{\text{crit}}$ of the transition material is expected to be much lower than that for the bulk material depending on the interfacial chemistry treatment, one should not underestimate the deleterious effect of residual stresses on fracture of bonded joints based only on this numerical study for PVAc. In fact, it was pointed out in the chapter 2 that if one estimates joint failure based on ultimate stress criteria, the contribution of the residual stresses is significant. With the uncertainty about the fracture toughness of the interface in mind, one wants to keep the maximum energy release rate for a given sandwich configuration as low as possible. Since the energy release rate is a decreasing function of the cooling time which processing parameter is desired to be short, the optimal cooling time for low energy release rate would still be around 600 to 10^3 sec as found earlier in chapter 2 for residual stresses.

3.5.3 Residually stressed sandwich under external loading

The energy release rate associated with the residual stresses have been calculated for a wide range of processing conditions. The range of the energy release rates varies from 0.02 to 500 $Joules/m^2$. Because these values are small compared to the fracture toughness for PVAc as discussed in the previous section, the residually stressed sandwich may carry (additionally) loads before failure can be anticipated. Of concern is thus the combined effect of residual stresses and external loads on the energy release rate. A basic difficulty of presentation in this regard is that additional stresses arising from external loads increase the energy release rate in a non-additive fashion since (a) the energy release rate is proportional to the square of combined stresses and (b) the present fracture problem is geometrically nonlinear. We consider, therefore, for demonstration

purposes, only one particular loading configuration, being well aware that a totally encompassing study transcends the scope and extent of this presentation.

In this portion of the study, we consider a residually stressed (finite) sandwich ($h_1 =$ 1.6 cm, $h_2 = 0.80$ mm) carrying some external loads. To avoid unnecessarily repeated calculations for the "total stresses" in the case of proportional loading, the (additional) stresses corresponding to the external loads are calculated from the linearly elastic analysis with the assumption that the whole sandwich is stress free before additional loads are applied to it. These stresses are then superposed on the original, residual stresses. A crack is then introduced into the polymer layer at the interface, and fracture analyses similar to that given in previous sections are carried out for a sandwich carrying "total" (residual plus mechanical) stresses.

All calculations in this section have been executed for a specific residual stress state and for a specific loading configuration (but the magnitudes of the forces for that loading configuration are allowed to vary by multiplying them by the same factor). In these calculations, the residual stresses correspond to the case of quench cooling ($t_R = 0.02$ sec) from an initial temperature of 60^0C (31^0C above T_g) to a final temperature of -91^0C (120^0C below T_g) (cf. Figures 2.30 and 2.31). These residual stresses, as shown in the previous sections, yield the highest energy release rate for all bond systems considered in this study.

The loading configuration imposed on the sandwich is based on the typical loading on a lap joint: the upper and lower metal plates are subjected to forces P as shown schematically in Figure 3.13. [3] The interface stresses σ_y and τ_{xy} for the sandwich under loads shown in Figure 3.13 and in the absence of residual stresses are presented in Figures 3.14 and 3.15 for $P = 0.1$ MPa-m (or $\sigma_f = P/h_1 = 6.25$ MPa). The interfacial shear stress τ_{xy} is approximately symmetric about the centerline ($x = l/2$) as expected

[3] In lap joints, two metal sheets of length $(c + l)$ are bonded together by a thin polymer layer over the length l (cf. Figure 3.13); for stress analysis purpose, the unjointed ends of the sheets are normally assumed to be simply supported and acted upon by tensile forces. However, these tensile forces at the unjointed ends result in tensile forces as well as the bending moments and transverse shears at the edges of the joint. Our assumed loading configuration is thus simpler than the realistic one for lap joints.

since the length of the sandwich is long (compared to the total thickness) so that the "end" effects disappear for $3 \leq x/h_1 \leq l/h_1 - 3$. In fact on that domain, τ_{xy} reaches a constant value while $\sigma_y = 0$. The small amount of asymmetry in τ_{xy} is due to the bending of the sandwich under the unsymmetric (moment) loading.

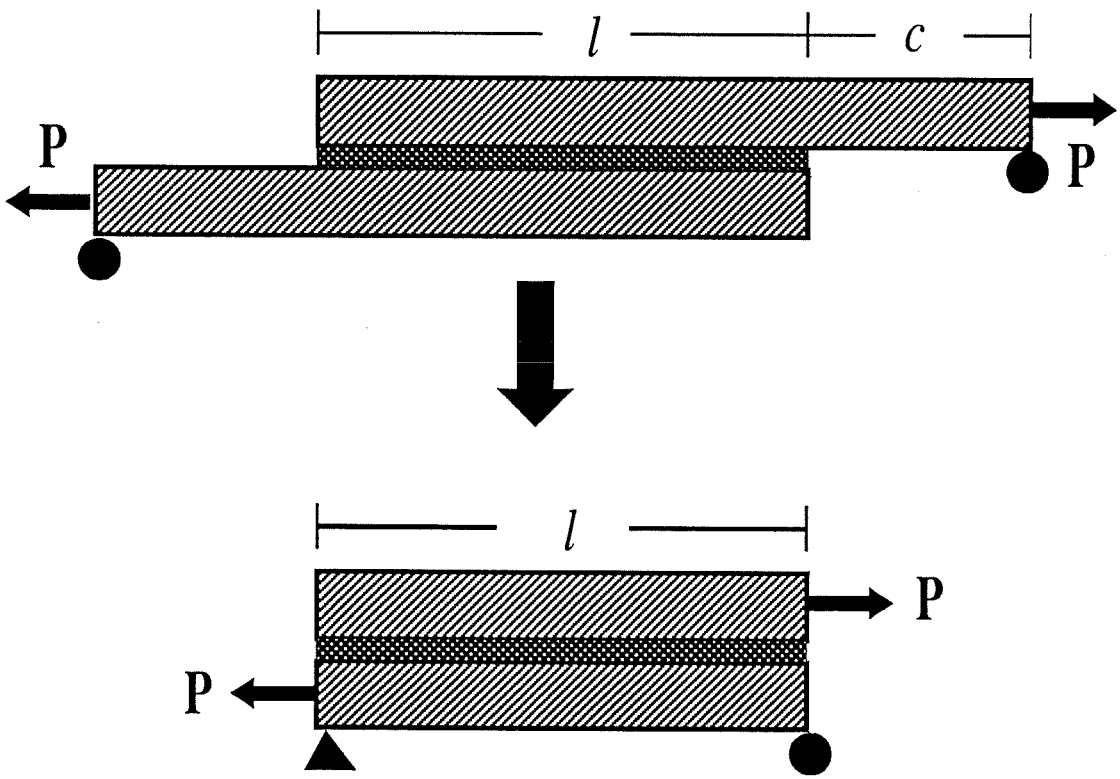

Figure 3.13: Loads acting on a sandwich. The upper figure shows the typical loading in a lap joint.

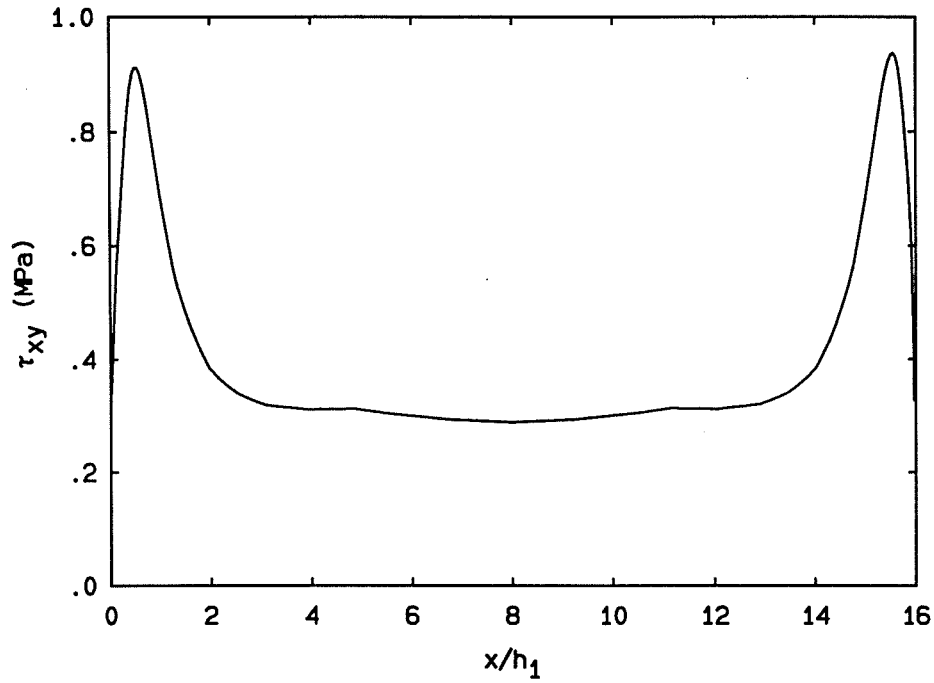

Figure 3.14: Interfacial shear stress τ_{xy} at $y = h_2/2$ for a sandwich under the loading shown in Figure 3.13 and in the absence of residual stresses.

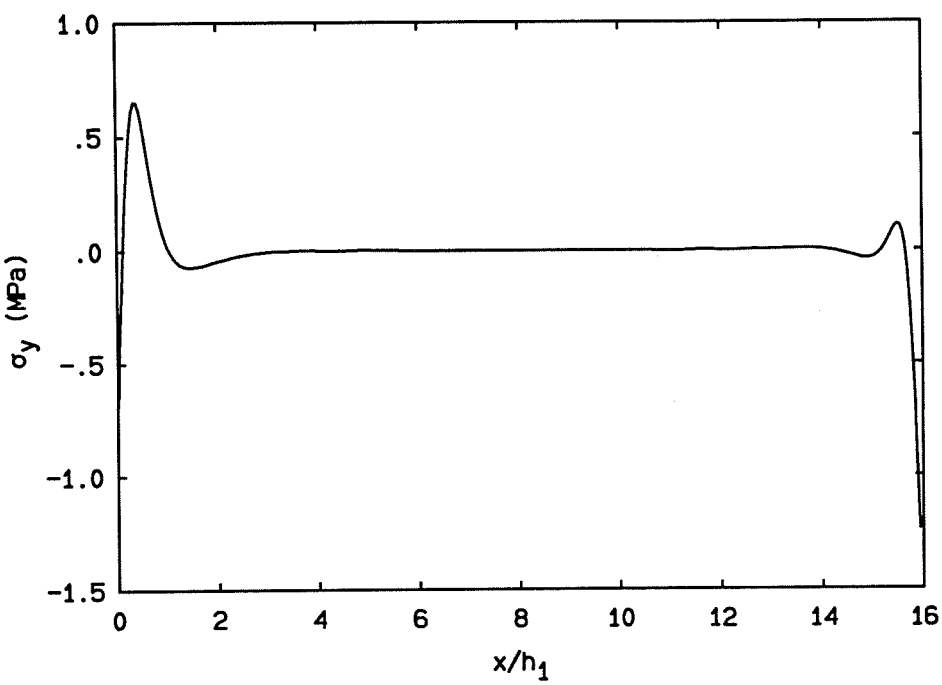

Figure 3.15: Interfacial normal stress σ_y at $y = h_2/2$ for a sandwich under the loading shown in Figure 3.13 and in the absence of residual stresses.

To exhibit the "combined" effect of residual stresses and load P on the total energy release rate, the (maximum) total energy release rate is plotted as a function of the dimensionless parameter $\frac{\sigma_f}{\sigma_R}$ in Figure 3.16, where $\sigma_f = P/h_1$, σ_R is the thickness-averaged residual stress $\bar{\sigma}_{x_1}$ in the adherend, at the centerline ($x = l/2$), and equals 1.8 MPa. We also include there the energy release rate for a sandwich under the same (external) loads but without residual stresses. [4] Although the residual stresses are zero in this case, for presentation purpose, we still normalize σ_f by 1.8 MPa. From Figure 3.16, the contribution of the residual stresses to the total energy release rate is smaller as the magnitude of P increases as expected. However, it is interesting to note that the total energy release rate is not necessarily higher than the sum of the individual contribution from external loads and from residual stresses separately.

3.6 Conclusions

The energy release rates resulting from thermally induced residual stresses in an adhesive bond have been considered. The bond is more prone to failure at the interface. The energy release rate is a decreasing function of the cooling times. For each cooling rate, there is a critical crack length in a finite sandwich for the maximum energy release rate. The front of this critical crack length does not coincide with the location where the (residually) interfacial normal stress σ_y reaches its maximum. Although the residual stresses in the polymer are high in comparison to the ultimate strength of the bulk material, the energy release rates are small since the polymer layer is very thin. From a fracture point of view, the contribution of the residual stress to bond failure becomes significant if the fracture toughness of the interface material is much lower than that of the bulk polymer.

Although the combined effect of residual stresses and external loads on the energy release rate has been addressed in the study, this aspect has been examined within

[4] For the purely mechanical loading case, no crack closure is observed for all crack lengths. The energy release rate is, therefore, proportional to the square of P. Moreover, the energy release rate increases monotonically with crack length for $\frac{a}{l} < \frac{1}{2}$ since the interfacial shear stress is constant (different from zero) at distance away from the free edges.

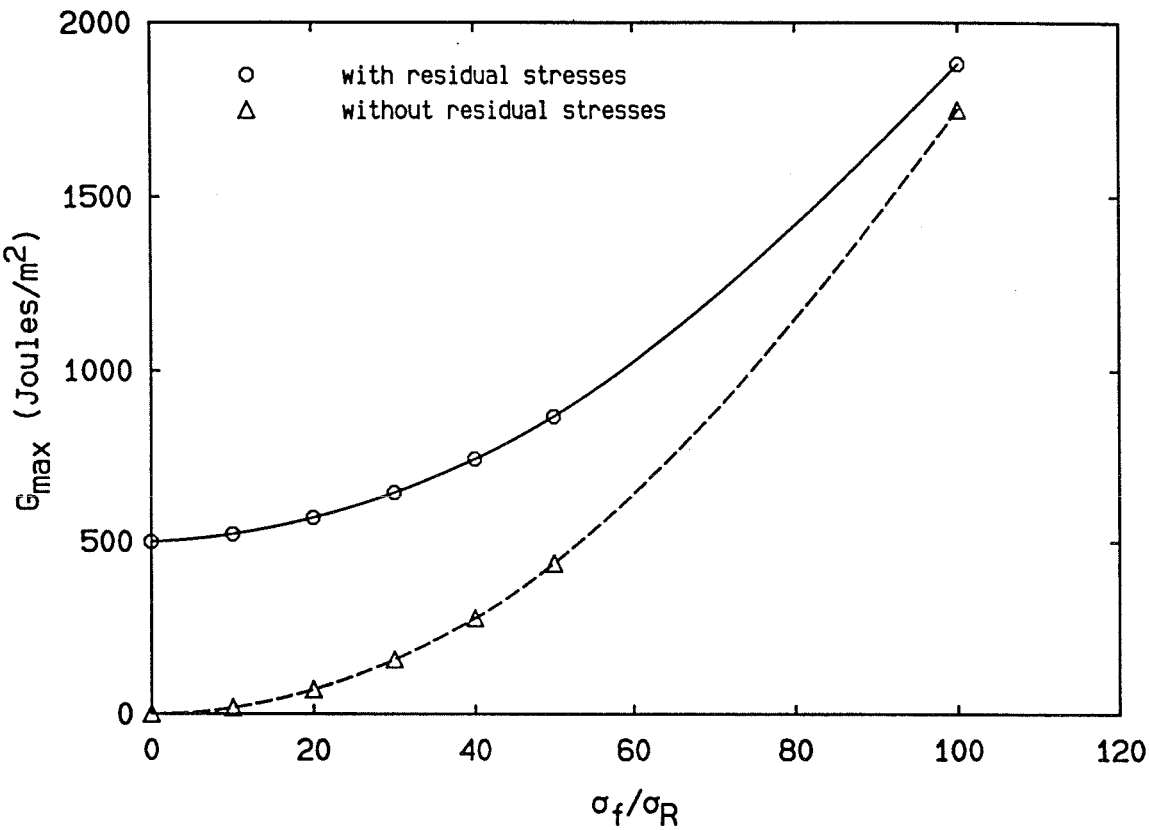

Figure 3.16: Maximum energy release rate for a residually stressed sandwich carrying loads shown in Figure 3.13. $\sigma_f = P/h_1$; $\sigma_R = \bar{\sigma}_{x_1}$. For Δ , $\sigma_R = 1.8$ MPa.

a simple context: The crack is assumed to propagate along the interface. In reality, the residual stresses as well as the external loads determine the subsequent path for the crack propagation [47, 48]. Furthermore, the present model for crack closure assumes the contact surfaces to be frictionless. Again this assumption may not be totally realistic. Future work should, therefore, be based on a more advanced crack model for which the friction of the contact surfaces and the dependence of crack propagation path on the external loads and residual stresses would be taken into account.

Appendix A: Material properties for PVAc and aluminum

The properties of PVAc are obtained from data given in [10, 18]. They are repeated here for reference.

$$
\begin{aligned}
f_0 &= 0.0095 \\
f_i \text{ (at T=60 deg)} &= 0.01414 \\
\beta_{f_0} &= 0.63 \\
A &= 2.0 \times 10^{-6} \\
B &= 0.1 \\
f_{crit} &= 0.0065 \\
\rho C_p &= 2.09 \times 10^6 \frac{J}{m^3 K} = \rho C_{p_l} \text{ for } f > f_{crit} \\
&= 1.29 \times 10^6 \frac{J}{m^3 K} = \rho C_{p_g} \text{ for } f < f_{crit} \\
k &= 0.19 \frac{Watt}{mK} \\
\alpha_{l_v} &= 6.0 \times 10^{-4} \frac{cm^3}{cm^3} deg\ C
\end{aligned}
$$

The material properties of the aluminum plate are

$$
\begin{aligned}
\alpha &= 0.236 \times 10^{-4} \frac{cm}{cm} deg\ C \\
k &= 237.1 \frac{Watt}{mK} \\
\rho C_p &= 2.417 \times 10^6 \frac{J}{m^3 K} \\
K &= 67.60 \text{ GPa} \\
G &= 25.90 \text{ GPa}
\end{aligned}
$$

Appendix B: Finite element modelling the thermoviscoelastic boundary value problem

The advent of the finite element method has opened new ways to compute transient and residual stresses in viscoelastic solids. This numerical method can be easily applied to complicated (arbitrary) geometries; for example, Crochet and Denayer [30] used the finite element method to study transient and residual stresses in glass bottles from the annealing process. An efficient computing algorithm for the thermoviscoelastic problem was also derived by Taylor et al. [35]. The nonlinear constitutive model described in chapter 1 was implemented into the finite element program FEAP, as used by Losi and Knauss in their investigation of residual stresses in a homogenous sphere and in an infinite cylinder cooling across the glass transition [18]. For these simple geometries, their analyses did not encounter any numerical instability. However, as we found in this study, there are some meshes for the present adhesive bonding problem which result in a spurious (spatial) oscillation in the stress field; this instability is attributed to the "incompressibility locking." A special finite element formulation, therefore, has been used in the present study. We, therefore, devote this appendix to the study of the incompressibility locking in viscoelastic solids, especially to the elimination of this numerical instability.

In this appendix, the finite element modelling of the governing field equations are detailed. The variational statements of the field equations, including the special form of the principle of virtual work, are first delineated. This development is followed by the descriptions of the strain-displacement and stress-displacement relations. The (finite element) equilibrium equations are then derived, and finally the effect of the different orders of numerical integration on the solution of the thermoviscoelastic problem is discussed.

Finite Element Implementation

The governing equations for the present thermoviscoelastic boundary value problem are (see section 2.2 of this chapter):

$$\kappa \bigtriangledown^2 T = \rho C_p \frac{dT}{dt} \tag{B.1}$$

$$\sigma_{ij,j} = 0 \tag{B.2}$$

$$\epsilon_{ij} = \frac{1}{2}(u_{i,j} + u_{j,i}) \tag{B.3}$$

$$\sigma_{ij} = \mathcal{F}(\epsilon_{ij}, T). \tag{B.4}$$

In the finite element method, we deal with the weak or variational forms of equations (B.1) and (B.2). These forms can be obtained as follows. We take the inner product of equation (B.1) with the weight function $\hat{T}$ and that of equation (B.2) with $\hat{u}_i$, and rearrange the resulting expressions to give

$$\sigma_{ij,j}\hat{u}_i = (\sigma_{ij}\hat{u}_i)_{,j} - \sigma_{ij}\hat{u}_{i,j} = 0$$

$$\kappa T_{,ii}\hat{T} = \kappa(T_{,i}\hat{T})_{,i} - \kappa T_{,i}\hat{T}_{,i} = \rho C_p \hat{T}\frac{\partial T}{\partial t}.$$

Integrating the above expressions over the volume V and applying the divergence theorem to the terms in the parentheses yields

$$\int_{\partial V} S_i \hat{u}_i ds + \int_V \sigma_{ij}\hat{\epsilon}_{ij} dV = 0 \tag{B.5}$$

$$\int_V \rho C_p \hat{T}\frac{\partial T}{\partial t} dV + \int_V \kappa T_{,i}\hat{T}_{,i} dV + \int_{\partial V} \kappa q \hat{T} ds = 0, \tag{B.6}$$

where S_i is the traction on the boundary ∂V and q is the (normal) derivative of the temperature field.

If we choose the weighting function $\hat{u}_i$ to be any compatible, small and virtual (or fictitious) displacement increment, *e.g.*, $\hat{u}_i = \delta u_i$, equation (B.5) is equivalent to the principle of virtual work in solid mechanics, and it can be applied to any material at any instant t. The finite element equations corresponding to equation (B.6) will not be presented here as detailed descriptions are available in many textbooks. We limit

our discussion to the implementation of equation (B.5) as applied to the nonlinearly viscoelastic materials. In matrix notation, the principle of virtual work is written as

$$\int_{\partial V} < \delta u > \{S\} dS + \int_{V} < \delta \epsilon > \{\sigma\} dV = 0, \tag{B.7}$$

where {} denotes a column vector and <> a row vector.

The constitutive relation for the polymer is described in detail in chapter 1. The pertinent mathematical description of this constitutive model are listed below for ready reference.

$$\begin{aligned} \sigma_{ij}(t) &= \int_{-\infty}^{t} 2G(\xi(t)-\xi(\tau))\frac{\partial \epsilon'_{ij}(\tau)}{\partial \tau} d\tau + \delta_{ij} \int_{-\infty}^{t} K(\xi(t)-\xi(\tau))\frac{\partial \epsilon_{kk}}{\partial \tau} d\tau \\ &\quad - \delta_{ij}\, \hat{K}_{\infty} \alpha_{l_V}\, \triangle T(t), \end{aligned} \tag{B.8}$$

where

$$\xi(t) = \int_0^t \frac{d\tau}{a_T} \tag{B.9}$$

$$\log a_T = B\left(\frac{1}{f} - \frac{1}{f_0}\right) \tag{B.10}$$

$$f(t) = f_i + \int_0^t \delta(f(\tau)) d\epsilon_{kk}(\tau) \tag{B.11}$$

$$\delta(f) = \frac{\beta_{f_0}\phi(f)}{1+\beta_{f_0}\phi(f)} \tag{B.12}$$

$$\phi(f) = \frac{1}{1-\frac{A}{2}[1-\frac{B}{f}]\exp(\frac{B}{f}-\frac{B}{f_0})} \tag{B.13}$$

$$K(t) = K_{\infty} + \sum_{i}^{M} K_i \exp^{-\frac{t}{\tau_i^K}} \tag{B.14}$$

$$G(t) = G_{\infty} + \sum_{i}^{N} G_i \exp^{-\frac{t}{\tau_i^G}} \tag{B.15}$$

$$\hat{K}_{\infty} = K_{\infty} \frac{1+\beta_{f_0}}{1+\beta_{f_0}\phi(f)} \tag{B.16}$$

$$\beta_{f_0} = \frac{\triangle V_{free}}{\triangle V_{occ}} = \frac{\alpha_l}{\alpha_g} - 1 - \sum_i \frac{K_i}{K_{\infty}}. \tag{B.17}$$

An alternate form of equation B.7, which is appropriate for the incompressible, viscoelastic solids, is given in the next section.

An alternate form of the principle virtual work

We used 4-node quadrilateral isoparametric finite elements. Because the long term bulk modulus is several orders of magnitude larger than the long term shear modulus in many polymers, the polymer is nearly incompressible in the rubbery regime. Isoparametric finite elements are known to behave poorly in incompressible elastic materials due to an inadequate representation of the volumetric strain energy (overestimation of this energy in bending modes). Since a similar "locking" is expected for the nearly incompressible viscoelastic materials, as in [25] the term $\sigma_{ij}\delta\epsilon_{ij}$ is split into the deviatoric and volumetric components with the (volume) integral of the latter component being "underintegrated."

$$\sigma_{ij}\ \delta\epsilon_{ij} = \underbrace{s_{ij}\ \delta e_{ij}}_{\text{deviatoric contribution}} + \underbrace{\frac{1}{3}\sigma_{kk}\ \delta\epsilon_{ii}}_{\text{volumetric contribution}} \tag{B.18}$$

where s_{ij} and e_{ij} are deviatoric stress and strain tensors, respectively.

Beside the time (history) independent term $p(t)$, the constitutive relation given in equation (B.8) can be rewritten in the following form,

$$\frac{1}{3}\sigma_{kk}(t) = K * \dot{\epsilon}_{kk} \tag{B.19}$$

$$s_{ij}(t) = 2G * \dot{e}_{ij}, \tag{B.20}$$

where $(*)$ denotes time convolution. Equations (B.19) - (B.20) are written in matrix notation suitable for finite element implementation and for plane (2-D) problem as

$$\{\bar{\sigma}(t)\} = [D]_K * \{\dot{\epsilon}\} \tag{B.21}$$

$$\{s(t)\} = [D]_G * \{\dot{\epsilon}\}. \tag{B.22}$$

In the above equations, $\{\bar{\sigma}\}$, $\{s\}$, $[D]_K$, $[D]_G$ and $\{\dot{\epsilon}\}$ are defined by

$$[D]_K = 3[R_1]K(t) \tag{B.23}$$

$$[D]_G = 2[R_2]G(t) \tag{B.24}$$

$$\{s\} = \begin{Bmatrix} s_1 \\ s_2 \\ s_3 \\ s_4 \end{Bmatrix} = \begin{Bmatrix} s_x \\ s_y \\ s_z \\ s_{xy} \end{Bmatrix} \quad ; \{\bar{\sigma}\} = \begin{Bmatrix} \sigma_x + \sigma_y + \sigma_z \\ \sigma_x + \sigma_y + \sigma_z \\ \sigma_x + \sigma_y + \sigma_z \\ 0 \end{Bmatrix} \quad ; \{\dot{\epsilon}\} = \begin{Bmatrix} \dot{\epsilon}_x \\ \dot{\epsilon}_y \\ \dot{\epsilon}_z \\ \dot{\epsilon}_{xy} \end{Bmatrix}, \tag{B.25}$$

where

$$[R_1] = \begin{bmatrix} 1 & 1 & 1 & 0 \\ 1 & 1 & 1 & 0 \\ 1 & 1 & 1 & 0 \\ 0 & 0 & 0 & 0 \end{bmatrix} \; ; \; [R_2] = \begin{bmatrix} \frac{2}{3} & -\frac{1}{3} & -\frac{1}{3} & 0 \\ -\frac{1}{3} & \frac{2}{3} & -\frac{1}{3} & 0 \\ -\frac{1}{3} & -\frac{1}{3} & \frac{2}{3} & 0 \\ 0 & 0 & 0 & 1 \end{bmatrix}.$$

By definition, e_{ij} and ϵ_{kk} are given by

$$\{e\} = [R_2]\{\epsilon\} \; ; \; \{\bar{\epsilon}\} = [R_1]\{\epsilon\}, \tag{B.26}$$

where

$$\{e\} = \begin{Bmatrix} e_x \\ e_y \\ e_z \\ e_{xy} \end{Bmatrix} \quad ; \quad \{\bar{\epsilon}\} = \begin{Bmatrix} \epsilon_x + \epsilon_y + \epsilon_z \\ \epsilon_x + \epsilon_y + \epsilon_z \\ \epsilon_x + \epsilon_y + \epsilon_z \\ 0 \end{Bmatrix}.$$

Using equations (B.21), (B.22), and (B.26), the deviatoric and volumetric components of the virtual strain energy density become

$$< \delta e > \{s\} = \{\delta\epsilon\}^T [R_2]^T [D]_G * \{\dot{\epsilon}\} \tag{B.27}$$

$$\frac{1}{3}\sigma_{kk}\delta\epsilon_{kk} = \frac{1}{3}\{\delta\epsilon\}^T [R_1]^T [D]_K * \{\dot{\epsilon}\}. \tag{B.28}$$

However, because

$$[R_2]^T [D]_G = [D]_G$$

$$[R_1]^T [D]_K = 3[D]_K$$

it follows that (B.27) and (B.28) can be rewritten as

$$< \delta e > \{s\} = \{\delta\epsilon\}^T [D]_G * \{\dot{\epsilon}\} \tag{B.29}$$

$$\frac{1}{3}\sigma_{kk}\delta\epsilon_{kk} = \{\delta\epsilon\}^T [D]_K * \{\dot{\epsilon}\}. \tag{B.30}$$

By substituting (B.29), (B.30) and (B.18) into equation (B.7), the desired (alternate) form of the principle of virtual work is

$$\int_V < \delta\epsilon > \{s\} dV + \int_V < \delta\epsilon > \{\bar{\sigma}\} dV + \int_{\partial V} < \delta u > \{S\} dV = 0, \tag{B.31}$$

where $\{s\}$ and $\{\bar{\sigma}\}$ are again given by (cf. equations B.21 and B.22):

$$\begin{aligned} \{s\} &= [D]_G * \{\dot{\epsilon}\} \\ \{\bar{\sigma}\} &= [D]_K * \{\dot{\epsilon}\}. \end{aligned}$$

Strain-displacement relation

In the context of finite element formulations, the strain-displacement relations are given by

$$\{\epsilon\} = [B]\{U\} \tag{B.32}$$

or

$$\epsilon_i = B_{ij} U_j, \tag{B.33}$$

where $\{U\}$ is the vector of nodal displacements.

Stress-displacement relation

We now express $\{\bar{\sigma}(t)\}$ and $\{s(t)\}$ at a material point as the hereditary integrals of the nodal displacement vector $\{U(t)\}$. Substituting equation (B.33) into (B.21) and (B.22) for the strains and using the Prony-Dirichlet series representation for $K(t)$ and $G(t)$ (as in equations B.14 and B.15) yields

$$\bar{\sigma}_i(t) = B_{jl} \sum_{p=0}^{M} D^{(p)}_{ij_K} \int_{-\infty}^{t} \exp[-\frac{(\xi(t) - \xi(\tau))}{\tau_p''}] \frac{\partial U_l}{\partial \tau} d\tau \tag{B.34}$$

$$s_i(t) = B_{jl} \sum_{p=0}^{N} D^{(p)}_{ij_G} \int_{-\infty}^{t} \exp[-\frac{(\xi(t) - \xi(\tau))}{\tau_p'}] \frac{\partial U_l}{\partial \tau} d\tau, \tag{B.35}$$

where

$$[D^{(p)}]_K = 3[R_1]K_p \tag{B.36}$$

$$[D^{(p)}]_G = 2[R_2]G_p. \tag{B.37}$$

K_p, τ_p'' and G_p, τ_p' are the components of the Prony series and the relaxation times for the bulk and shear behaviors, respectively. τ_0'' and τ_0' are chosen to be infinitely large to represent the possible asymptotic behavior.

Because the evaluations of the heredity integrals for $\bar{\sigma}_i(t)$ and $s_i(t)$ are conceptually the same, we show only the calculation for $\bar{\sigma}_i(t)$. Rewrite equation (B.34) as

$$\bar{\sigma}_i(t) = B_{jl} \sum_{p=0}^{M} D_{ij_K}^{(p)} \int_0^{\xi(t)} \exp[-\frac{(\xi(t) - \xi'))}{\tau_p''}] \frac{\partial U_l}{\partial \xi'} d\xi', \tag{B.38}$$

where we have used $\frac{\partial U_l}{\partial \tau} d\tau = \frac{\partial U_l}{\partial \xi'} d\xi'$ and $\xi' = \xi(\tau)$.

Assume that the relation between the internal time ξ and t is known for all t, and that the nodal displacement vector $U_l(t)$ is known at each discrete time t_1, t_2, $\cdots t_L$ (with $t = t_L$), thus also at $\xi_1, \xi_2, \cdots \xi_L$ where $\xi_1 = \xi(t_1)$, *etc.* If the time domain from t_1 to t is discretized accordingly and if $\frac{\partial U_l}{\partial \xi'}$ in each time interval from t_r to t_{r+1} (for $r = 1, 2, \cdots L-1$) is assumed to be constant and given by $\frac{U_l(t_{r+1}) - U_l(t_r)}{\xi_{r+1} - \xi_r}$, then the heredity integral in equation (B.38) can be evaluated exactly to yield

$$\begin{aligned} \bar{\sigma}_i(t) &= B_{jl} \sum_{p=0}^{M} \sum_{r=1}^{L-1} D_{ij_K}^{(p)} \tau_p'' \frac{U_l(t_{r+1}) - U_l(t_r)}{\xi_{r+1} - \xi_r} \{\exp[-\frac{(\xi(t) - \xi_{r+1})}{\tau_p''}] - \exp[-\frac{(\xi(t) - \xi_r)}{\tau_p''}]\} \\ &= \sum_{p=0}^{M} \bar{\sigma}_i^{(p)}(t). \end{aligned} \tag{B.39}$$

$\bar{\sigma}_i^{(p)}(t)$ is the contribution of p th Prony element to the component $\bar{\sigma}_i$ at time t. The formula for $\bar{\sigma}_i(t + \triangle t)$ is obtained in a similar manner and is given by

$$\begin{aligned} \bar{\sigma}_i(t + \triangle t) &= B_{jl} \sum_{p=0}^{M} \sum_{r=1}^{L-1} D_{ij_K}^{(p)} \tau_p'' \frac{U_l(t_{r+1}) - U_l(t_r)}{\xi_{r+1} - \xi_r} \\ &\times \{\exp[-\frac{(\xi(t + \triangle t) - \xi_{r+1})}{\tau_p''}] - \exp[-\frac{(\xi(t + \triangle t) - \xi_r)}{\tau_p''}]\} \\ &+ B_{jl} \sum_{p=0}^{M} D_{ij_K}^{(p)} \tau_p'' \frac{[1 - \exp(-\frac{\triangle \xi}{\tau_p''})]}{\triangle \xi} \triangle U_l \end{aligned}$$

$$\bar{\sigma}_i(t + \triangle t) = \sum_{p=0}^{M} \bar{\sigma}_i^{(p)}(t) \exp(-\frac{\triangle \xi}{\tau_p''}) + B_{jl} \sum_{p=0}^{M} D_{ij_K}^{(p)} \tau_p'' \frac{[1 - \exp(-\frac{\triangle \xi}{\tau_p''})]}{\triangle \xi} \triangle U_l, \tag{B.40}$$

where

$$\begin{aligned} \triangle U_l &= U_l(t + \triangle t) - U_l(t) \\ \triangle \xi &= \xi(t + \triangle t) - \xi(t). \end{aligned}$$

An identical expression is obtained for $s_i(t + \triangle t)$ except that $D_{ij_K}^{(p)}$, τ_p'' and $\bar{\sigma}_i^{(p)}$ are replaced by $D_{ij_G}^{(p)}$, τ_p' and $s_i^{(p)}$, respectively.

Finite element equations

To simplify the notation, in the previous section we express the stresses and the internal time at a given material point as $s_i(t)$, $\bar{\sigma}_i(t)$ and $\xi(t)$ while the precise notations for them should be $s_i(t, \underline{x})$, $\bar{\sigma}_i(t, \underline{x})$ and $\xi(t, \underline{x})$ where $\underline{x}$ denotes the location of that material point. However, we will use the precise notation (rather than the simplified version) for stresses and the internal time in this section for reason of clarity.

Substituting the recursive formula (equation B.40) for $\{s(t + \triangle t, \underline{x})\}$ and $\{\bar{\sigma}(t + \triangle t, \underline{x})\}$ into equation (B.7) applied to the time $t + \triangle t$ and then dividing out the variational term δU_l from the resulting equation, yields the following (finite element) equilibrium equation

$$\begin{aligned}
&\int_{\partial V} S_i(t + \triangle t, \underline{x}) B_{ik} dS + \int_V B_{ik} \sum_{p=0}^{N} s_i^{(p)}(t, \underline{x}) \exp[-\frac{\triangle \xi(\underline{x})}{\tau_p'}] dV \\
&+ \int_V B_{ik} \sum_{p=0}^{M} \bar{\sigma}_i^{(p)}(t, \underline{x}) \exp[-\frac{\triangle \xi(\underline{x})}{\tau_p''}] dV \\
&+ \left(\int_V B_{ik} B_{jl} \sum_{p=0}^{N} D_{ij_G}^{(p)} \tau_p' \frac{(1 - \exp[-\frac{\triangle \xi(\underline{x})}{\tau_p'}])}{\triangle \xi(\underline{x})} dV \right) \triangle U_l \\
&+ \left(\int_V B_{ik} B_{jl} \sum_{p=0}^{M} D_{ij_K}^{(p)} \tau_p'' \frac{(1 - \exp[-\frac{\triangle \xi(\underline{x})}{\tau_p''}])}{\triangle \xi(\underline{x})} dV \right) \triangle U_l = 0. \qquad \text{(B.41)}
\end{aligned}$$

Here B_{ij} is also a function of $\underline{x}$.

If the current internal time ξ (at time $t + \triangle t$) is known, the above equation renders a system of linearly algebraic equations for the unknown vector $\triangle U_l$ (and also for $U_l(t + \triangle t)$) with the incremental stiffness matrix given by the last two terms. However, the current internal time ξ in general is not known since it depends on the current values of strains, temperature and possibly solvent concentration. The current mechanical state must, therefore, be obtained through iteration.

Numerical integration

We consider next how the volume integrals in equation (B.41) are evaluated numerically. As is shown later, two different integration schemes are employed in the evaluation of

the volume integrals in equation (B.41), and they are summarized here.

- All volume integral terms are integrated by using 2×2 quadrature rules (full integration).

- The third and fifth terms are integrated by 1×1 rule. The second and fourth terms are integrated by 2×2 rule but with $\sum_{p=0}^{N} s_i^{(p)}(t, \underline{x}) \exp[-\frac{\triangle\xi(\underline{x})}{\tau'_p}]$ and $\sum_{p=0}^{N} D_{ijG}^{(p)} \tau'_p \frac{(1 - \exp[-\frac{\triangle\xi(\underline{x})}{\tau'_p}])}{\triangle\xi(\underline{x})}$ always evaluated at the centroid of the element. By doing so, we can eliminate the mesh locking associated with material incompressibility.

The results may be significantly different depending on the integration scheme used. An in-depth discussion on this subject is given in the next section.

Effect of the order of numerical integration

As already mentioned, 4-node isoparametric finite elements are used in the computation. The selection of the appropriate order of integration in such a (materially) nonlinear analysis is important since the conditions governing the material behavior are only computed at the integration points. Nonlinear material conditions should be sampled to sufficient accuracy. In fact, by using a different integration order, the results can be affected significantly, especially for a nearly incompressible nonlinear viscoelastic solid unless proper precautions are met. The ultimate check on whether the use of a given order of integration is appropriate is through comparing the reality of the predicted response with the expected physical processes and its insensitivity to fine finite element meshes. Since the global response of a structure or body is an assemblage of each individual element response governed by energy minimization, a good understanding of the behavior of a single element will help us in the selection of the appropriate order of integration and also in the interpretation of the results.

A 4-node rectangular isoparametric element has five deformation modes beside the three rigid body modes. These are two "bending modes" (in two directions), an exten-

sion mode, an expansion mode, and a shearing mode. Under applied loads, the element will respond as the combination of these modes with each mode possessing different weight. In many circumstances, the elemental response under the same applied loads will be different depending on the numerical integration rule used. In search for the optimal integration scheme for our nearly incompressible, nonlinear viscoelastic element, we consider two integration rules. These are the full 2x2 quadrature rule and the selective reduced integration scheme.

We examine the behavior of the 4-node element under each of these rules. Just as in the linearly elastic case, the element under full integration will be very stiff in the bending modes for incompressible media because those modes will result in an incorrect volumetric strain at the integration points even though its total volume is preserved. As a consequence the element is excessively stiff, and it may cause "mesh locking" as demonstrated later.

In the selective reduced integration rule, different strain terms are integrated with different orders of integration. The volumetric strain term is segregated and treated with reduced quadrature (1x1 rule) while the remaining deviatoric term is integrated by full quadrature to retain the rank of the elemental matrices [25]. Since the volumetric strain is exactly zero at a reduced quadrature in the bending modes, this scheme will alleviate mesh locking. However, unlike the linearly elastic case, the incorrect volumetric strain at the full (2x2) quadrature points also affects the deviatoric strain energy of the element, thus the global response of the structure, since the thermal mechanical response of the polymer depends on the history of the volumetric strain. The thermal mechanical response functional (or material property) is, therefore, chosen to be evaluated based on the volumetric strain history at the reduced quadrature point where this strain component is most accurate for the bending modes. The material property of an element is assumed to be uniform.

We demonstrate the superiority of the last integration rule over the former through examples. In these examples, all meshes considered have approximately the same num-

ber of nodes (around 5500 nodes) and either simple rectangular grids or distorted grids. Based on the results in [27], the stresses at the corner of the interface and the free edge are expected to be singular. However, the normal stress σ_y and the shear stress τ_{xy} will gradually vanish at some distance away from the free edge while the distribution of the normal stress σ_x across thickness will eventually become independent of the x coordinate. Therefore, a very refined mesh must be employed at the corner while a coarser one may be used for the remote area. The rectangular grids have small square elements at the corner and slender elements in the remote area. On the other hand, the distorted grids have more elements per unit thickness at the free edge than at the remote area with elemental reduction through transition areas as shown in Figure B.1.

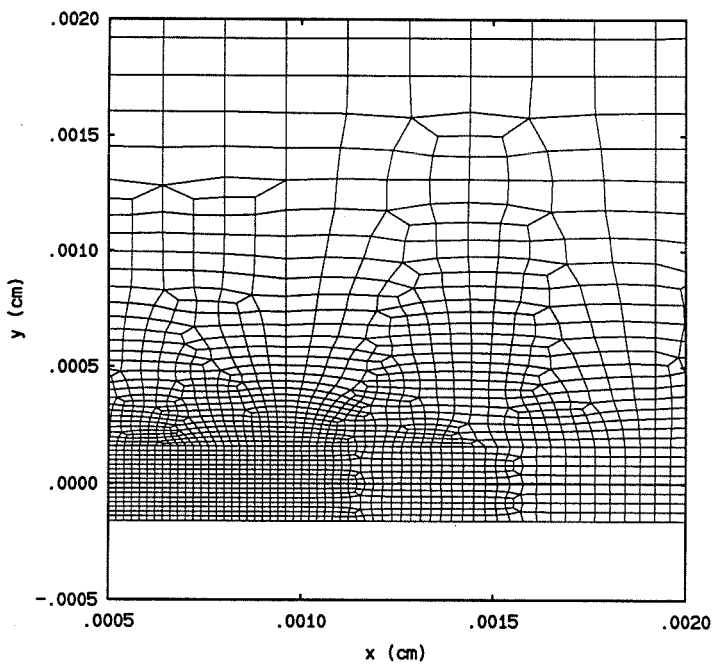

Figure B.1: Elements at transition areas in the "distorted" mesh.

The tractions along the interface based on the rectangular and distorted meshes are given in Figures B.2 and B.3 for the full integration scheme and in Figures B.4 and B.5 for the new integration scheme. The results based on two meshes under the full integration rule are in excellent agreement overall except at locations coinciding with the transition areas of the distorted mesh, where the solutions "oscillate" suddenly

and rapidly. These local oscillations are the manifestations of mesh locking in 4-node isoparametric elements, and can be explained as follows. As mentioned earlier with reference to Figure B.1, the mesh outside of the transition area is a rectangular grid while the mesh in the transition areas has many irregular elements. As the plate is cooled, the polymer will contract and shears occurs at the transition locations. Since the rectangular element is oriented parallel to the contracted direction, it will contract and shear in this case without any bending nor locking. In contrast, the response of the distorted elements to such action may involve bending because of their relative orientation and geometries with respect to the contracted direction. As a result, the elements in the transition areas will appear much stiffer than those of the neighboring areas which leads to the mentioned oscillation. A "standard" linear analysis of the same problem with a Poisson ratio of 0.499 for the adhesive gives the same local oscillations and thus supports this argument. Results from Figures B.4 - B.5 indicate that distorted elements under the reduced integration scheme have minimal locking.

Based on the above numerical study, the reduced integration scheme appears to be the most appropriate choice for the nonlinearly viscoelastic solids. Thus, all results obtained in this study are based on this reduced integration scheme. It is worthwhile to mention that there is no bending involved in the infinite sandwich; for that case, our calculations show that there are no difference in stresses and displacement under these two rules.

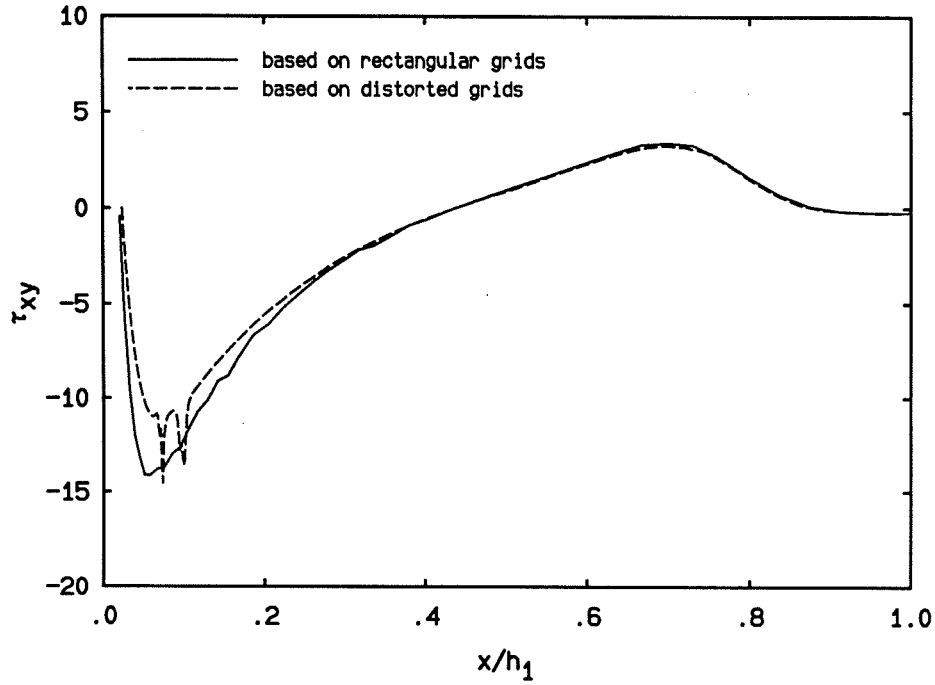

Figure B.2: Interfacial shear stress τ_{xy} based on two meshes and the under full integration scheme.

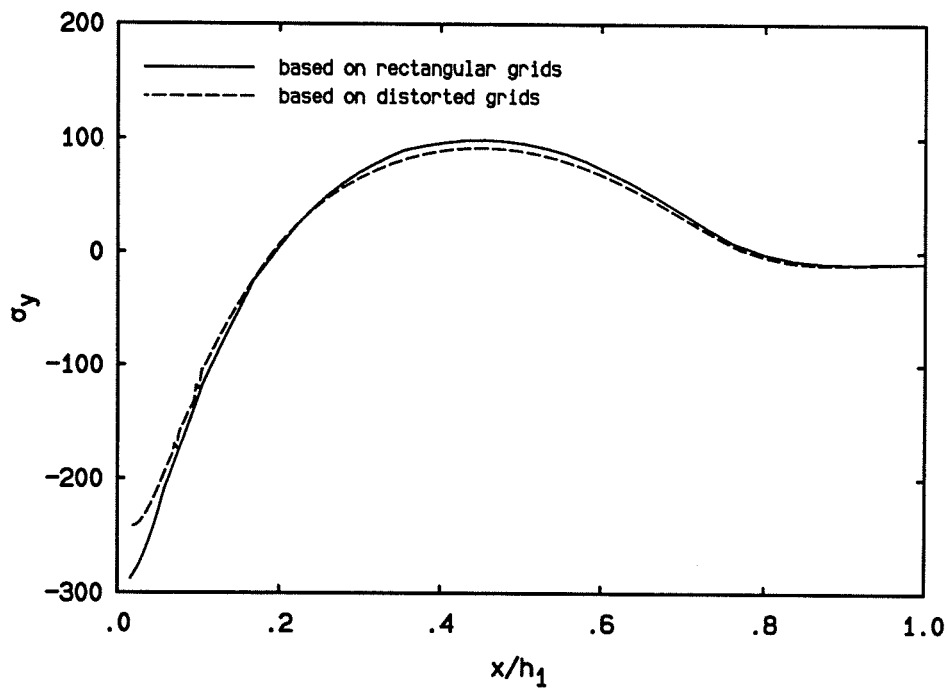

Figure B.3: Interfacial normal stress σ_y based on two meshes and under the full integration scheme.

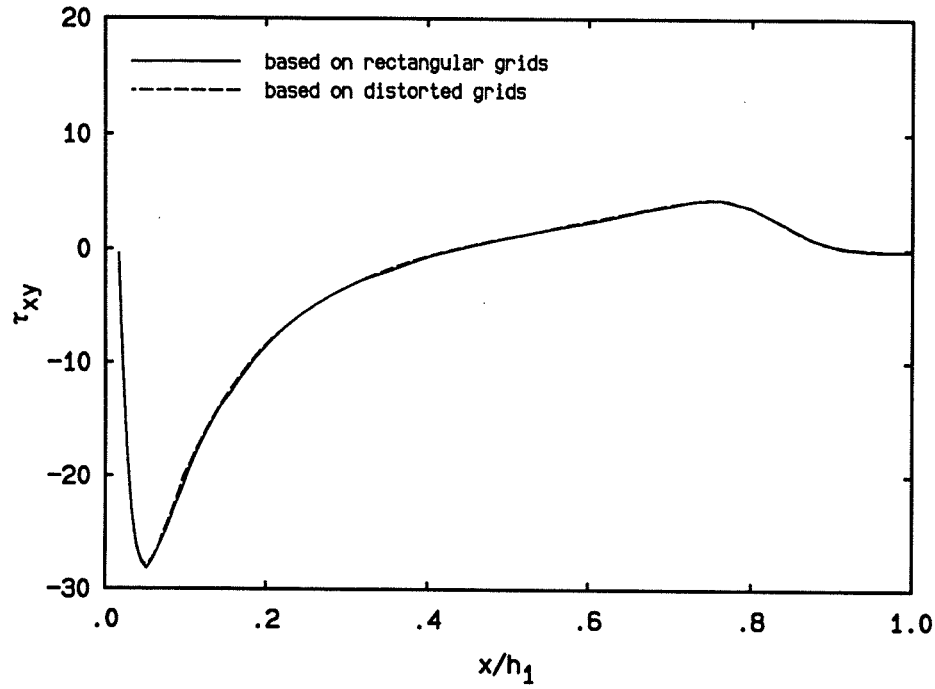

Figure B.4: Interfacial shear stress τ_{xy} based on two meshes and under the new integration scheme.

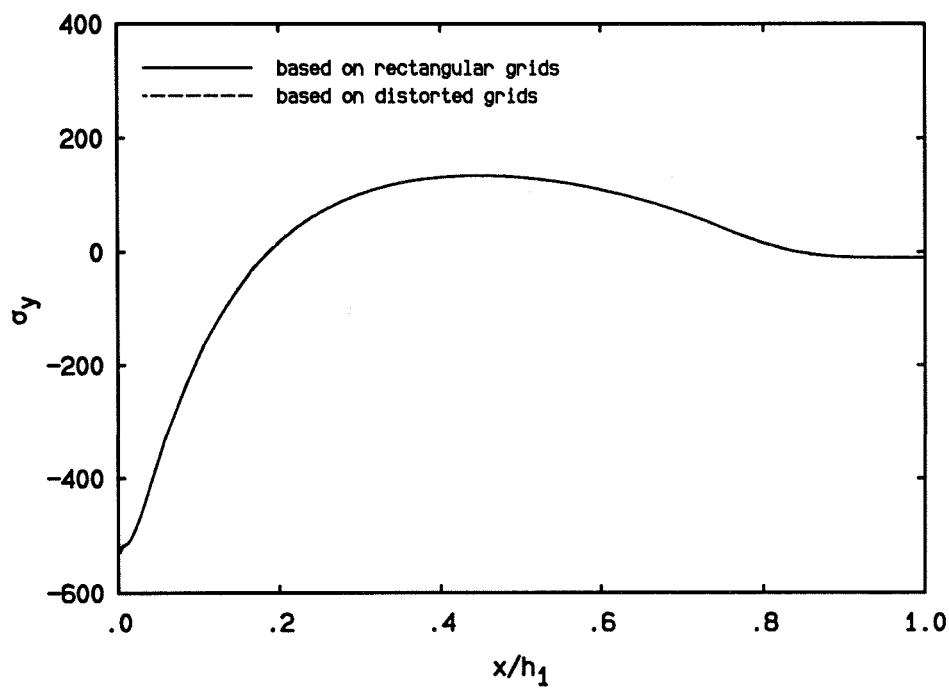

Figure B.5: Interfacial normal stress σ_y based on two meshes and under the new integration scheme.

Appendix C: Effect of cooling rates and geometries

There is a large number of parameters that control the residual stress state(s), as for example (for the case of the infinite domain) the thicknesses h_1, h_2, the stiffness properties of the two materials E_1 and $E_2 \cdots$ yielding a total of 20 parameters. By the Buckingham Pi-theorem this list generates 16 nondimensional parameters. The influences of different thermoviscoelastic material behaviors, the weight of changes in the temperature and the geometries as well as the cooling rates on residual stresses have been discussed separately in chapter 2. It is also of interest to examine the "combined effect" of the cooling rates and geometries on the residual stresses when both the geometry and the cooling rate are the design parameters. For this situation, one wants to characterize the results in terms of the governing dimensionless parameters. For that purpose, we find that the most important of these 16 nondimensional parameters are $\frac{\kappa_1 t_R}{h_1^2}$, $\frac{h_2}{h_1}$ and $\frac{t_R}{\bar{\tau}}$ with κ_1 and $\bar{\tau}$ being the thermal diffusivity and the characteristic relaxation time, respectively. In order to establish the latter fact we have repeated the calculations for the infinitely large sandwich for 21 cases with a wide range of these variables,[5] but because these do not explore the full range of all the variables we do not present them in detail here and merely summarize briefly their effect on the residual stresses.

To begin, we review the results from the heat conduction in a homogenous slab cooled symmetrically from its large lateral surfaces with the expectation that the pertinent parameters are also appropriate for the sandwich problem.

For the immediately following discussion we consider time-independent material response in order to recall certain basic characteristics of the thermal solution. The temperature distribution in a homogeneous plate cooled symmetrically from the outer surfaces to the final temperature in the time t_R is given by

$$\frac{T(t,y)-T_i}{T_f-T_i} = \begin{cases} \frac{t}{t_R} - \frac{t}{t_R} F(\frac{\kappa t}{4h^2}, y) & \frac{t}{t_R} < 1 \\ 1 - \frac{t}{t_R} F(\frac{\kappa t}{4h^2}, y) + (\frac{t}{t_R} - 1) F(\frac{\kappa \triangle t}{4h^2}, y) & \frac{t}{t_R} > 1 \end{cases}, \qquad \text{(C.1)}$$

[5] $h_1 = 5$ - 23 mm, $h_2 = 0.32$ - 1.6 mm, and $t_R = 0.01 - 10^5$ sec.

where h is the half thickness of the plate, κ is the thermal diffusitivity and is given by $\frac{k}{\rho C_p}$, and

$$F(\bar{t}, y) = \sum_{n=1,3\cdots 2n+1}^{\infty} \frac{4}{n\pi} \frac{(1 - e^{-n^2\pi^2\bar{t}})}{n^2\pi^2\bar{t}} \sin(\frac{n\pi y}{2h}).$$

$$\triangle t = t - t_R$$

For a large value of $\frac{\kappa t_R}{h^2}$, $F(\frac{\kappa t}{4h^2}, y) = F(\frac{\kappa t_R}{4h^2} \cdot \frac{t}{t_R}, y) \to 0$, and $\frac{T(t,y) - T_i}{T_f - T_i} \to \frac{t}{t_R}$ for $\frac{4h^2}{\kappa t_R} < \frac{t}{t_R} < 1$. Then the temperature distribution reaches uniformity across the plate thickness (independent of y) after the time $t = \frac{4h^2}{\kappa}$. For other values of $\frac{\kappa t_R}{h^2}$, no such general statement can be made except that based on the first term of the series (C.1), the time to approximately reach thermal equilibrium is given by

$$t_e = t_R + \beta \frac{h^2}{\kappa}, \tag{C.2}$$

where β is a constant and $\frac{h^2}{\kappa}$ is called thermal diffusion time.

This expression indicates that the temperature changes in the midplane lag those at the outer surfaces by an interval proportional to the thermal diffusion time $\frac{h^2}{\kappa}$.

By rewriting $\frac{\kappa t}{h^2}$ as $\frac{\kappa t_R}{h^2} \cdot \frac{t}{t_R}$, equation (C.1) can be recast into

$$\frac{T(t,y) - T_i}{T_f - T_i} = \mathcal{R}(\frac{\kappa t_R}{h^2}, \frac{t}{t_R}, \frac{y}{h}). \tag{C.3}$$

The function $\mathcal{R}$ has been compiled in most text books on the subject for step cooling, *i.e.*, for a parameter $\frac{\kappa t_R}{h^2}$ equal zero.

The generalization of (C.3) to the sandwich may take the following form

$$\frac{T(t,y) - T_i}{T_f - T_i} = \mathcal{R}(\frac{\kappa_1 t_R}{h_1^2}, \frac{h_2}{h_1}, \frac{\kappa_2 \bar{\tau}_b}{h_2^2}, \frac{t}{t_R}, \frac{y}{2h_1 + h_2}), \tag{C.4}$$

where $\mathcal{R}$ depends also on $\frac{h_2}{h_1}$ and $\frac{\kappa_2 \bar{\tau}_b}{h_2^2}$ with $\bar{\tau}_b$ being the characteristic (average) bulk relaxation time for a particular polymer.[6] The above functional form of $\mathcal{R}$ includes the influence of the nonlinearly viscoelastic behavior of the heat capacity of the polymer on transient thermal response.

[6]The discontinuity of the heat capacity is determined by the fractional free volume which in turn depends on the bulk modulus.

For the present we continue to use the earlier material (PVAc) for modeling purposes and compute residual stresses for different combinations of geometry and cooling rate. In that case the dependence of $\mathcal{R}$ on $\frac{\kappa_2 \bar{\tau}_b}{h_2^2}$ is (probably) weak as long as the polymer layer is thin, which is usually the case in bonding, and equation (C.2) applies in the form

$$t_e = t_R + \frac{\beta h_1^2}{\kappa_1} \tag{C.5}$$

and the temperature field is described implicitly by

$$\frac{T(t,y) - T_i}{T_f - T_i} = \mathcal{R}(\frac{\kappa_1 t_R}{h_1^2}, \frac{h_2}{h_1}, \frac{t}{t_R}, \frac{y}{2h_1 + h_2}). \tag{C.6}$$

The temperature field depends, therefore, on three parameters $\frac{\kappa_1 t_R}{h_1^2}$, $\frac{h_2}{h_1}$, and t_R. Since material properties do not vary in this part of the study, the stress field also depends on these three parameters. In the sequel we consider variations of these parameters such that any two are held constant for any case.

Case 1: Variation in t_R with $\frac{\kappa_1 t_R}{h_1^2}$ and $\frac{h_2}{h_1}$ constant: $\frac{\kappa_1 t_R}{h_1^2} = c_1$, $\frac{h_2}{h_1} = c_2$

In this situation the temperature distribution in the sandwich is characterized by equation (C.6) as

$$\frac{T(t,y) - T_i}{T_f - T_i} = \mathcal{R}(c_1, c_2, \frac{t}{t_R}, \frac{y}{2h_1 + h_2}) = \mathcal{P}(\frac{t}{t_R}, \frac{y}{2h_1 + h_2}) \tag{C.7}$$

from where the average temperatures in the adherend and in the polymer are computed as

$$\frac{\bar{T}_1 - T_i}{T_f - T_i} = \frac{1}{h_1} \int_{\frac{h_2}{2}}^{h_1 + \frac{h_2}{2}} \mathcal{P}(\frac{y}{2h_1 + h_2}, \frac{t}{t_R}) dy = (2 + c_2) \int_{\frac{c_2}{2(2+c_2)}}^{\frac{1}{2}} \mathcal{P}(\eta, \frac{t}{t_R}) d\eta$$

$$\frac{\bar{T}_2 - T_i}{T_f - T_i} = \frac{1}{h_2} \int_{-\frac{h_2}{2}}^{\frac{h_2}{2}} \mathcal{P}(\frac{y}{2h_1 + h_2}, \frac{t}{t_R}) dy = (\frac{2 + c_2}{c_2}) \int_{-\frac{c_2}{2(2+c_2)}}^{\frac{c_2}{2(2+c_2)}} \mathcal{P}(\eta, \frac{t}{t_R}) d\eta$$

with

$$\eta = \frac{y}{2h_1 + h_2}.$$

$\bar{T}_1$ and $\bar{T}_2$ are functions of the single variable $\frac{t}{t_R}$ so that the thermal strain mismatch is also a function of $\frac{t}{t_R}$ since it is determined by

$$\epsilon_m = \alpha_1(\bar{T}_1 - T_i) - \bar{\alpha}_2(\bar{T}_2 - T_i) = \mathcal{L}(\frac{t}{t_R}),$$

where the time and temperature-dependent thermal expansion coefficient of the polymer is represented, for estimation purposes, by its "effective" value $\bar{\alpha}_2$.

The strain rate associated with the thermal contraction mismatch therefore is

$$\frac{d\epsilon_m}{dt} = \frac{1}{t_R}\mathcal{L}'(\frac{t}{t_R})$$

for

$$0 \leq \frac{t}{t_R} \leq 1 + \frac{\beta}{c_1},$$

where a prime denotes the differentiation with respect to the argument.

Since the functions $\mathcal{L}$, $\mathcal{L}'$ and the normalized time for attaining thermal equilibrium are the same for all cases with $\frac{\kappa_1 t_R}{h_1^2}$ and $\frac{h_2}{h_1}$ constant, it is clear that the case with a higher cooling rate (smaller t_R) among them would yield a higher strain rate and produces a higher residual stress as indicated in Figure C.1.

Case 2: Variation in $\frac{\kappa_1 t_R}{h_1^2}$ with $\frac{h_2}{h_1}$ and t_R constant: $\frac{h_2}{h_1} = c_2$, $t_R = c_1$

This consideration follows the same procedures as in case 1; the strain rate $\frac{d\epsilon_m}{dt}$ for this case turns out to depend on two variables since

$$\frac{T(t,y) - T_i}{T_f - T_i} = \mathcal{R}(\frac{\kappa_1 c_1}{h_1^2}, c_2, \frac{t}{c_1}, \frac{y}{2h_1 + h_2}) = \mathcal{D}(\frac{\kappa_1}{h_1^2}, t, \frac{y}{2h_1 + h_2})$$

$$\epsilon_m = \mathcal{H}(t, \frac{\kappa_1}{h_1^2})$$

for

$$0 < t < c_1 + \beta\frac{h_1^2}{\kappa_1}.$$

The dependence of ϵ_m on $\frac{\kappa_1}{h_1^2}$ beside time t makes the comparison of residual stresses for different cases with $\frac{h_2}{h_1}$ and t_R constant less appealing unless the explicit form of the function $\mathcal{H}$ is known. However, a qualitative prediction can be made.

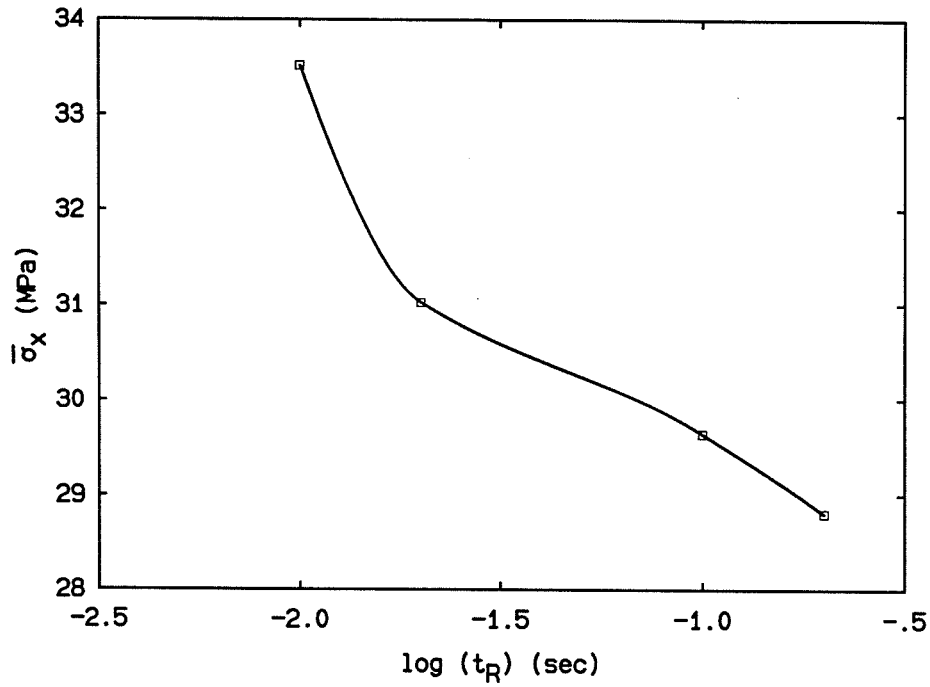

Figure C.1: Thickness-averaged stress σ_x in the polymer of an infinite sandwich for $\frac{\kappa_1 t_R}{h_1^2} = 0.03832$ and for $\frac{h_2}{h_1} = 5$ %.

As shown earlier, the time for attaining thermal equilibrium is given by equation (C.5). Based on that equation, the case with a smaller thermal diffusion time, *e.g.*, $\frac{h_1^2}{\kappa_1}$, would result in a shorter thermal equilibrium time, thus a higher strain rate. Therefore, we expect that residual stress is an increasing function of the parameter $\frac{\kappa_1 t_R}{h_1^2}$.[7] This trend is evident from Figure C.2.

Case 3: Variation in $\frac{h_2}{h_1}$ with $\frac{\kappa_1 t_R}{h_1^2}$ and t_R constant: $\frac{\kappa_1 t_R}{h_1^2} = c_1$, $t_R = c_2$

In this situation, the thickness of the adherend and the cooling time are kept constant while the polymer thickness varies. We already present the result for this case in section 2.4.1.7 of chapter 2 (cf. Figures 2.6). For high cooling rates, the residual stresses increase with $\frac{h_2}{h_1}$ but decrease with that ratio for low cooling rates. However, the influence of thickness ratio is only minor for all cooling rates. We now explain the increase in residual

[7] t_R is constant in this situation so that $\frac{\kappa_1 t_R}{h_1^2}$ is proportional to the inverse of the thermal diffusion time.

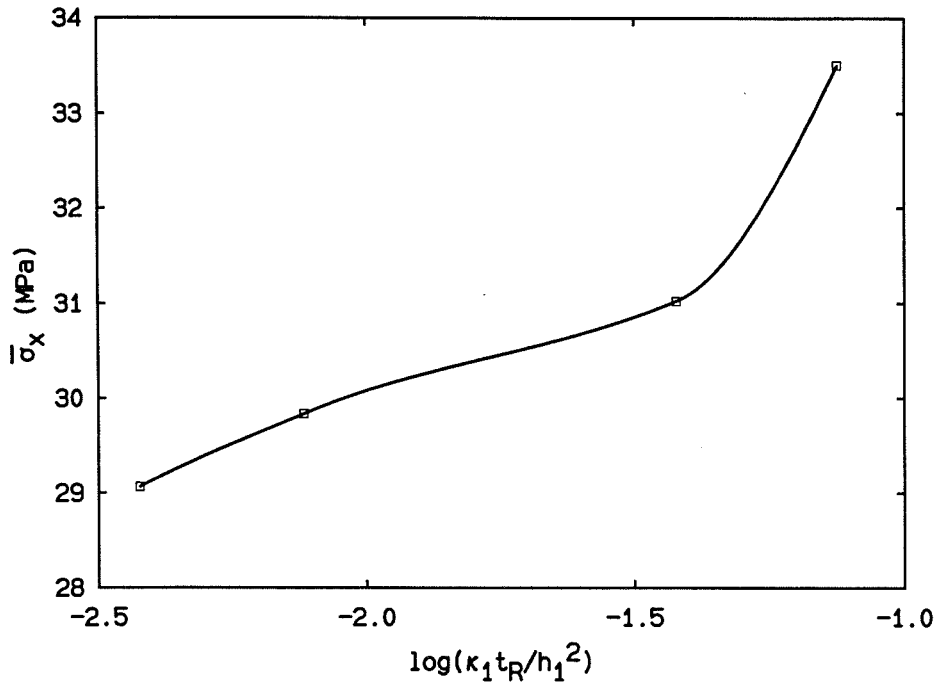

Figure C.2: Thickness-averaged stress σ_x in the polymer of an infinite sandwich for $\frac{h_2}{h_1} = 5\%$ and for $t_R = 0.02$ sec.

stresses with thickness ratio at high cooling rates: A thicker polymer layer produces larger (transient) temperature gradients across the sandwich thickness while, for the present situation, the time required for attaining thermal equilibrium remains nearly unchanged since (a) the thermal diffusion time for the adherend and the cooling time are kept constant and (b) the polymer is much thinner than the adherends ($\frac{h_2}{h_1} \leq 10\%$). The applied strain rate is, therefore, higher for a thicker polymer layer which leads to a higher residual stress. On the other hand, for low cooling rates, the effect of transient temperature gradients is essentially absent so that the stress behavior for that case follows the same trend as what thermoelastic analysis predicts.

Appendix D: Linearly Thermal Stress Analysis

This appendix presents an engineering analysis of bonding stresses at the interface between an elastic adhesive layer and an elastic adherend of a sandwich plate exposed to a uniform temperature change. The bonding stresses at the interface of the similar or closely related problem have been studied in [3, 36, 37] by using either a beam analysis or a variational method. Our approach to solve this problem is based on the work by Suhir in [37]. The adherend is considered as a plate on an elastic foundation. Due to symmetric lay up of the adherends, the polymer layer will not bend as a plate, thus it is modelled as a thin elastic strip (see Figure D.1).

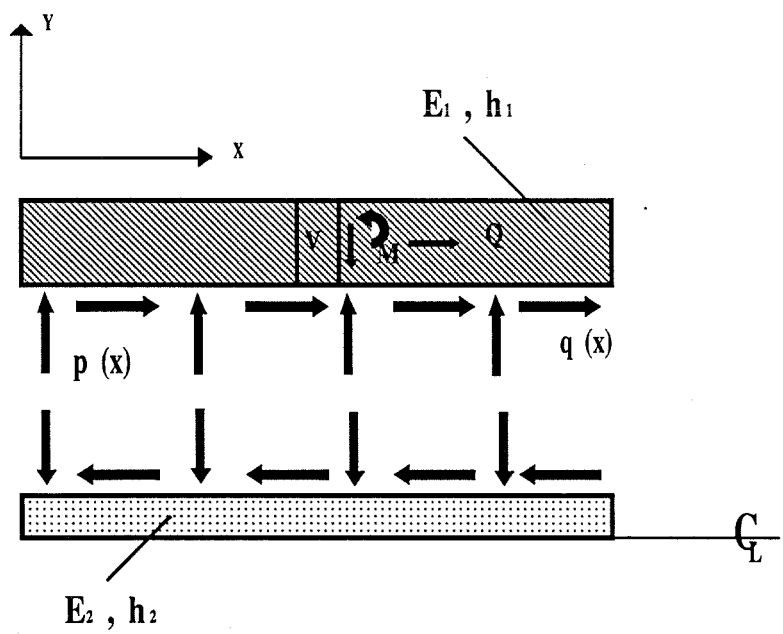

Figure D.1: Forces and moments acting on the adherend and the polymer. The convention of the forces and moment acting on a cut across the thickness is also given in the figure for the adherend. (Note that $x = 0$ corresponds to the center line).

Let us denote the subscript 1 and 2 of any quantity to be that of the adherend and polymer, respectively. The displacement of the lower extreme fiber of the adherend in

the direction of the bond line is given by

$$u_1(x) = (1+\nu_1)\alpha_1 \triangle T x + \frac{1-\nu_1^2}{E_1 h_1}\int_0^x Q(\zeta)\,d\zeta + \kappa_1 q(x) + \frac{h_1}{2}\int_0^x v''(\zeta)\,d\zeta,$$

where E_1, ν_1, and α_1 are the elastic constants and the thermal expansion coefficient of the adherend, respectively. Q, q, and v are the axial force, shear force per unit plate length, and normal displacement, respectively. The first term in the above equation is the free thermal expansion (contraction). The second and third terms are the displacements due to distributed shearing force. The last term is due to bending. Typical for plate analysis are the following relations

$$\begin{aligned}
\kappa_1 &= \frac{2(1+\nu_1)h_1}{3E_1} \\
Q(x) &= -\int_{-l}^{x} q(\zeta)d\zeta \\
M &= D_1 v'' \\
D_1 &= \frac{E_1 h_1^3}{12(1-\nu_1^2)} \\
\frac{dM}{dx} &= V - q\frac{h_1}{2} \\
\frac{dV}{dx} &= p \\
\frac{dQ}{dx} &= -q.
\end{aligned}$$

A similar expression for the axial (x) displacement of the upper extreme fiber of the polymer layer can be obtained as

$$u_2(x) = (1+\nu_2)\alpha_2 \triangle T x - \frac{1-\nu_2^2}{E_2 h_2}\int_0^x Q(\zeta)\,d\zeta - \kappa_2 q(x) + \frac{\nu_2(1+\nu_2)}{E_2}\int_0^x p(\zeta)\,d\zeta.$$

In this case, the last bending term has been substituted by a Poisson ratio induced term, *e.g.*, the term with the normal distributed force p(x). By assuming that the polymer layer is very thin compared to the adherends and that p(x) is smooth without any step change, it follows from linear elasticity theory that

$$\frac{p}{E_2} = -\frac{v}{h_2(1-\nu_2^2)} + \frac{(1+\nu_2)\alpha_2 \triangle T}{(1-\nu_2^2)}.$$

After enforcing the axial (x) displacement continuity across the interface, the above equations can be reduced to

$$Q'' - \left(\frac{1-\nu_1^2}{E_1 h_1 \kappa} + \frac{1-\nu_2^2}{E_2 h_2 \kappa}\right) Q = \frac{h_1}{2\kappa} v'' + \frac{\nu_2}{(1-\nu_2) h_2 \kappa} - \frac{\triangle\alpha \, \triangle T}{\kappa} - \frac{\nu_2(1+\nu_2)\alpha_2 \, \triangle T}{(1-\nu_2)\kappa}$$

$$v'''' + \frac{E_2}{h_2 D_1 (1-\nu_2^2)} v = \frac{h_1}{2D_1} Q'' + \frac{\alpha_2 E_2 \, \triangle T}{(1-\nu_2) D_1},$$

where

$$\begin{aligned} \kappa &= \kappa_1 + \kappa_2 \\ \triangle\alpha &= (1+\nu_2)\alpha_2 - (1+\nu_1)\alpha_1 \end{aligned}$$

subject to boundary conditions

$$\begin{aligned} v'(0) &= 0 \\ v'''(0) &= 0 \\ v''(l) &= 0 \\ Q(l) &= 0 \\ Q'(0) &= 0 \\ D_1 v'''(l) - \frac{h_1}{2} Q'(l) &= 0. \end{aligned}$$

The above two coupled differential equations can be solved by rewriting them as a system of six coupled first order equations, *e.g.*, $\underline{w'} = [A]\,\underline{w} + \underline{r}$ and then reducing them further to an uncoupled first order system through a proper variable transformation. The solution for $\underline{w}$ is finally given as

$$w_i = \sum_{j=1}^{6} w_{0i} N_{ij} e^{\lambda_j x} - A_{ij}^{-1} r_j$$

where

$$[A] = \begin{bmatrix} 0 & 1 & 0 & 0 & 0 & 0 \\ \frac{1-\nu_1^2}{E_1 h_1 \kappa} + \frac{1-\nu_2^2}{E_2 h_2 \kappa} & 0 & \frac{\nu_2}{h_2 \kappa (1-\nu_2)} & 0 & \frac{h_1}{2\kappa} & 0 \\ 0 & 0 & 0 & 1 & 0 & 0 \\ 0 & 0 & 0 & 0 & 1 & 0 \\ 0 & 0 & 0 & 0 & 0 & 1 \\ \frac{h_1}{2D_1}\left(\frac{1-\nu_1^2}{E_1 h_1 \kappa} + \frac{1-\nu_2^2}{E_2 h_2 \kappa}\right) & 0 & \frac{\nu_2}{2\kappa D_1 (1-\nu_2)} \frac{h_1}{h_2} - \frac{E_2}{h_2 D_1 (1-\nu_2^2)} & 0 & \frac{h_1^2}{4\kappa D_1} & 0 \end{bmatrix},$$

$$\underline{r} = \left\{ \begin{array}{c} 0 \\ -\dfrac{\triangle\alpha\,\triangle T}{\kappa} - \dfrac{\nu_2\alpha_2(1+\nu_2)\,\triangle T}{(1-\nu_2)\kappa} \\ 0 \\ 0 \\ 0 \\ -\dfrac{h_1\,\triangle\alpha\,\triangle T}{2\kappa D_1} - \dfrac{\nu_2 h_1\alpha_2(1+\nu_2)\,\triangle T}{2D_1\kappa(1-\nu_2)} + \dfrac{\alpha_2 E_2\,\triangle T}{(1-\nu_2)D_1} \end{array} \right\},$$

w_{0i} are the constants of integration determined by the boundary conditions, N_{ij} is the i^{th} component of the j^{th} eigenvector of the matrix [A], and λ_j are the corresponding eigenvalues. If $\frac{E_2}{E_1} \ll \frac{h_1}{h_2}$ as in most typical adhesive joints, the eigenvalues can be approximated by the following expressions

$$\begin{aligned} \lambda_{1,2} &\approx \pm\sqrt{\frac{3(1-\nu_2)}{2(1+\beta)}}\frac{1}{h_2} \\ \lambda_{3,4,5,6} &\approx \pm\frac{\sqrt{2}}{2h_1}\left[\frac{12(1-\chi\nu_2)\beta}{1-\nu_2}\right]^{1/4}(1\pm i) \\ \beta &= \frac{E_2 h_1(1+\nu_1)}{E_1 h_2(1+\nu_2)} \\ \chi &= \frac{\nu_1}{\nu_2}. \end{aligned}$$

Based on these λ_i, the homogeneous solution of $\underline{w}$ decays to zero at a distance of several adherend thicknesses away from the free edge as expected.

We compare the results based on this analytical model with those from (finite element) thermoelastic analysis in Figures D.2 and D.3.

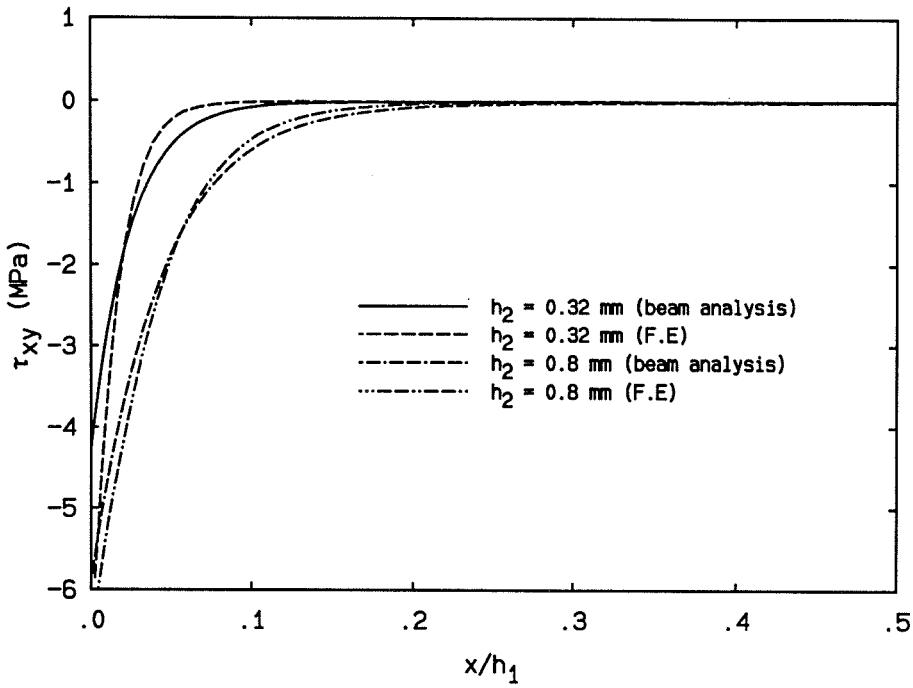

Figure D.2: Comparison of the analytical and the finite element solutions for the interfacial shear stress τ_{xy} in thermoelastic analysis.

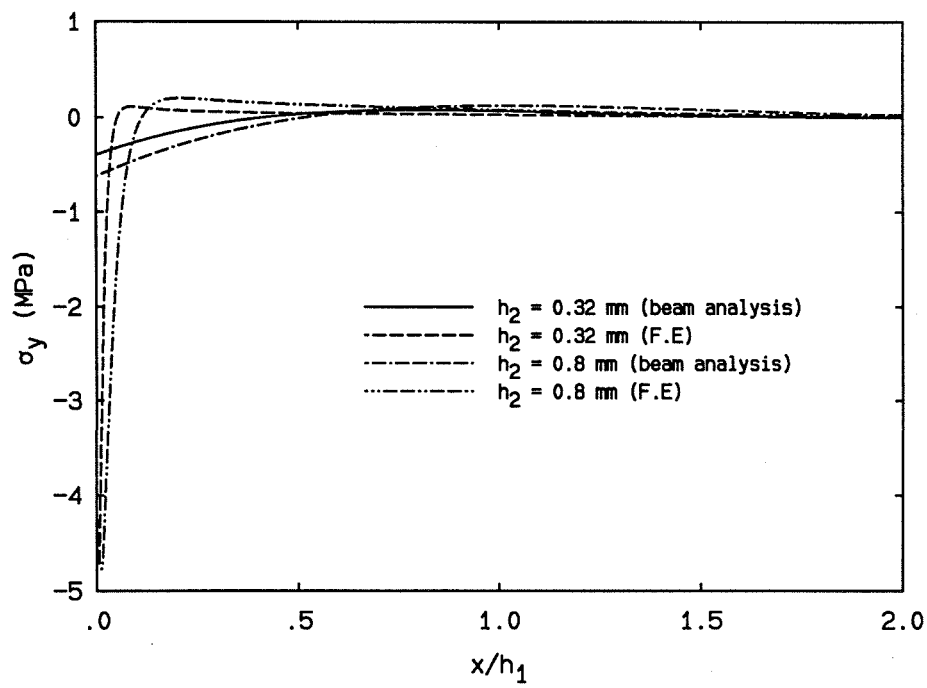

Figure D.3: Comparison of the analytical and the finite element solutions for the interfacial normal stress σ_y in thermoelastic analysis.

Appendix E: Energy Release Rate For A Semi-infinite Crack

Consider the sandwich to be separated by a hypothetical plane through the polymer and along which a crack is introduced later. This plane is not necessarily located in the (large) plane of symmetry of the sandwich. The two segments defined by the plane constitute bi-material plates, each (possibly) possessing a different layer thickness of polymer. Before introduction of the crack there exists a net force F_0 and a net moment M_0 resulting from the residual stresses in each of these hypothetical plates (see Figure E.1). If the assembly were cut along this hypothetical plane the stresses reduce to yield a vanishing net force and moment across each section, but these segments then deflect into each other at the free end. As a consequence there must be a contact force P acting on each segment to keep them from interpenetrating. For the present analysis the length of the crack is assumed to equal "a," and "a" is the half length of the sandwich with the goal of letting $a \to \infty$ for a semi-infinite crack. Figure E.1 depicts the deformed configurations of this cracked sandwich after the (stress) unloading process. The energy release rate for this problem can be computed with the aid of a dual bi-material cantilever type plate model. Since this computation uses results from the bi-material plate analysis, we review the latter briefly in the next section. All equations are derived for plane strain with E' denoting $\dfrac{E}{1-\nu^2}$.

Results from bi-material plate analysis

Consider a bi-material plate under an applied force F and/or under a moment M as shown in Figure E.2. One then wants to derive the stresses, strains and the strain energy in the plate. We show the calculation for the plate under F first. The stresses $\bar{\sigma}'_{x_1}$ and $\bar{\sigma}'_{x_2}$ in layers 1 and 2, respectively, of the plate due to the force F are given by

$$\bar{\sigma}'_{x_1} = \frac{FE'_1}{h_1 E'_1 + t_2 E'_2} \tag{E.1}$$

$$\bar{\sigma}'_{x_2} = \frac{FE'_2}{h_1E'_1 + t_2E'_2}, \tag{E.2}$$

as determined from the two following equations

$$\bar{\sigma}'_{x_1}h_1 + \bar{\sigma}'_{x_2}t_2 = F \quad \text{(sum of forces)} \tag{E.3}$$

$$\frac{\bar{\sigma}'_{x_1}}{E'_1} = \frac{\bar{\sigma}'_{x_2}}{E'_2} \quad \text{(identical strain).} \tag{E.4}$$

The corresponding strain energy is

$$U = (\frac{\bar{\sigma}'^2_{x_1}}{2E'_1} + \frac{\bar{\sigma}'^2_{x_2}}{2E'_2})a. \tag{E.5}$$

We next consider the plate subjected to an applied moment M. As in the homogenous case, the strain-curvature relation follows from the assumption that plane sections remain plane, *i.e.*,

$$\epsilon_x(y) = -(y - y_0)\kappa, \tag{E.6}$$

where y_0 is the location of the neutral axis as measured from a reference axis as indicated in Figure E.2. The axial stress profile in the plate (across the thickness) is

$$\sigma_x(y) = \begin{cases} E_2\epsilon_x & 0 < y < t_2 \\ E_1\epsilon_x & t_2 < y < h_1 + t_2 \end{cases}. \tag{E.7}$$

This stress profile $\sigma_x(y)$ must satisfy the force and moment equilibrium conditions

$$\int_0^{h_1+t_2} \sigma_x(y)dy = 0 \tag{E.8}$$

$$\int_0^{h_1+t_2} (y - y_0)\sigma_x(y)dy = M. \tag{E.9}$$

Substituting (E.7) and (E.6) for the stress and strain, respectively, into (E.7) and (E.9) and carrying out the integrations yield

$$y_0 = \frac{\frac{E'_2t_2^2}{2} + \frac{E'_1h_1^2}{2} + E'_1h_1t_2}{E'_2t_2 + E'_1h_1} \tag{E.10}$$

$$M = (E'I)_*\kappa, \tag{E.11}$$

where

$$(E'I)_* = \frac{E'_2t_2^3}{3} + \frac{E'_1h_1^3}{3} + E'_1h_1^2t_2 + E'_2t_2^2h_1 - \frac{\left[\frac{E'_2t_2^2}{2} + \frac{E'_1h_1^2}{2} + E'_1h_1t_2\right]^2}{E'_2t_2 + E'_1h_1}. \tag{E.12}$$

The strain energy in the plate for this (moment) loading follows: From the definition of the strain energy for a plate, one has

$$U = \frac{1}{2}\int_0^a \int_0^{h_1+t_2} \sigma_x \epsilon_x \, dy dx \tag{E.13}$$

with a being the length of the plate. By substituting (E.6) into (E.13) and by invoking (E.9) and (E.11), one finds

$$U = \frac{1}{2}\int_0^a \frac{M^2}{(E'I)_*} dx. \tag{E.14}$$

So far M has been assumed to be constant but allowing $M = M(x)$ does not change the results in any way. One can also show that the total strain energy of the plate under a combined axial force F and moment M equals the sum of the strain energies arising from each load component separately. It is thus clear that all results from the homogenous plate analysis also apply to the bi-material case but with the "effective" flexure rigidity $(E'I)_*$.

Energy release rate

As mentioned at the beginning of this appendix, a contact force P acts on each segment of the cracked sandwich during the (moment) unloading process. This contact force is determined from the continuity in the transverse displacement at the end of the two bi-material plates, *e.g.*, $(u_2)_1 - (u_2)_2 = 0$, as

$$P = \frac{3}{2a}\left[\frac{M_{0_u}(E'I)_{*_l} + M_{0_l}(E'I)_{*_u}}{(E'I)_{*_l} + (E'I)_{*_u}}\right], \tag{E.15}$$

where M_{0_u} and M_{0_l} are the net moments resulting from residual stresses as defined below on a cut (cross) section in the upper and lower segments, respectively; $(E'I)_*$ is the effective flexural rigidity.

The energy release rate for a cracked geometry is

$$\mathcal{G} = -\frac{\partial U}{\partial a}, \tag{E.16}$$

where a is the crack length. With the aid of Figure E.1 and by linear superposition the energy release rate for the present cracked sandwich can be computed from equation

(E.16) via a dual cantilever plate model, in which U is the total strain energy of the two bi-material plates, each being subjected to its own force $-F_0$ and moment $-M_0$ but a common load P at the end $x = 0$. We deal next with (either) one of the two bi-material plates.

If $\sigma_{x_0}(y)$ is the residual stress in the (infinite) plate before the crack is introduced, y_1, y_2 and y_0 are the positions of the bottom fiber, the upper fiber and the neutral axis of the bi-material plate, respectively, then F_0 and M_0 resulting from this residual stress are given by

$$\begin{aligned} F_0 &= \int_{y_1}^{y_2} \sigma_{x_0} dy \\ M_0 &= \int_{y_1}^{y_2} \sigma_{x_0}(y - y_0) dy. \end{aligned}$$

The calculation of the energy release rate for one (generic) bi-material plate is outlined next. As mentioned in the previous section, the contribution of the bending strain energy and that of the stretching counterpart to the total strain energy can be computed separately. Both expressions for stretching and bending strain energies are also derived in that section as given by equations (E.5) and (E.14), from which $\mathcal{G}$ follows by (E.16).

The contribution of $-F_0$ to $\mathcal{G}$ is determined through equations (E.5) and (E.16) for $F = -F_0$ as

$$\mathcal{G} = \frac{F_0^2(E_1' + E_2')}{2(E_1'h_1 + E_2't_2)^2}. \tag{E.17}$$

Similarly, by using equations (E.14) and (E.16) with $M = -M_0 + Px$, the contribution of $-M_0$ and P to $\mathcal{G}$ is given by

$$\mathcal{G} = \frac{M_0^2 + P^2a^2 - 2M_0Pa}{2(E'I)_*}. \tag{E.18}$$

The above equation for $\mathcal{G}$ is independent of a since P is proportional to $\frac{1}{a}$. The total energy release rate of the cracked sandwich is then calculated by evaluating equations (E.17) and (E.18) for each bi-material plate and combining the results. This final result also holds for a semi-infinite crack since its expression is independent of the crack length "a."

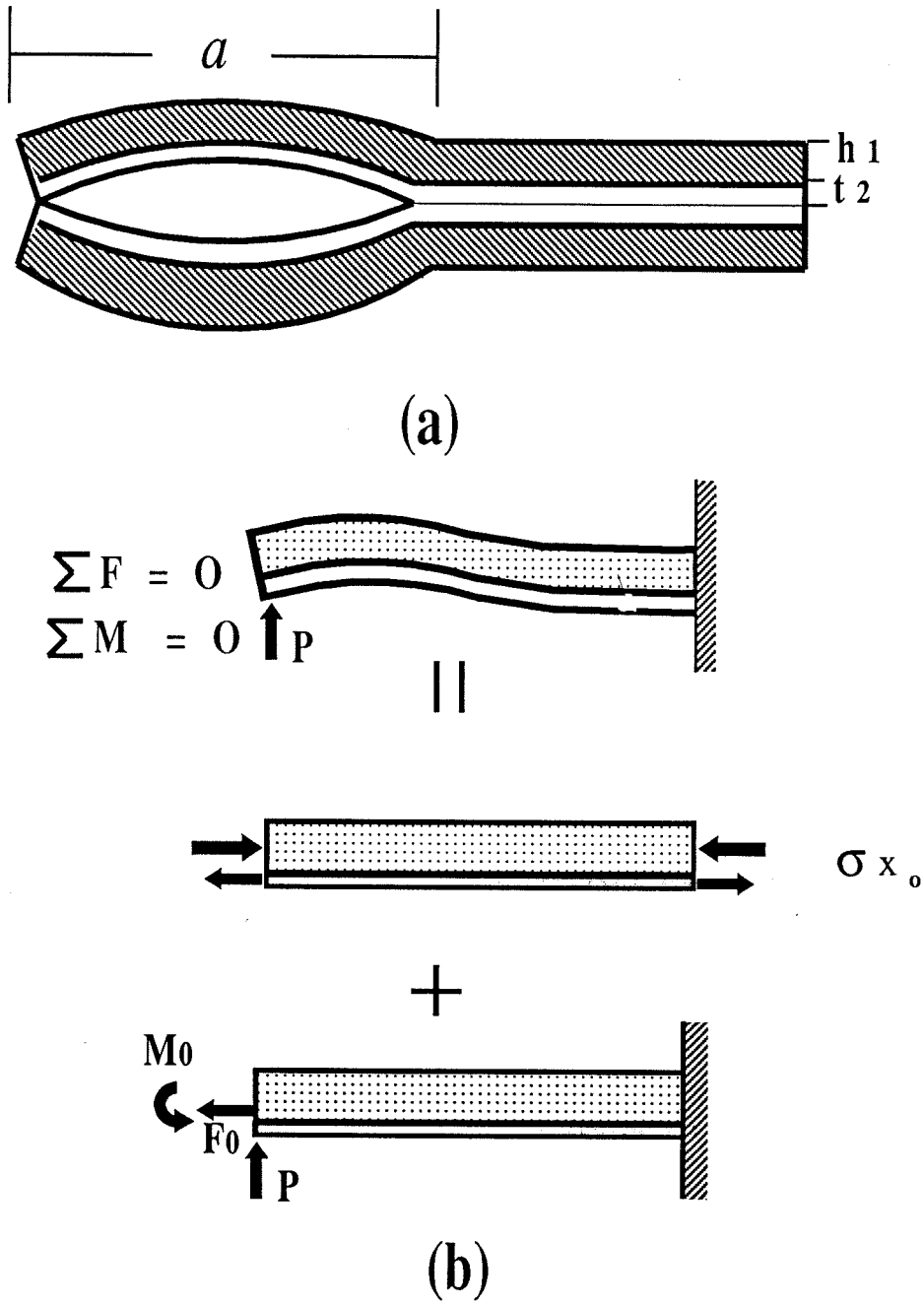

Figure E.1: Deformed configuration of the cracked sandwich and schematic representation of superposition method used. (a) Deformed configuration of a cracked sandwich. (b) Schematic representation of superposition method used (shown only for the upper segment of the cracked sandwich).

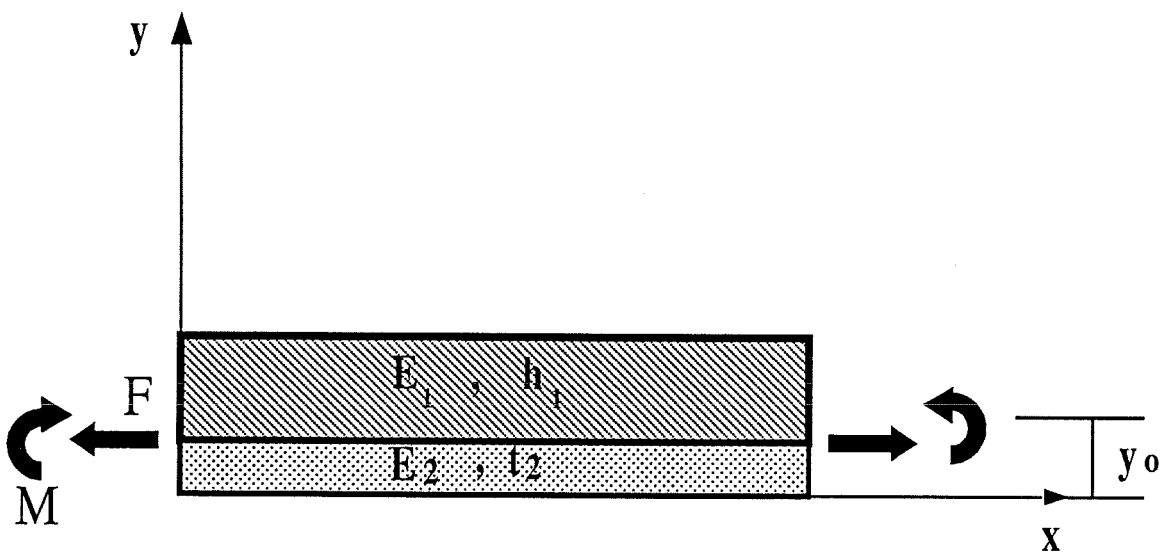

Figure E.2: A bi-material plate under a force F and a moment M.

References

[1] Losi, G. U., (1990), "Nonlinear Thermoviscoelastic Behavior of Polymers," Ph.D. Thesis, California Institute of Technology.

[2] Lee, E. H., Rogers, T. G., Woo, T. C., (1965), "Residual Stresses in a Glass Plate Cooled Symmetrically from Both Surfaces," Journal of The American Ceramic Society, Vol. 48, pp. 480-487.

[3] Heymans, L., (1983), "An Engineering Analysis of Polymer Film Adhesion to Rigid Substrates," Ph.D Thesis, California Institute of Technology.

[4] Gardon, R., Narayanaswamy, O. S., (1970), "Stress and Volume Relaxation in Annealing Flat Glass," Journal of The American Ceramic Society, Vol. 53, pp. 380-385.

[5] Narayanaswamy, O. S., (1978), "Stress and Structural Relaxation in Tempering Glass," Journal of The American Ceramic Society, Vol. 61, pp. 146-152.

[6] Scherer, G. W., Rekhson, S. M., (1982) "Viscoelastic-Elastic Composites: II, Sandwich Seal," Journal of The American Ceramic Society, Vol. 65, pp. 399-406.

[7] Ferry, J. D., Straton, R. A., (1960), "The Free Volume Interpretation of the Dependence of Viscosities and Viscoelastic Relaxation Times on Concentration, Pressure and Tensile Strain," Kolloid-Zeitschrift, Vol. 171, pp. 107-111.

[8] Knauss, W. G., Emri, I. J., (1981), "Non-linear Viscoelasticity Based on Free Volume Considerations," Journal of Computers and Structures, Vol. 13, pp. 123-128.

[9] Knauss, W. G., Emri, I., (1987), "Volume Change and the Nonlinearly Thermo-Viscoelastic Constitution of Polymers," Polymer Engineering and Science, Vol. 27, pp. 86-100.

[10] Losi, G. U., Knauss, W. G., (1992), "Freee Volume Theory and Nonlinear Thermoviscoelasticity," Polymer Engineering and Science, Vol. 32, pp. 542-557.

[11] Cohen, M. H., Turnbull, D., "Molecular Transport in Liquids and Glasses," Journal of Chemical Physics, Vol. 31, pp. 1164-1169.

[12] Doolittle, A. K., (1951), "Studies in Newtonian Flow. II. The Dependence of the Viscosity of Liquids on Free-Space," Journal of Applied Physics, Vol. 22, pp. 1471-1475.

[13] Struik, L. C. E., (1978), "Physical Aging in Amorphous Polymers and Other Materials," Elsevier Scientific Publishing Company.

[14] McKenna, G. B., (1990), "Glass Formation and Glassy Behavior," Comprehensive Polymer Science, Vol. 2, Polymer Properties, edited by Booth, C. and Price, C., pp. 311-362, Pergamon Press, Oxford.

[15] Carlson, J. A., Sapetta, L. P., (1967), "Stresses in Assemblies Bonded With Thermosetting Adhesive," Adhesive Age, Vol. 19, pp. 26-67.

[16] Weitsman, Y., (1980), "Residual Thermal Stresses in a Symmetric, Double-Lap Joint," Journal of Thermal Stresses, Vol. 3, pp. 521-535.

[17] Weitsman, Y., (1979), "Residual Thermal Stresses Due to Cool-Down of Epoxy-Resin Composites," Journal Applied Mechanics, Vol. 46, pp. 563-567.

[18] Losi, G. U., Knauss, W. G., (1992), " Thermal Stresses in Nonlinearly Viscoelastic Solids," Journal of Applied Mechanics, Vol. 59, pp. 43-49.

[19] McKinney, J. E., Belcher, H. V., (1963), "Dynamic Compressibility of Poly(Vinyl Acetate) and Its Relation to Free Volume," Journal of Research of the National Bureau of Standards-A. Physics and Chemistry, Vol. 67A, pp. 43-53.

[20] Armero, F., Simo, J. C., (1991), "A New Unconditionally Stable Fractional Step Method for Nonlinear Coupled Thermomechanical Problems," SUDAM Report no. 91-5, Stanford University.

[21] Farhat, C., Park, K. C., Dubois-Pelerin, Y. , (1991), "An Unconditionally Stable Staggered Algorithm for Transient Finite Element Analysis of Coupled Thermoelastic Problems," Computer Methods in Applied Mechanics and Engineering, Vol. 85, pp. 349-365.

[22] Zienkiewicz, O. C., Paul, D. K., Chan, A. H. C., (1988), " Unconditionally Stable Staggered Solution Procedure for Soil-Pore Fluid Interaction Problems," International Journal for Numerical Methods in Engineering, Vol. 26, pp. 1039-1055.

[23] Belytschko, T., Tsay, T., Liu, W. K., (1981), "A Stabilization Matrix for the Bilinear Mindlin Plate Element," Computer Methods in Applied Mechanics Engineering, Vol. 20, pp. 313-327.

[24] Moran, B., Knauss, W. G., (1992), "Crack Tip Stress and Deformation Fields in Strain-Softening Nonlinearly Viscoelastic Materials," Journal of Applied Mechanics, Vol. 59, pp. 95-101.

[25] Hughes, T. J. R., (1980), "Generalization of Selective Integration Procedures to Anisotropic and Nonlinear Media," International Journal for Numerical Methods in Engineering, Vol. 15, pp. 1413-1418.

[26] Taylor, R. L., (1980), "Chapter 15: Computer Procedures for Finite Element Analysis," in "*Finite Element Method*" by Zienkiewics, O. C., McGraw Hill, pp. 436-495.

[27] Bogy, D. B., (1968), "Edge-Bonded Dissimilar Orthogonal Elastic Wedges under Normal and Shear Loading," Journal of Applied Mechanics, Vol. 35, pp. 460-466.

[28] Carslaw, H. S., Jaeger, J. C., (1959), "Conduction of Heat in Solids," Oxford at the Clarendon Press, London.

[29] Miyano, Y., Nakamura, S., Sugimori, S., Kunio, T., Woo, T. C., (1986), "A Simplified Optical Method for Measuring Residual-Stress by Rapid Cooling in Thermosetting Resin Strip," Experimental Mechanics, Vol. 26, pp. 185-192.

[30] Crochet, M. J., Denayer, A., (1980), "Transient and Residual Thermoviscoelastic Stresses in Glass," Journal of Applied Mechanics, Vol. 47, pp. 254-260.

[31] Ferry, J. D., (1980), "Viscoelastic Properties of Polymers," Third edition, John Wiley and Sons, Inc.

[32] Negami, S., Ruch, R. J., Myers, R. R., (1982), "The Dielectric Behavior of Polyvinyl Acetate as a Function of Molecular Weight," Journal of Colloid and Interface Science, Vol. 90, pp. 117-126.

[33] Pagano, personal communication.

[34] Tobolsky, A. V., (1960), "Properties and Structures of Polymers," John Wiley & Sons, Inc.

[35] Taylor, R. L., Pister, K. L., Goudreau, G. L., (1970), "Thermomechanical Analysis of Viscoelastic Solids," International Journal for Numerical Methods in Engineering, Vol. 2, pp. 45-59.

[36] Weitsman, Y., (1979) "Stresses in Adhesive Joints Due to Moisture and Temperature," Journal of Composite Material, Vol. 11, pp. 378-394

[37] Suhir, E., (1986) "Stresses in Bi-Metal Thermostats," Journal of Applied Mechanics, Vol. 53, pp. 657-660.

[38] Geubelle, P. H., Knauss, W. G., (1993), "Propagation of a Crack in Homogenous and Bimaterial Sheet Under General In-plane Loading: Nonlinear Analysis," to appear in Journal of Applied Mechanics.

[39] Liechti, K. M., Chai, Y. S., (1992), "Asymetric Shielding In Interfacial Fracture Under In Plane Shear," Journal of Applied Mechanics, Vol. 59, pp. 295-304.

[40] William, M. L., (1959), "The Stress Around a Fault or a Crack in Dissimilar Media," Bulletin of the Seismological Society of America, Vol. 49, pp. 199-204.

[41] Rice, J. R., Sih, G. C., (1965), "Plane Problems of Cracks in Dissimilar Media," Journal of Applied Mechanics, Vol. 32, pp. 418-423.

[42] England, A. H., (1965), "A Crack Between Dissimilar Media," Journal of Applied Mechanics, Vol. 32, pp. 400-402.

[43] Moran, B., Shih, C. F., (1987), "Crack Tip and Associated Domain Integrals From Momentum and Energy Balance," Engineering Fracture Mechanics, Vol. 27, pp. 615-642.

[44] Wilson, W. K., Yu, I. W., (1979), "The Use of the J-integral in Thermal Stress Crack Problem," International Journal of Fracture, Vol. 15, pp. 377-387.

[45] Matos, P. L., McMeeking, R. M., et al, (1989), "A Method for Calculating Stress Intensities in Bimaterial Fracture," International Journal of Fracture, Vol. 40, pp. 235-254.

[46] Parvin, M., Knauss, W. G., (1988), "An Experimental Arrangement to Estimate the Failure Behavior of an Uncrosslinked Polymer Under High Spatial Constraint," Adhesive, Sealants, and Coating for Space and Harsh Environments, edited by Lieng-Huang Lee, Plenum Publishing Corporation.

[47] He, M. Y., Hutchinson, J. W., (1989), "Kinking of a Crack Out of an Interface," Journal of Applied Mechanics, Vol. 56, pp. 270-278.

[48] Fleck, N. A., Hutchinson, J. W., and Suo, Z., (1991), "Crack Path Selection in a Brittle Adhesive Layer," International Journal of Solids and Structures, Vol. 27, pp. 1683-1703.